Diffraction of Plane Radio Waves by a Parabolic Cylinder

Calculation of Shadows Behind Hills

By S. O. RICE

(Manuscript received April 3, 1953)

Expressions are given for the diffraction field far behind, and the surface currents on, a parabolic cylinder. Approximate values for the field strength and current density are given when the radius of curvature of the cylinder is large compared to a wavelength. The formulas may have value in predicting the shadows that are cast by hills in microwave propagation. The idea of representing hills by knife-edges has been used successfully by a number of investigators. The theory of the parabolic cylinder indicates that such a representation is valid even for gently rounded hills when the angle of diffraction is small. On the other hand, when the angle of diffraction is so large that the knife-edge calculations do not apply, the results presented here may be used.

1. INTRODUCTION

A number of investigators have studied the effect of hills on the propagation of short radio waves. Experiment has shown that the field far behind a hill may be computed, to a reasonable degree of accuracy, by assuming that the hill acts like a knife-edge (half-plane)[1]. The question naturally arises as to the conditions under which such an assumption is permissible. Here we attempt to throw some light on this question by taking the hill to be a parabolic cylinder.

Our results indicate that, for small angles of diffraction, even gently curved hills act like knife-edges. However, for larger angles corresponding to points deep in the shadow or to points high in the illuminated region, it may be necessary to use the more exact formulas which take the curvature of the hill into account.

[1] See, for example, Ultra-Short-Wave Propagation, J. C. Schelleng, C. R. Burrows and E. B. Ferrell, Proc. I.R.E., **21**, pp. 423–463, 1933.

As an application of our results, a brief study is made of the hypothesis that very short radio waves are transmitted far beyond the horizon by successive diffractions over hills or ridges. The ridges are assumed to be of equal height, to be 40 miles apart, and to have a radius of curvature of 100 meters at their crests. At the frequencies considered (30 and 300 mc) and at the small angles of diffraction required to go from one crest to the next, the ridges act like knife-edges.

At 30 mc and a distance of 280 miles the calculated field is in fair agreement with the observed field[2]. At 300 mc and at the same distance the calculated field is about 50 db below the observed field. This suggests that the 30 mc long distance propagation may possibly be explained by successive diffractions. The discrepancy at 300 mc may be due to any one of a number of reasons. For example, it may be due to the effect of the non-uniformity of the atmosphere, or to the roughness of our approximations (for one thing, we neglect reflections from the ground between the ridges).

The first theoretical work on the diffraction of plane electromagnetic waves by a parabolic cylinder apparently was done by P. S. Epstein.[3] His work makes use of a series of parabolic cylinder functions. When the cylinder is large many terms are required for computation. By "large" we mean that the radius of curvature at the vertex of the cylinder is large compared to the wavelength of the radio wave.

An entirely different approach was used by V. Fock[4,5] in 1946. In the first paper Fock sketches the derivation of an integral for the current density on a large paraboloid of revolution. In the second paper he rederives this integral by considering the form assumed by the field equations when a plane wave strikes a gently curved conductor at grazing incidence. His result gives the change in current density on a large and highly conducting parabolic cylinder as we go from the illuminated region into the shadow.

In 1950 K. Artmann[6] examined the diffraction field far behind a large circular cylinder. He showed that, for small angles of diffraction, the

[2] A summary of experimental data is given by K. Bullington, Radio Transmission beyond the Horizon in the 40-400 Megacycle Band, Proc. I.R.E., **41**, pp. 132–135, 1953.

[3] Dissertation, Munich (1914). A more accessible account of this work is given in the Encyklopäedie der Math. Wiss. 5, Part 3 (1909–1926) Phys. p. 511. See also H. Bateman, *Partial Differential Equations of Math. Phys.*, (Cambridge Univ. Press 1932) p. 488.

[4] The Distribution of Currents Induced by a Plane Wave on the Surface of a Conductor, J. Phys. (U.S.S.R.), **10**, pp. 130–136, 1946.

[5] The Field of a Plane Wave Near the Surface of a Conducting Body, J. Phys. (U.S.S.R.), **10**, pp. 399–409, 1946.

[6] Beugung polarisierten Lichtes an Blenden endlicher Dicke im Gebiet der Schattengrenze, Zeitschr. für Phys. **127**, pp. 468–494, 1950.

diffraction pattern is shifted by an amount proportional to the $\frac{1}{3}$ power of the radius of curvature. Whether the shift is towards the shadow or in the opposite direction depends upon the polarization of the incident wave.

In this paper we derive some of the results given by Fock and Artmann by starting with Epstein's series. In addition we investigate the diffracted field at a great distance behind the cylinder. The cylinder is assumed to be a perfect conductor in all of our work except for a few equations given near the ends of Sections 4, 6, and 7. The procedure is similar to that used in the smooth-earth theory.[7] The series is converted into an integral and then the path of integration is deformed so as to gain as much simplification as possible. As might be expected, the results for a large parabolic cylinder are similar in some respects to those for a smooth earth. Much of the work requires a knowledge of the behavior of parabolic cylinder functions of large complex order. Although several studies of this behavior have been published, the results are not in the form required. For this reason, and for the sake of completeness, several sections dealing with the properties of parabolic cylinder functions have been included.

Incidentally, W. Magnus[8] has studied the field produced by a line source located at the focus of a parabolic cylinder. However, his problem is somewhat different from the one with which we are concerned.

I am grateful to Prof. Erdélyi of the California Institute of Technology and to my colleagues at Bell Telephone Laboratories for helpful discussions and references which resulted in a number of improvements throughout the paper. I am also indebted to Miss Marian Darville for performing the rather laborious computations upon which the various curves and tables are based.

2. DISCUSSION OF RESULTS

Various expressions are given later for the electromagnetic field in terms of parabolic cylinder functions. In this section we shall confine a good share of our attention to the case in which the cylinder is very large compared to a wavelength so that the cylinder functions may be approximated by Airy integrals. As in the remainder of the paper, we shall be concerned chiefly with the field behind the cylinder and the current density on the cylinder.

[7] By "Smooth-earth theory" we mean the formulas for the field produced by a dipole near a large sphere. A complete discussion of the theory is given in the book by H. Bremmer, *Terrestrial Radio Waves* (Elsevier, 1949).

[8] Zur Theorie des zylindrisch-parabolischen Spiegels, Zeitschr. für Physik, **118**, pp. 343–356, 1941.

It turns out that the results for the parabolic cylinder are closely related to those obtained by Sommerfeld[9] for the diffraction of a plane wave by a perfectly conducting half-plane. In fact, the two fields are surprisingly similar in the region of the shadow boundary. More precisely, the fields are similar for values of the angle ψ, defined in Fig. 2.3, such that (roughly)

$$|\psi \text{ in radians}| < \frac{1}{4}\left[\frac{\text{wavelength}}{\text{radius of curvature of cylinder at its crest}}\right]^{1/3},$$

where the coefficient $\frac{1}{4}$ has been selected somewhat arbitrarily. For larger values of $|\psi|$ the difference between the fields becomes pronounced. As we go deeper and deeper into the shadow, i.e. as ψ becomes more and more negative, the field behind a cylinder ultimately decreases exponentially with ψ. On the other hand, the field behind a half-plane decreases roughly as $1/|\psi|$. Since the exponential function decreases more rapidly than does $1/|\psi|$, the shadow behind a hill is darker than the one behind a half-plane. High in the illuminated region the field consists of the incident wave plus the wave reflected from the illuminated portion of the cylinder. For the half-plane this reflected wave is negligibly small until ψ reaches 180°.

First we shall review the situation pictured in Fig. 2.1. An incident wave comes in from the left and strikes a perfectly conducting vertical half-plane which casts a shadow as shown. The electric and magnetic intensities are proportional to $\exp(i\omega t)$ where t is the time and ω is the radian frequency. The unit of length is chosen so that λ, the wavelength, is equal to 2π. This is done in order to simplify the expressions we have to deal with. For example, a plane wave of unit amplitude traveling in the positive x direction, as shown in Fig. 2.1, is represented by $\exp(-ix)$.

Sommerfeld's exact expressions, for the special case of horizontal incidence shown in Fig. 2.1, may be written as

$$\text{(hp)} \qquad E = (e^{-ix} + S_1) + S_2(0), \tag{2.1}$$

$$\text{(vp)} \qquad H = (e^{-ix} + S_1) + S_3(0), \tag{2.2}$$

where (2.1) holds when the electric intensity E is parallel to the edge, and (2.2) when the magnetic intensity H is parallel to the edge. From

[9] Math. Annalen, **47**, p. 317, 1896. Sommerfeld's results have been described in a number of texts on optics. The book, *Huygens' Principle* by Baker and Copson (Oxford 2nd edition, 1950) deals with this and many similar problems. See also Chap. 20 of Frank-von Mises, *Die Differential-und Integralgleichungen der Mechanik und Physik*, 2nd edition, Braunschweig: F. Vieweg and Sohn (1935).

the analogy with the radio case, these two polarizations will be termed "horizontal polarization" (hp) and "vertical polarization" (vp), respectively. The incident plane wave for hp is assumed to have an E of unit amplitude. This is indicated by the exp $(-ix)$ in (2.1). For vp the incident wave is assumed to have an H of unit amplitude. The S's are defined by the Fresnel integrals

$$e^{-ix} + S_1 = (i/\pi)^{1/2} e^{-ix} \int_{-\infty}^{t_1} e^{-it^2}\, dt,$$

$$S_1 = -(i/\pi)^{1/2} e^{-ix} \int_{t_1}^{\infty} e^{-it^2}\, dt, \tag{2.3}$$

$$S_2(0) = -S_3(0) = -(i/\pi)^{1/2} e^{+ix} \int_{t_2}^{\infty} e^{-it^2}\, dt,$$

$$t_1 = (2r)^{1/2} \sin\frac{\varphi}{2}, \qquad t_2 = (2r)^{1/2} \cos\frac{\varphi}{2}, \qquad i^{1/2} = \exp(i\pi/4),$$

where (r, φ) are the polar coordinates shown in Fig. 2.1 [S_1 and $S_2(0) = -S_3(0)$ for an arbitrary angle of incidence are given by Equations (5.3), (5.6), and (5.20) of Section 5]. We use the notation $S_2(0)$, $S_3(0)$ to indicate that these functions are special cases of the functions $S_2(h)$, $S_3(h)$ which appear in the analysis for the parabolic cylinder.

The principal part of the field far to the right of the half-plane, where x is positive, is given by exp $(-ix) + S_1$ whose absolute value is plotted in Fig. 2.2. The function S_1 almost cancels the incident wave in the shadow, and then drops down to small values outside the shadow. The function $S_2(0)$ is always small in the region we shall consider. It becomes large only when φ exceeds π. It then corresponds to the wave reflected from the front (left-hand side) of the half-plane.

When we are far enough away from the shadow boundary to make

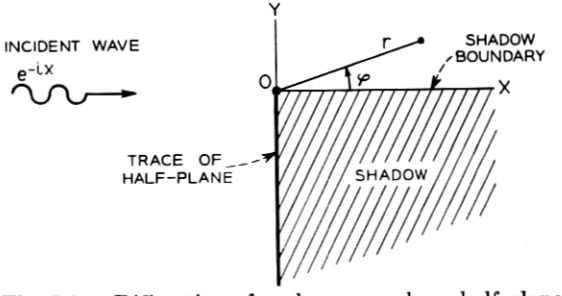

Fig. 2.1 — Diffraction of a plane wave by a half-plane.

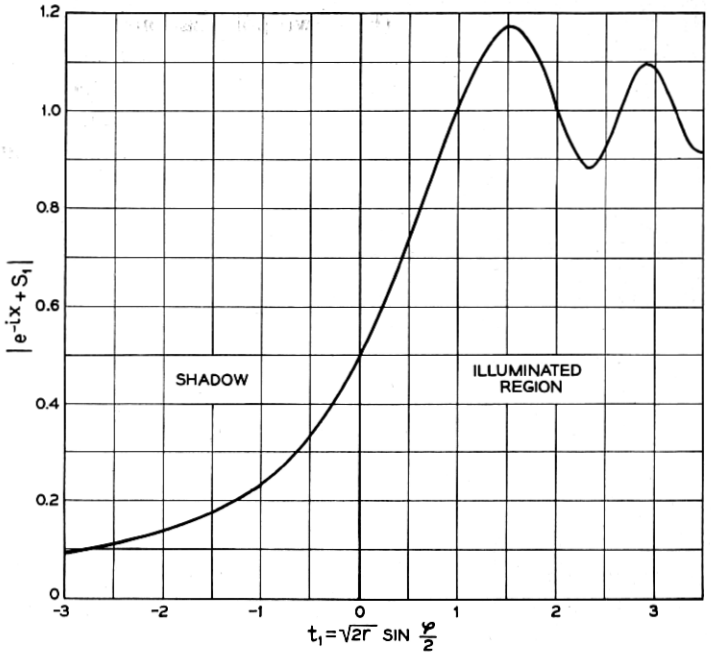

Fig. 2.2 — The approximate value $|e^{-ix}+S_1|$ of $|E|$ for hp and of $|H|$ for vp at a great distance r behind a half-plane. Here, as in all of our work, the wavelength λ is 2π. For an arbitrary wavelength replace r by $2\pi r/\lambda$, etc.

$\varphi^2 r \gg 1$, $\exp(-ix)+S_1$ has the asymptotic expressions [see Equations (7.7) and (7.8)]

$$e^{-ix}+S_1 \sim \begin{cases} c(r)/2\,\sin\frac{\varphi}{2}, & \varphi<0 \text{ (shadow)} \\ e^{-ix}+c(r)/2\,\sin\frac{\varphi}{2}, & \varphi>0 \end{cases} \tag{2.4}$$

$$c(r) = i^{3/2}(2\pi r)^{-1/2}e^{-ir}. \tag{2.5}$$

These expressions lead us to picture the field to the right of the half-plane as the sum of the incident wave and a wave, $c(r)/\varphi$, spreading out from the diffracting edge[10] (for the small φ's of interest, $2\sin\varphi/2 \approx \varphi$ even though $\varphi^2 r \gg 1$). In the illuminated region these two waves interfere with each other to give the oscillations around unity shown in Fig.

[10] See, for example, R. W. Wood, *Physical Optics*, 3rd edition, p. 220 (MacMillan, 1935). Curves of equal phase and amplitude have been computed and plotted by W. Braunbeck and G. Laukien, Einzelheiten zur Halbebenen-Beugung, Optik, **9**, pp. 174–179, 1952.

2.2. In the shadow only the edge wave is present and there is no interference. S_1 is not the edge wave in the shadow.

The edge does not radiate uniformly in all directions. The φ in the denominator of $c(r)/\varphi$ indicates that the edge sends out its strongest wave in the direction of the shadow boundary where $\varphi = 0$. This accounts for the decreasing size of the oscillations in Fig. 2.2 as φ becomes more and more positive. It likewise accounts for the steady decrease as φ becomes more and more negative.

That $S_2(0)$ is small in comparison with $\exp(-ix) + S_1$ follows from

$$S_2(0) \sim c(r)/2 \cos\frac{\varphi}{2} \tag{2.6}$$

and the fact that this is small compared to the $c(r)/2 \sin(\varphi/2)$ in (2.4) when φ is small.

So far, we have been discussing a special case of Sommerfeld's results. Now we turn to the case of the perfectly conducting parabolic cylinder shown in Fig. 2.3. Here, as in Fig. 2.1, the incident plane wave $\exp(-ix)$ comes in from the left. The fields for the two kinds of polarization are given by

$$\text{(hp)} \qquad E = (e^{-ix} + S_1) + S_2(h), \tag{2.7}$$

$$\text{(vp)} \qquad H = (e^{-ix} + S_1) + S_3(h), \tag{2.8}$$

where, just as in the half-plane case, the fundamental vectors E and H are perpendicular to the plane of Fig. 2.3 and the incident waves are of unit amplitude.

The $[\exp(-ix) + S_1]$ in (2.7) and (2.8) is exactly the same Fresnel integral (2.3) as for the half-plane. $S_2(h)$ is a rather complicated integral

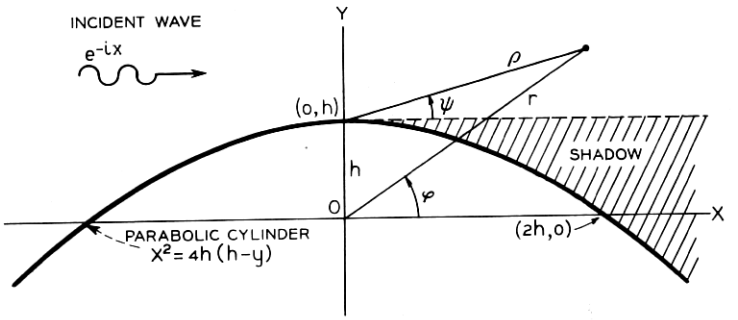

Fig. 2.3 — Coordinates used in the discussion of the parabolic cylinder. The coordinates such as $(0, h)$ refer to (x, y). The origin 0 of coordinates is at the focus of the parabola and h is the height of the vertex or crest, above the origin.

(obtained by setting the angle of incidence θ equal to $\pi/2$ in equation (5.4)) involving parabolic cylinder functions. When $h = 0$ the parabolic cylinder reduces to a half-plane and $S_2(h)$ reduces to the value $S_2(0)$ appearing in (2.3). The symbol $S_3(h)$ represents an integral much like $S_2(h)$ except that it contains derivatives of the parabolic cylinder functions. As we might expect, $S_2(h)$ and $S_3(h)$ behave in much the same way as does $S_2(0)$. In particular, they are small compared to $\exp(-ix) + S_1$ at the shadow boundary, and their asymptotic expressions analogous to (2.6) hold as φ and ψ pass through zero.

$S_2(h)$ and $S_3(h)$ have been put in a form suitable for computation in two cases, (1) when $h = 0$, which is the half-plane case already discussed, and (2) when h and r/h^2 are very large. In the second case it is convenient to introduce new polar coordinates (ρ, ψ) with their origin at the crest of the parabola as shown in Fig. 2.3. In these coordinates a circular cylindrical wave spreading out from the crest is asymptotically proportional to

$$c(\rho) = i^{3/2}(2\pi\rho)^{-1/2} e^{-i\rho}. \tag{2.9}$$

In Section 8 it is shown that

$$E \approx [e^{-ix} + S_1]_\rho - \frac{c(\rho)}{\psi} + c(\rho)h^{1/3}\left[\Psi(\tau) + \frac{1}{\tau}\right]\exp(i\tau^3/3), \tag{2.10}$$

$$\tau = h^{1/3}\psi$$

is an approximation which gives the field (for horizontal polarization) in the region of the shadow boundary far behind a large cylinder. Our τ is an approximation to the g used there. Here the subscript ρ on $[\exp(-ix) + S_1]_\rho$ means that the quantity within the brackets is to be computed as though it corresponded to a half-plane with its edge at the crest of the parabolic cylinder, so that ρ, ψ are to be used in (2.3) instead of r, φ. Also,

$$\Psi(\tau) = 2i^{-1/3}\int_0^\infty \frac{Ai(u)\exp(i^{-1/3}u\tau)\,du}{Ai(u) - iBi(u)} + 2i\int_0^\infty \frac{Ai(u)\exp(iu\tau)\,du}{Ai(u) + iBi(u)} \tag{2.11}$$

where $Ai(u)$ and $Bi(u)$ are Airy integrals defined by equations (13.12) and (13.16), and tabulated in reference.[11] In this paper we find it convenient to use the Airy integrals instead of the related Bessel functions

[11] The Airy Integral, Brit. Asso. Math. Tables, Part — Vol. B (Cambridge, 1946).

of order $\frac{1}{3}$. As in (2.3), the fractional powers of i are made precise by taking $i \equiv \exp(i\pi/2)$.

Three kinds of approximations have been made in the derivation of (2.10), namely those associated with the assumptions (1) that the angle ψ is small, (2) that h is large, and (3) that r/h^2 is large. The terms in $1/\psi$ and $1/\tau$ do not cause trouble at $\psi = 0$ because their infinities cancel each other.

The counterpart of (2.10) for vertical polarization is obtained from (2.10) by replacing E by H and $\Psi(\tau)$ by $\Psi_v(\tau)$, where the subscript v stands for "vertical"; and $\Psi_v(\tau)$ is given by (2.11) when $Ai(u)$ and $Bi(u)$ are replaced by their derivatives with respect to u.

Series for $\Psi(\tau) + 1/\tau$ and $\Psi_v(\tau) + 1/\tau$ which converge for negative (shadow) values of τ are given by Equations (7.31) and (7.53), respectively, with g in place of τ. Table 2.1 gives values of $\Psi(\tau)$ and $\Psi_v(\tau)$ which were obtained from the series for τ negative, and from numerical integration of (2.11) and its analogue for $\tau \geqq 0$.

When τ is large and positive Equations (7.35) and (7.55) show that

$$\begin{aligned} \Psi(\tau) + 1/\tau &\sim (i\pi\tau)^{1/2} \exp(-i\tau^3/12), \\ \Psi_v(\tau) + 1/\tau &\sim (i\pi\tau)^{1/2} \exp(i\pi - i\tau^3/12). \end{aligned} \tag{2.12}$$

When τ is large and negative the leading terms in (7.31) and (7.53) give

$$\begin{aligned} \Psi(\tau) + 1/\tau &\sim -i^{1/3}\, 2.03 \exp[(2.025 + i\ 1.169)\tau], \\ \Psi_v(\tau) + 1/\tau &\sim -i^{1/3}\, 3.42 \exp[(0.882 + i\ 0.509)\tau]. \end{aligned} \tag{2.13}$$

Now that we have expressions for the field what do they tell us? For one thing, they may be used to show that the field near the shadow

TABLE 2.1 — VALUES OF $\Psi(\tau)$ AND $\Psi_v(\tau)$

τ	$\lvert\Psi(\tau)\rvert$	arg. $\Psi(\tau)$	$\lvert\Psi_v(\tau)\rvert$	arg. $\Psi_v(\tau)$
3	3.13	−93.5°	3.16	+104.3°
2	2.21	−1.8°	2.80	192.4°
1.5	1.945	+21.6	2.44	211.3
1.0	1.715	+32.5	1.985	219.5
0.5	1.486	34.2	1.522	218.6
0	1.254	30.0	1.089	210.0
−0.5	1.030	22.9	0.724	193.7
−1.0	0.823	15.2	0.459	167.8
−1.5	0.648	8.48	0.317	130.6
−2.0	0.511	+3.79	0.281	92.0
−3.0	0.338	+0.12	0.288	45.1
−4.0	0.250	−0.12	0.264	22.3
−5.0	0.200	−0.02	0.221	9.71

boundary is almost the same as for a half-plane. Away from the shadow boundary, the field in the shadow can be interpreted as a "crest wave" which reduces to the "edge wave" for a half-plane. The crest wave decreases as an exponential function of ψ in the shadow instead of as $1/\varphi$ in the case of a half-plane. In other words it is much darker behind a parabolic cylinder than behind a half-plane — and the larger the cylinder the darker it is. (A glance at Fig. 2.8 shows that this statement must be qualified for vertical polarization by requiring the observer to be deep in the shadow.) As Figs. 2.7 and 2.8 show, deep in the illuminated region the crest wave behaves like the wave reflected (as computed by geometrical optics) from the illuminated portion of the cylinder.

Now we consider expressions for the surface currents. Let J and J_v be the densities of the conduction currents which flow on the surface of the perfectly conducting parabolic cylinder for the cases of horizontal and vertical polarizations, respectively. J is parallel to E and is perpendicular to the plane of Fig. 2.3 while J_v flows in the plane of the figure. J_v is positive when the current flows in the direction of increasing x. In Section 6 it is shown that when h is large, J and J_v are given approximately by

$$\zeta_0 J \approx \frac{\exp(-ix - i\gamma^3/3)}{\pi h^{1/3}} \int_0^\infty \left[\frac{i^{-2/3} \exp(-i^{1/3} u\gamma)}{Ai(u) - iBi(u)} + \frac{\exp(-iu\gamma)}{Ai(u) + iBi(u)} \right] du, \tag{2.14}$$

$$J_v \approx \frac{i \exp(-ix - i\gamma^3/3)}{\pi} \int_0^\infty \left[-\frac{\exp(-i^{-1/3} u\gamma)}{Ai'(u) - iBi'(u)} + \frac{\exp(-iu\gamma)}{Ai'(u) + i\,Bi'(u)} \right] du. \tag{2.15}$$

These expressions are obtained when the relations (13.17) for Airy integrals are used in equations (6.16) and (6.23). Here ζ_0 is the intrinsic impedance of free space. In the rational MKS system which we use $\zeta_0 = 120\pi$ ohms. The factor ζ_0 appears in (2.14) but not in (2.15) because we assume the incident wave for vertical polarization ($H = 1$, $E = \zeta_0 H = 120\pi$) to be 120π times stronger than the one for horizontal polarization ($E = 1$). The primes on $Ai(u)$ and $Bi(u)$ denote their derivatives with respect to u. The parameter γ depends upon the coordinate x of the point at which the current is being observed:

$$\gamma = x/2h^{2/3}. \tag{2.16}$$

Equations (2.14) and (2.15) hold only in the region of the crest of the cylinder and for large h. Under these conditions $x + \gamma^3/3$ is very nearly equal to the distance along the surface measured from the crest of the cylinder.

An expression equivalent to the one for J_v in (2.15) has been derived and tabulated by V. Fock.[4]

Series for $\zeta_0 J$ and J_v which converge for positive (shadow) values of γ are given by equations (6.17) and (6.24). When γ is large and negative the application of the method of steepest descent to integrals (6.16) and (6.23) leads to

$$\begin{aligned} \zeta_0 J &\approx -(x/h)e^{-ix}\,[1 + i/4\gamma^3 + \cdots], \\ J_v &\approx 2e^{-ix}\,[1 - i/4\gamma^3 + \cdots], \end{aligned} \tag{2.17}$$

in which $x/h = 2\gamma h^{-1/3}$.

Table 2.2 gives values of $h^{1/3}\zeta_0 J \exp(ix)$ and $J_v \exp(ix)$. The values of J for $\gamma > 0$ were computed from the series, and the ones for $\gamma \leqq 0$ were obtained by numerical integration of (2.14). The entries for J_v were taken from the more extensive table given by Fock.[4] In order to express his results in our terms it is necessary to use the fact that the radius of curvature at the vertex of the parabola is $2h$. A change in the sign of i is also necessary because the time enters Fock's work through $\exp(-i\omega t)$ instead of $\exp(i\omega t)$. The values shown were checked for $\gamma > 0$ by the series and for $\gamma \leqq 0$ by numerical integration of (2.15)

Fock's table shows that by the time γ has reached -2 the value of $J_v \exp(ix)$ has become 1.982 at an angle of $+1.45$ degrees. This is close to the limiting value of 2 predicted at $\gamma = -\infty$ by (2.17).

It will be noted that, for large values of h, J is smaller than J_v by

TABLE 2.2 — SURFACE CURRENT DENSITIES

γ	$h^{1/3}\zeta_0 J \exp(ix + i\gamma^3/3)$		$J_v \exp(ix + i\gamma^3/3)$	
	modulus	Argument in degrees	mod.	Arg.
−1.0	2.16	−25.9	1.861	−15.43°
−0.5	1.38	−16.8	1.682	+1.52
0.0	0.77	−30.0	1.399	0.00
0.3	0.515	−44.8	1.197	−6.06
0.6	0.327	−62.9	0.991	−14.23
1.0	0.167	−90.1	0.738	−26.63
1.5	0.066	−125.9	0.488	−42.57
2.0	0.025	−161.6	0.315	−57.98
3.0	0.0033	−230.7	0.130	−87.57
4.0	0.00043	−298.0	0.054	−116.75

the order of $h^{-1/3}$ when γ is of moderate size. It will be shown later that the current density decreases exponentially as one moves into the shadow, and that its rate of decrease is related to that of the field as shown in Fig. 2.6.

We now take up the detailed discussion of the expressions for the field and the current density. It is convenient to consider the current density first. When a plane wave strikes a perfectly conducting plane, the surface current is proportional to the tangential component of H in the incident wave, and flows at right angles to it. In the rational MKS units we are using, the surface current density is two times the incident tangential H. When we consider the illuminated side of a large parabolic cylinder and calculate the current density by doubling the tangential component of the incident H we obtain the approximations

$$\begin{aligned} \zeta_0 J &\approx -2x(4h^2 + x^2)^{-1/2}\, e^{-ix}, \\ J_v &\approx 2e^{-ix}, \end{aligned} \tag{2.18}$$

which hold when x is large and negative. When h is very large but $x/2h$ small these formulas agree with the leading terms of (2.17) which were obtained from our integrals for the current density.

Expressions for the current density deep in the shadow may be obtained from the leading terms of the convergent series by letting γ become large and positive. The exponential decrease is found to be

$$\begin{aligned} |\, \zeta_0 J \,| &\approx 1.43 h^{-1/3} \exp\,(-1.013 x h^{-2/3}), \\ |\, J_v \,| &\approx 1.83 \exp\,(-0.44 x h^{-2/3}), \end{aligned} \tag{2.19}$$

where the numbers appearing in these equations are associated with the smallest zeros of $Ai(u)$ and $Ai'(u)$, respectively. These formulas for a large cylinder are roughly similar to those for propagation over a smooth earth. The radius of curvature at the crest of the cylinder is $2h$. Setting this equal to the radius of the earth gives an exponential rate of decrease for J and J_v which is the same as that over a smooth earth for the two polarizations. Of course, the coefficients multiplying the exponential functions are different. This agreement is not surprising since the Airy integrals are closely related to the Hankel functions of order $\frac{1}{3}$ used in the smooth earth theory.

The surface current densities as a function of the distance $h - y$ below the crest for $h = 1000$ and for $h = 0$ are shown in Fig. 2.4. The equation of the cylinder shows that $h - y = x^2/4h$ so that, from (2.19), $\zeta_0 J$ and J_v decrease in proportion to $h^{-1/3} \exp\,[-2.025 h^{-1/6}\,(h - y)^{1/2}]$ and $\exp\,[-.88 h^{-1/6}\,(h - y)^{1/2}]$, respectively, far down in the shadow.

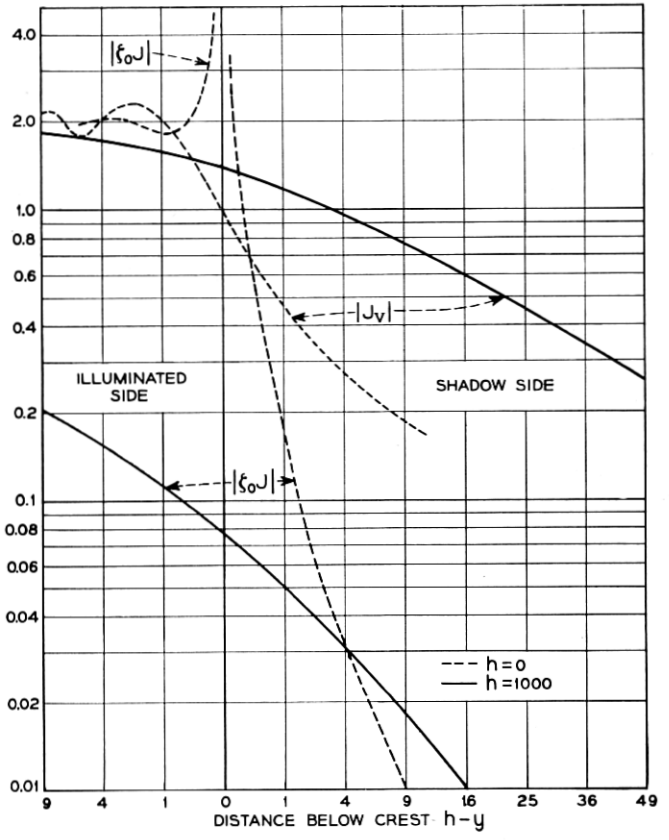

Fig. 2.4 — The surface current density is plotted as a function of the vertical distance below the crest or edge. The curves for $h = 1000$ and $h = 0$ are obtained from Table 2.2 and equations (2.20), respectively. Here, as always, the units are such at $\lambda = 2\pi = 6.28 \ldots$

The equations used to compute the curves marked $h = 0$ are

$$\zeta_0 J = (i\pi r)^{-1/2}\left[e^{-ir} \mp 2ir^{1/2}\int_{\pm\sqrt{\tau}}^{\infty} e^{-it^2}dt\right], \qquad J_v = 2(i/\pi)^{1/2}\int_{\pm\sqrt{\tau}}^{\infty} e^{-it^2}dt, \tag{2.20}$$

where the upper signs are for the shadow side and the lower ones for the illuminated side. The computations are made easier by the relations

$$(\zeta_0 J)_- - (\zeta_0 J)_+ = 2,$$
$$(J_v)_- + (J_v)_+ = 2,$$

where the subscripts "$-$" and "$+$" denote opposite points on the illuminated side and shadow side, respectively, of the half-plane. These relations follow from (2.20).* The radius vector r from the origin is equal to $-y$ on the half-plane. Equations (2.20) follow quite readily from (2.3). The values of J and J_v for an arbitrary angle of incidence and $h = 0$ are given by expressions (6.6) and (6.22), respectively.

All of the curves in Fig. 2.4, even $| \zeta_0 J |$ for $h = 1{,}000$, eventually approach the value 2 far down on the illuminated side. It may be shown that $| J_v |$ and $| \zeta_0 J |$ for the half-plane decrease like $(\pi r)^{-1/2}$ and $1/(2\pi^{1/2} r^{3/2})$, respectively, deep in the shadow. Hence as we go to the right in Fig. 2.4, the dashed curves will eventually cross over and lie above the solid curves, which decrease exponentially. The larger h, the lower and flatter is the curve for $| \zeta_0 J |$.

Now we turn to the diffraction field at points far to the right of the cylinder. When $| \psi | \ll 1$, so that we are not too far from the shadow boundary, and h is large, the field is given by (2.10), or by its analogue for vertical polarization. In order to get acquainted with (2.10) we first examine the field when $| \psi | \ll 1$ but $\psi^2 \rho \gg 1$.

When we are so far behind the cylinder that $\psi^2 \rho \gg 1$ even though $| \psi | \ll 1$, the asymptotic expressions (2.4) show that

$$[e^{-ix} + S_1]_\rho \sim \begin{cases} c(\rho)/\psi, & \psi \text{ negative (shadow)} \\ e^{-ix} + \dfrac{c(\rho)}{\psi}, & \psi \text{ positive} \end{cases} \tag{2.21}$$

Substitution of (2.21) in (2.10) gives

$$E \sim \begin{cases} c(\rho) h^{1/3} \left(\Psi(\tau) + \dfrac{1}{\tau} \right) \exp\,(i\tau^3/3), & \psi < 0 \\ c(\rho) h^{1/3} \left(\Psi(\tau) + \dfrac{1}{\tau} \right) \exp\,(i\tau^3/3) + e^{-ix}, & \psi > 0 \end{cases} \tag{2.22}$$

The presence of $c(\rho)$ shows that the total wave may be regarded as the sum of the incident wave and a wave spreading out from the crest. The crest wave is the analogue of the edge wave, $c(r)/\varphi$, for the half-plane. In fact, when we are in the region where the $1/\tau$ in (2.22) is the most important term, the crest wave is approximately

$$c(\rho)/\psi \tag{2.23}$$

* They also follow from superposition and consideration of the symmetry of the currents produced on the half-plane $y < 0$, $x = 0$ when $-A$ is impressed. Here A denotes the system of currents which flows in the upper half-plane $y > 0$, $x = 0$ when the incident wave falls on a complete plane at $x = 0$.

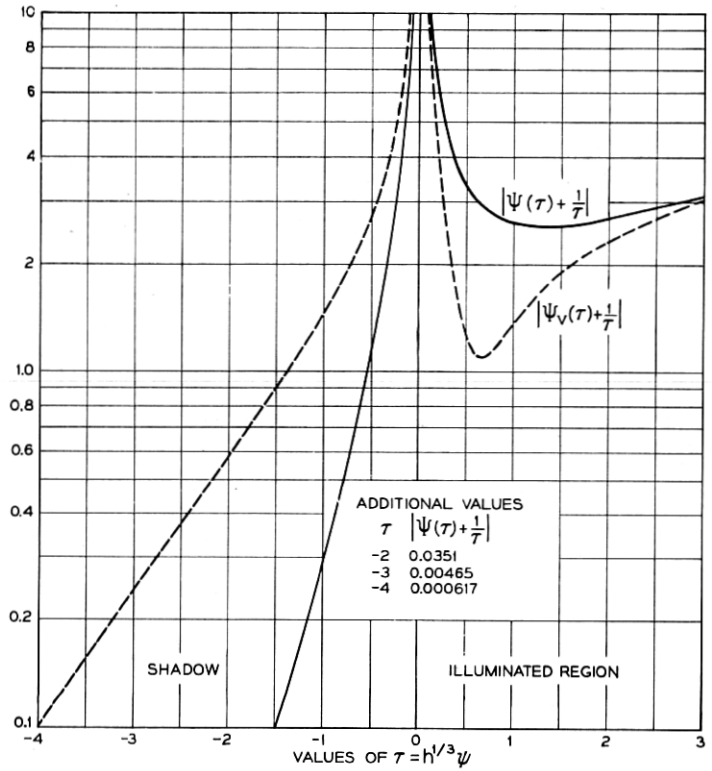

Fig. 2.5 — The amplitude of the crest wave may be obtained from these curves and expressions (2.24). Here $\tau = h^{1/3}\psi$ where ψ is small. However ρ must be large enough to make $\psi^2\rho \gg 1$.

and this corresponds to a half-plane with its edge at the crest of the cylinder. τ may be small even though we are considering $|\psi|$ to be large enough to make (2.21) and (2.22) hold, i.e. large enough to make $|\psi|\rho^{1/2} \gg 1$. Indeed, multiplying by $h^{1/3}$ gives $|\tau|\rho^{1/2} \gg h^{1/3}$ which may be achieved for small values of τ by making ρ large enough.

It follows from (2.22) and its analogue for vertical polarization that the amplitudes of the crest waves are

$$\begin{aligned} &\text{(hp)} && (2\pi\rho)^{-1/2}\, h^{1/3}\, |\,\Psi(\tau) + 1/\tau\,|, \\ &\text{(vp)} && (2\pi\rho)^{-1/2}\, h^{1/3}\, |\,\Psi_v(\tau) + 1/\tau\,|, \end{aligned} \tag{2.24}$$

where the expression (2.9) for $c(\rho)$ has been used. The last factors in (2.24) may be computed from Table 2.1. They are plotted in Fig. 2.5.

When we go deep down into the shadow where τ is large and negative

we see from (2.13) that

$$\begin{aligned} |\Psi(\tau) + 1/\tau| &\sim 2.03\, e^{2.025\tau}, \\ |\Psi_v(\tau) + 1/\tau| &\sim 3.42\, e^{0.882\tau}, \end{aligned} \tag{2.25}$$

so that the absolute value of the field is

$$\begin{aligned} &\text{(hp)} \qquad |E| \sim (2\pi\rho)^{-1/2}\, h^{1/3}\, 2.03 \exp\,(2.025\, h^{1/3}\psi), \\ &\text{(vp)} \qquad |H| \sim (2\pi\rho)^{-1/2}\, h^{1/3}\, 3.42 \exp\,(0.882\, h^{1/3}\psi). \end{aligned} \tag{2.26}$$

where the angle ψ is negative. Thus, as Artmann[6] has pointed out, the field decreases exponentially as we go into the shadow. The larger h is, the more rapid is the decrease. This supports the statement made earlier that it is darker behind a large cylinder than behind a half-plane.

Comparison of the expressions for the current density and field strength for the shadow regions shows that there is a simple approximate relation between them. Near the crest of the cylinder, where x is small, the radius of curvature is nearly $2h$. Hence the tangent to the parabola drawn from the point P (located at (ρ, ψ) deep in the shadow) touches the parabola at T where x is approximately $-2h\psi$. This is shown in Fig. 2.6. Replacing x by $-2h\psi$ in the expressions (2.19) shows that the current density at T is proportional to the field at P as given by (2.26). It follows that

$$\begin{aligned} &\text{(hp)} \qquad |E/\zeta_0 J| \sim 1.41\, h^{2/3}\, (2\pi\rho)^{-1/2} \\ &\text{(vp)} \qquad |H/J_v| \sim 1.87\, h^{1/3}\, (2\pi\rho)^{-1/2}. \end{aligned} \tag{2.27}$$

This leads us to picture the field at P as being produced principally by the surface currents around T. The effect of the stronger currents

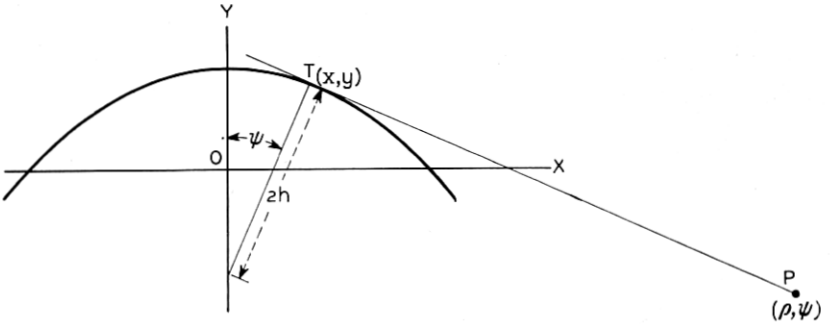

Fig. 2.6 — The field strength at point P (deep in the shadow) specified by the polar coordinates (ρ, ψ) is nearly proportional to the current density at the tangent point T specified by the rectangular coordinates (x, y).

closer to the crest is perhaps blocked out by the curvature of the cylinder. For comparison with the horizontal polarization case we note that E at (ρ, ψ) for an infinitely long current filament at the origin $\rho = 0$ is given by

$$|E/\zeta_0 I| \sim .5(2\pi\rho)^{-1/2} \tag{2.28}$$

where I is the current carried by the filament and the frequency is is such that $\lambda = 2\pi$. There is some difficulty with the picture for vertical polarization because the current element at T points directly towards P and hence should produce very little field there. This is perhaps associated with the fact that the (vp) ratio in (2.27) is smaller than the (hp) ratio by approximately the factor $h^{-1/3}$.

We now leave the shadow region and consider the field at points well inside the illuminated region. Fig. 2.5 shows that for large positive values of τ the amplitude of the crest wave tends to increase with τ. The asymptotic expressions (2.12) show that when τ is large and positive

$$|\Psi(\tau) + 1/\tau| \approx |\Psi_v(\tau) + 1/\tau| \sim (\pi\tau)^{1/2} = (\pi\psi)^{1/2}h^{1/6}, \tag{2.29}$$

and hence the amplitude of the crest wave deep in the illuminated region is, from (2.22) and its analogue,

$$\begin{aligned} &\text{(hp)} \qquad |E - e^{-ix}| \sim (2\pi\rho)^{-1/2}\,(\pi\psi h)^{1/2}, \\ &\text{(vp)} \qquad |H - e^{-ix}| \sim (2\pi\rho)^{-1/2}\,(\pi\psi h)^{1/2}. \end{aligned} \tag{2.30}$$

Since (2.30) is derived from the general expression (2.10) it is subject to the restrictions mentioned just below equation (2.11). In particular the angle ψ should be small (but we must still have $\psi^2\rho \gg 1$ as assumed in (2.22)). When ψ is positive, an application of the laws of geometrical optics to determine the reflection from the curved surface of the parabolic cylinder leads to the expressions[12]

$$\begin{aligned} &\text{(hp)} \quad |E - e^{-ix}| \sim \left[\frac{h\tan(\psi/2)}{\rho}\right]^{1/2} \sec(\psi/2), \qquad \psi > 0 \\ &\text{(vp)} \quad |H - e^{-ix}| \sim \left[\frac{h\tan(\psi/2)}{\rho}\right]^{1/2} \sec(\psi/2), \qquad \psi > 0 \end{aligned} \tag{2.31}$$

for the reflected wave. When ψ is small these expressions reduce to (2.30) as they should.

Expressions (2.31) may also be obtained from our analysis by start-

[12] In our two-dimensional case the calculation of the required radius of curvature, etc., is not difficult. General theorems dealing with problems of this sort and references to earlier work are given in the paper, A General Divergence Formula, H. J. Riblet and C. B. Barker, J. Appl. Phys. **19**, pp. 63–70, 1948.

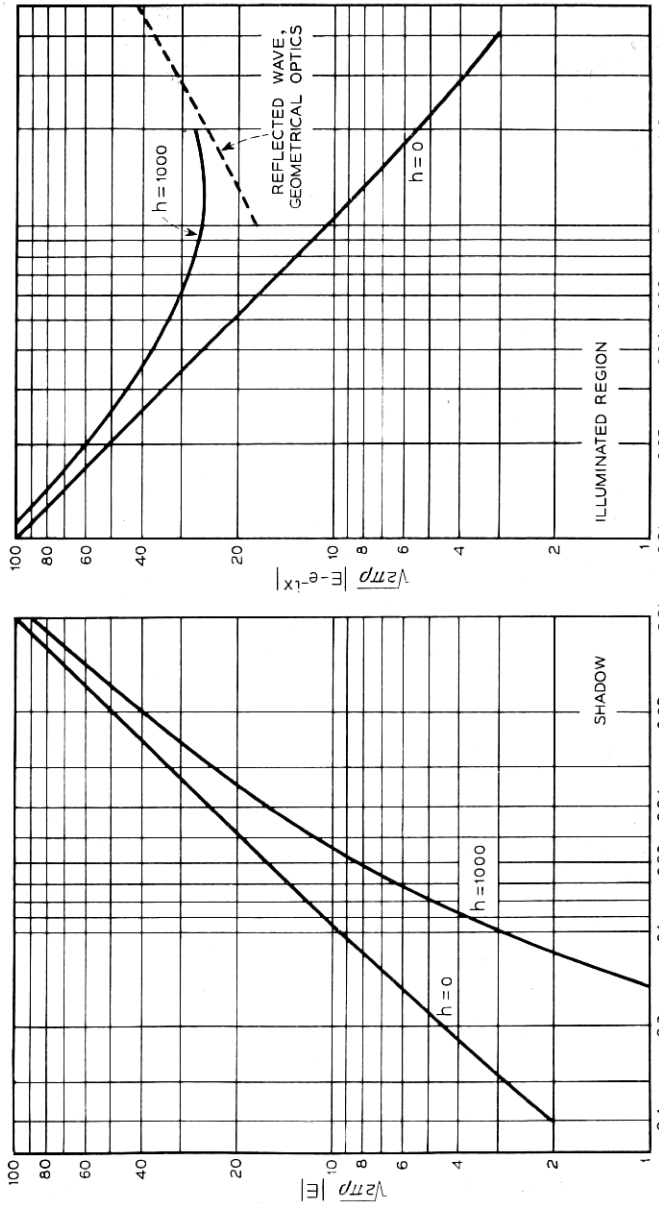

Fig. 2.7 — Strength of crest wave for horizontal polarization. The curves fail for $|\psi| < \rho^{-1/2}$, and the $h = 1000$ curve becomes less reliable as ψ increases. The exponential decrease deep in the shadow is given by equation (2.26). The dashed curve for the reflected wave is computed from equation (2.31).

ing with equations (7.36) and (7.56). Furthermore, it may be verified that the phase angles of the reflected waves as computed from (7.36) and (7.56) agree with those computed from geometrical optics when reflection coefficients of -1 and $+1$ are assumed for hp and vp, respectively.

The amplitudes of the crest waves for $h = 1{,}000$ and $h = 0$ are shown for hp in Fig. 2.7 and for vp in Fig. 2.8. Of course, when $h = 0$ the crest wave reduces to the edge wave from a half-plane. The curves for $h = 1{,}000$ were computed from equations (2.24) and the curves of Fig. 2.5 (or their equivalent when τ is small). The curves for $h = 0$ were computed from

$$
\begin{aligned}
&|E| \sim (2\pi\rho)^{-1/2} \left| \frac{1}{2\sin(\psi/2)} + \frac{1}{2\cos(\psi/2)} \right|, \qquad \psi < 0 \\
&\text{(hp)} \\
&|E - e^{-ix}| \sim (2\pi\rho)^{-1/2} \left| \frac{1}{2\sin(\psi/2)} + \frac{1}{2\cos(\psi/2)} \right|, \qquad \psi > 0 \\
&|H| \sim (2\pi\rho)^{-1/2} \left| \frac{1}{2\sin(\psi/2)} - \frac{1}{2\cos(\psi/2)} \right|, \qquad \psi < 0 \\
&\text{(vp)} \\
&|H - e^{-ix}| \sim (2\pi\rho)^{-1/2} \left| \frac{1}{2\sin(\psi/2)} - \frac{1}{2\cos(\psi/2)} \right|, \qquad \psi > 0
\end{aligned}
\tag{2.32}
$$

which follow from (2.1), (2.2), (2.4) and (2.6).

From equation (2.21) onward we have been discussing the field for values of ψ and ρ such that $\rho\psi^2 \gg 1$. For these values the concept of the crest wave is helpful in visualizing the behavior of the field. Now we consider the field at points close to the boundary of the geometric shadow far behind the cylinder. This is the region in which Artmann[6] was especially interested. His results for the shift of the field may be obtained from (2.10) and its analogue by taking $|\psi|$ to be very small.

At the shadow boundary $\psi = 0$ and $[\exp(-ix) + S_1]_\rho = \frac{1}{2}$. Hence the region of interest at present is in the neighborhood of the point point $t_1 = 0$, $|\exp(-ix) + S_1| = \frac{1}{2}$ of Fig. 2.2. A magnified view of this region showing the shift of the field is given in Fig. 2.9. The figure shows that, for a given value of $\rho\psi$, $|E|$ for hp is less than $|H|$ for vp. As Artmann has pointed out, this is to be expected since the reflection coefficient for E (hp) is roughly -1 and the reflected wave therefore

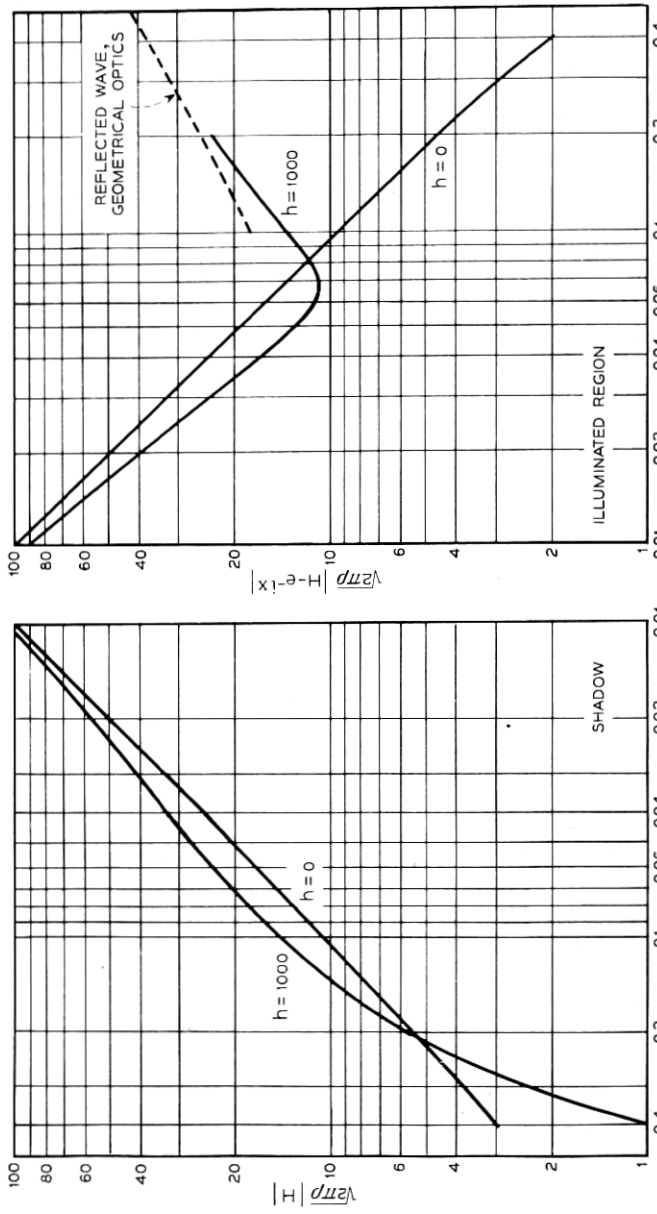

Fig. 2.8 — Strength of crest wave for vertical polarization. The remarks made in the caption of Fig. 2.7 also hold here. Incidentally, a value of $h = 1000$ corresponds to a radius of curvature of $2000/2\pi = 318$ wavelengths at the crest.

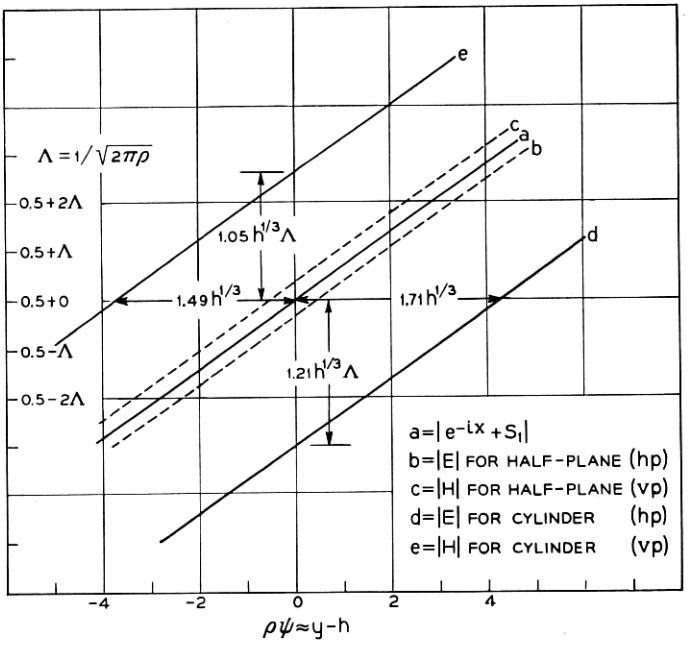

Fig. 2.9 — Behavior of $|E|$ and $|H|$ on the shadow boundary far behind the half-plane or parabolic cylinder. This is a magnified view of the region around $t_1 = 0$, $|\exp(-ix) + S_1| = \frac{1}{2}$ in Fig. 2.2.

tends to cancel the direct wave when ψ is very small. On the other hand, the reflection coefficient for H (vp) is $+1$ and the reflected wave tends to add to the direct wave.

The distances $1.71h^{1/3}$ and $-1.49h^{1/3}$ appearing in Fig. 2.9 are the amounts, measured in units for which the wavelength is 2π, by which $|E|$ and $|H|$ are shifted by the curvature of the parabolic cylinder. If $y' - h'$ is the shift in meters for $|E|$ and if the radius of curvature of the crest is $a = 2h'$ meters, Fig. 2.9 gives $\beta(y' - h') = 1.71\ (\beta h')^{1/3} = 1.71\ (\beta a/2)^{1/3}$ where $\beta = 2\pi/\lambda$. Thus $y' - h' = 0.399\lambda\ (a/\lambda)^{1/3}$ meters. The corresponding shift for $|H|$ is $-0.346\lambda(a/\lambda)^{1/3}$ meters. Artmann gives the values 0.39 and -0.20 for the respective coefficients. The discrepancy between -0.346 and -0.20 is cause for worry because it seems to indicate either a mistake in our work, which I have been unable to locate, or a shortcoming in the approximations made by Artmann for the case of vertical polarization.

As h approaches zero the parabolic cylinder becomes a half-plane and the curves d and e should approach curves b and c, respectively. According to Fig. 2.9 both d and e approach curve a. This failure is an

indication of the errors introduced by the approximations used in the derivation of (2.10) and its analogue.

3. RADIO PROPOGATION OVER A SUCCESSION OF RIDGES ON THE EARTH'S SURFACE

The results mentioned in Section 1 concerning propagation over a succession of ridges may be obtained from the expressions and curves of Section 2 as follows: Consider the situation shown in Fig. 3.1. Let a radio wave start out from a transmitter at T. We assume that by the time it arrives at the first ridge at P it has become equivalent to a plane wave of amplitude A/ℓ traveling in the direction TP, where A is a constant depending on the strength of the transmitter. For the sake of simplicity the waves reflected from the ground are neglected. In a more careful study they would have to be included.*

In order to calculate the strength of the wave at the second ridge, we assume it to be a crest wave coming from P. Let G denote the value of $|E|$ (we assume the case of horizontal polarization since the reflection coefficient of physical materials approaches -1 for almost grazing incidence) at Q corresponding to a plane wave of unit amplitude incident on P. From Fig. 3.1 we see that the values of ψ and ρ to be used in computing G are $\psi \approx -\ell/R$, $\rho = 2\pi\ell/\lambda$, λ = wavelength, R = radius of earth. The value of h depends upon the radius of curvature of the ridge: $2h = 2\pi$ (radius of curvature)$/\lambda$.

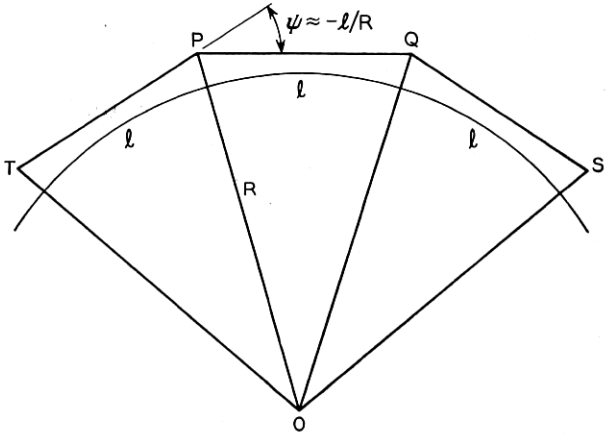

Fig. 3.1 — Diagram showing ridges at P and Q which diffract the radio wave starting from T so that a portion of it is received at S.

* A method for doing this (for one hill) is given in Reference 1, page 417.

The amplitude of the wave striking the ridge at Q is $AG/\ell\sqrt{2}$. The $\sqrt{2}$ comes from the horizontal sidewise spreading of the wave in going from ℓ to 2ℓ. If we were dealing with the energy instead of the amplitude, the factor would be 2 instead of $\sqrt{2}$. When this wave is assumed to be plane and traveling in the PQ direction, similar reasoning shows that the amplitude of the disturbance at the receiver S is $AG^2/\ell\sqrt{3}$.

If, instead of two ridges at P and Q, as shown in Fig. 3.1, there are N ridges between the transmitter at T and the receiver at S, the amplitude of the radio wave at S is $AG^N/\ell\sqrt{N+1}$. The distance between T and S is approximately $(N+1)\ell$, and the free space amplitude at S is $A/(N+1)\ell$. Hence

$$\frac{\text{Actual Amplitude at S}}{\text{Free Space Amplitude at S}} = G^N(N+1)^{1/2}. \tag{3.1}$$

The actual field at S is therefore

$$20\,N\log_{10}(1/G) - 10\log_{10}(N+1) \tag{3.2}$$

db below the free space field.

As an example, let us assume a distance of 280 miles between the transmitter and receiver, and a distance of 40 miles between successive ridges. This gives $N = 6$. For a wavelength of 10 meters and a radius of curvature of 100 meters for the diffracting ridges, the formulas of Section 2 show that the ridges behave like half-planes and that $G \approx 0.227$. Equation (3.2) then says that, for a distance of 280 miles and a wavelength of 10 meters the actual field should be about 69 db below the free space field. Although this is in fair agreement with the experimental results, calculations for other distances indicate that the field strengths predicted by (3.2) tend to be smaller than the ones observed.

When the work is carried through for $\lambda = 1$ meter and a distance of 280 miles, (3.2) says that the field is 120 db below free space. The observed fields are 70 ± 15 db below the free space value.

These figures suggest that the roughness of the earth's surface might possibly account for transmission far beyond the horizon for wavelengths of the order of 10 meters. For wavelengths of the order of 1 meter either the approximations leading to (3.2) break down or some other explanation is required.

4. SERIES FOR THE ELECTROMAGNETIC FIELD

Here we set down series for the electromagnetic field when a plane wave strikes a perfectly conducting parabolic cylinder. Since Epstein's

classical work deals with the general case of finite conductivity, the series we use are special cases of the ones discussed by him.

The parabolic coordinates (ξ, η) which we shall use are related to the rectangular coordinates (x, y) and polar coordinates (r, φ) as follows:

$$\begin{aligned} x + iy &= (\xi + i\eta)^2/2i = r\, e^{i\varphi}, \\ x &= \xi\eta = r\cos\varphi, \qquad y = (\eta^2 - \xi^2)/2 = r\sin\varphi, \\ r &= (x^2 + y^2)^{1/2} = (\xi^2 + \eta^2)/2, \\ dx^2 + dy^2 &= (\xi^2 + \eta^2)\,(d\xi^2 + d\eta^2) = 2r(d\xi^2 + d\eta^2), \\ \xi &= (2r)^{1/2}\cos(\varphi/2 + \pi/4), \\ \eta &= (2r)^{1/2}\sin(\varphi/2 + \pi/4). \end{aligned} \tag{4.1}$$

The lines η = constant are a series of downward-curving confocal parabolas having their focus at the origin. The parabolic cylinder $x^2 = 4h(h - y)$ is given by $\eta^2 = 2h$. This special value of η will be called η_0:

$$\eta_0 = (2h)^{1/2} \geqq 0, \qquad h = \eta_0^2/2. \tag{4.2}$$

When $\eta_0 = 0$, the cylinder reduces to the half-plane $x = 0$, $y \leqq 0$. The lines ξ = constant are halves of upward-curving confocal parabolas having their common focus at the origin. Outside the cylinder $\eta > \eta_0 \geqq 0$, so η is always positive in our work. ξ is positive in the half-plane $x > 0$ and negative in $x < 0$.

For much of our work we shall assume the incident wave to come in at the angle θ, $0 \leqq \theta \leqq \pi$, as shown in Fig. 4.1. As mentioned in Section

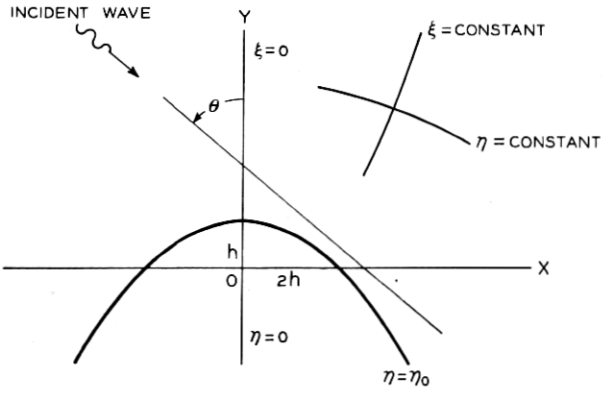

Fig. 4.1 — This diagram shows the angle θ of the incident wave and the surface of the perfectly conducting cylinder $x^2 = 4h(h - y)$ (or $\eta = \eta_0$).

2, the field quantities are assumed to depend upon the time through the factor $\exp(i\omega t)$ where ω is the radian frequency.

The wave equations for horizontal and vertical polarization are, respectively,

$$\frac{\partial^2 E}{\partial \xi^2} + \frac{\partial^2 E}{\partial \eta^2} + (\xi^2 + \eta^2)E = 0 \tag{4.3}$$

$$\frac{\partial^2 H}{\partial \xi^2} + \frac{\partial^2 H}{\partial \eta^2} + (\xi^2 + \eta^2)\, H = 0 \tag{4.4}$$

where, as explained in Section 2, the unit of length has been chosen so that the wavelength $\lambda = 2\pi$. On the surface of the perfectly conducting cylinder, i.e. for $\eta = \eta_0$, we must have $E = 0$ and $\partial H/\partial \eta = 0$. When E and H are known the remaining components of the field may be computed from Maxwell's equations.

Special solutions of (4.3) (and (4.4)) are

$$\exp\,[i(\eta^2 - \xi^2)/2]\; U_n(\xi i^{1/2})\; U_n(\eta i^{-1/2}), \tag{4.5}$$

$$\exp\,[i(\eta^2 - \xi^2)/2]\; U_n(\xi i^{1/2})\; W_n(\eta i^{-1/2}), \tag{4.6}$$

where $i^{1/2}$ stands for $\exp(i\pi/4)$ and $U_n(z)$, $W_n(z)$ satisfy the equation

$$\frac{d^2 T_n(z)}{dz^2} - 2z\,\frac{dT_n(z)}{dz} + 2nT_n(z) = 0. \tag{4.7}$$

Another solution of (4.7) with which we shall be concerned is $V_n(z)$. These three solutions are defined by contour integrals of the form

$$(2\pi i)^{-1} \int \exp\,[f(t)]\, dt \qquad \text{where} \qquad f(t) = -t^2 + 2zt - (n+1)\log t.$$

The path of integration for $U_n(z)$ comes in from $-\infty$ where $\arg t = -\pi$, encircles the origin counterclockwise and runs out to $-\infty$ with $\arg t = \pi$. The path for $V_n(z)$ runs from $-\infty$ where $\arg t = \pi$ to $+\infty$ where $\arg t = 0$, and the path for $W_n(z)$ runs from $+\infty$ to $-\infty$ where $\arg t = -\pi$. The integrals are written at greater length in equations (9.1) and the paths of integration are shown in Fig. 9.1. Since the paths may be joined to form a closed path containing no singularities of the integrand it follows that

$$U_n(z) + V_n(z) + W_n(z) = 0. \tag{4.8}$$

When n is a non-negative integer

$$U_n(z) = H_n(z)/n! = \frac{(-)^n}{n!}\, e^{z^2}\, \frac{d^n}{dz^n}\, e^{-z^2} \tag{4.9}$$

where $H_n(z)$ is Hermite's polynomial. When z becomes very large the leading terms in (9.17) and (9.16) give

$$U_n(z) \sim (2z)^n/n!, \tag{4.10}$$

$$W_n(\eta i^{-1/2}) \sim i(i^{1/2}/\eta)^{n+1}\, e^{-i\eta^2}/2\pi^{1/2}. \tag{4.11}$$

In order to obtain a series for the incident wave

$$\exp\,[-ix \sin\theta + iy \cos\theta]$$

shown in Fig. 4.1 we consider the special case $\theta = 0$. In this case the wave is simply $\exp(iy)$ or $\exp\,[i(\eta^2 - \xi^2)/2]$ and may be obtained by setting $n = 0$ in (4.5). This suggests that the incident wave may be expressed as the sum of terms like (4.5). The series turns out to be

$$\begin{aligned}
&\exp\,[-ix \sin\theta + iy \cos\theta] \\
&\quad = \exp\,[-i\xi\eta \sin\theta + i \cos\theta(\eta^2 - \xi^2)/2] \\
&\quad = \exp\,[-izz' \sin\theta - \cos\theta(z^2 + z'^2)/2] \\
&\quad = e^{iy} \sec(\theta/2) \sum_{n=0}^{\infty} n!(-iw/2)^n U_n(z) U_n(z')
\end{aligned} \tag{4.12}$$

where

$$\begin{aligned}
w &= \tan(\theta/2), \\
z &= \xi i^{1/2}, \\
z' &= \eta i^{-1/2}.
\end{aligned} \tag{4.13}$$

This series has been studied by a number of writers. It goes back to Mehler[13] who obtained it by evaluating the integral

$$\pi^{-1/2}\, e^{x^2} \int_{-\infty}^{\infty} \exp\,[-(t - iy)^2 - (x + iat)^2]\, dt$$

first in closed form, and then as a series (by using the generating function $\exp\,[-(-iat)^2 + 2(-iat)x]$ for $H_n(x)$ and integrating termwise). This leads to

$$\begin{aligned}
&(1 - a^2)^{-1/2} \exp\left[\frac{2xya - (x^2 + y^2)a^2}{1 - a^2}\right] \\
&\qquad = \sum_{0}^{\infty} H_n(x) H_n(y)\, a^n/2^n n!
\end{aligned} \tag{4.14}$$

which is equivalent to (4.12). Since (4.14) converges when $|a| < 1$, (4.12) converges when $|w| < 1$ or $|\theta| < \pi/2$.

[13] Reihenentwicklungen nach Laplaceschen Functionen höher Ordnung, J. Reine Angew., Math., **66**, pp. 161–176, 1866.

When the incident wave strikes the cylinder the reflected wave has some of the characteristics of a wave spreading radially outwards. Such a wave contains the factor $\exp(-ir) = \exp[-i(\xi^2+\eta^2)/2]$. Consideration of the exponential factors in (4.6) and (4.11) suggests that the reflected wave may be expressed as the sum of terms of the form (4.6). The coefficients in this series are to be determined so that $E = 0$ or $\partial H/\partial\eta = 0$ at the surface $\eta = \eta_0$, the incident wave being represented by (4.12).

For the case of horizontal polarization this procedure gives

$$E = e^{iy}\sec(\theta/2)\sum_0^\infty n!(-iw/2)^n U_n(z)\,[U_n(z') - W_n(z')U_n(z_0')/W_n(z_0')] \tag{4.15}$$

$$E = \exp[-ix\sin\theta + iy\cos\theta] - e^{iy}\sec(\theta/2)\sum_0^\infty n!(-iw/2)^n U_n(z)W_n(z')U_n(z_0')/W_n(z_0') \tag{4.16}$$

for the complete field. These are special cases of Epstein's results. Here z_0' is the value of z' which corresponds to the surface of the cylinder:

$$z_0' = i^{-1/2}\eta_0 = (2h/i)^{1/2} \tag{4.17}$$

The entries for regions II and II′ (these are regions in the m-plane ($m = n+1$) which, as Figs. 11.2 and 12.2 show, contain the large positive values of n) in Tables 12.2 and 12.4 of Section 12 may be used to show that as $n \to \infty$

$$\begin{aligned} V_n(z_0')/W_n(z_0') &\sim i^{-2n}\exp[2\eta_0(2in)^{1/2}], \\ U_n(z_0')/W_n(z_0') &= -1 - V_n(z_0')/W_n(z_0'), \\ U_n(z)W_n(z') &\sim -\frac{\exp[-iy - \eta(2n/i)^{1/2}]}{4[\Gamma(1+n/2)]^2} \\ &\quad \{\exp[-\xi(2n/i)^{1/2}] + i^{2n}\exp[\xi(2n/i)^{1/2}]\}. \end{aligned} \tag{4.18}$$

Since

$$n!/[\Gamma(1+n/2)]^2 \sim 2^n(\pi n/2)^{-1/2}$$

the series in (4.15) and (4.16) converge if $|w| = |\tan\theta/2| < 1$.

Series for H similar to those of (4.15) and (4.16) may be obtained for the case of vertical polarization. The boundary condition at $\eta = \eta_0$ is now $\partial H/\partial\eta = 0$. It is convenient to introduce the functions $'U_n(z)$, $'V_n(z)$, $'W_n(z)$ defined by

$$'U_n(z) = -zU_n(z) + \partial U_n(z)/\partial z \tag{4.19}$$

and the two other equations obtained when U is replaced by V and W. The prime is placed in front of U instead of behind to avoid mistaking $'U_n(z)$ for $\partial U_n(z)/\partial z$. The function $'U_n(z')$ makes its appearance when $\partial H/\partial \eta$ is calculated for the boundary condition. Since $iy = -(z^2 + z'^2)/2$ we have

$$\frac{\partial}{\partial \eta} e^{iy} U_n(z') = i^{-1/2} e^{iy} {}'U_n(z'). \tag{4.20}$$

The analogues of (4.15) and (4.16) for vertical polarization are (assuming now that H for the incident wave is of unit amplitude).

$$H = e^{iy} \sec(\theta/2) \sum_0^\infty n!(-iw/2)^n U_n(z) \\ [U_n(z') - W_n(z')'U_n(z_0')/'W_n(z_0')], \tag{4.21}$$

$$= \exp[-ix \sin\theta + iy \cos\theta] \\ - e^{iy} \sec(\theta/2) \sum_0^\infty n!(-iw/2)^n U_n(z) W_n(z')'U_n(z_0')/'W_n(z_0'), \tag{4.22}$$

and these series converge if $|w| < 1$.

If the parabolic cylinder is merely a good conductor, instead of being perfect, the boundary conditions at $\eta = \eta_0$ are approximately[14] $E = -\zeta H_\xi$, $E_\xi = \zeta H$. Here E_ξ and H_ξ denote the ξ components of the electric and magnetic intensities and ζ is the intrinsic impedance

$$\zeta = [i\omega\mu/(g + i\omega\epsilon)]^{1/2} \tag{4.23}$$

of the cylinder material. ζ is assumed to be small compared to the intrinsic impedance $\zeta_0 = (\mu_0/\epsilon_0)^{1/2} = \omega\mu_0$ (since $\lambda = 2\pi$) of the external medium. In these expressions μ, ϵ, g are the permeability, dielectric constant, and conductivity of the cylinder; and μ_0 and ϵ_0 refer to the external medium.

When we set

$$\sigma = i^{-1/2}(\xi^2 + \eta_0^2)^{1/2} \zeta_0/\zeta, \\ \tau = i^{-1/2}(\xi^2 + \eta_0^2)^{1/2} \zeta/\zeta_0, \tag{4.24}$$

the boundary conditon for hp becomes $\sigma E = -\partial E/\partial z'$ at $z' = z_0'$. When σ is assumed to be constant we obtain

$$E = e^{iy} \sec(\theta/2) \sum_0^\infty n!(-iw/2)^n U_n(z) \\ \{U_n(z') - W_n(z')[\sigma U_n(z_0') + {}'U_n(z_0')]/[\sigma W_n(z_0') + {}'W_n(z_0')]\} \tag{4.25}$$

[14] *Electromagnetic Waves*, S. A. Schelkunoff, D. Von Nostrand Co., N. Y. (1943) p. 89. See also G. A. Hufford, Quart. Appl. Math. **9**, pp. 391–403, 1952, where reference is made to the work of Leontovich and Fock.

which reduces to (4.15) when $\sigma \to \infty$. The constancy of σ may be achieved by either taking the properties of the cylinder material to change in a suitable way or, roughly, by taking η_0^2 (and hence h) to be so large that only the nearly constant values of σ at the crest of the cylinder have an effect on the result (assuming $\theta = \pi/2$, and restricting our attention to the region near the shadow boundary).

The corresponding expression for vertical polarization may be obtained from (4.25) by replacing E and σ by H and τ, respectively. We shall refer to (4.25) and its analogue later in connection with the field in the shadow (Section 7) and with Fock's[5] investigation of the surface currents on gently curved conductors (Section 6).

5. INTEGRALS FOR THE FIELD

When the curvature of the cylinder is small, i.e., when h is many wavelengths, the series of Section 4 converge slowly. The work initiated by G. N. Watson[15] on the smooth earth problem suggests that we convert the series into contour integrals with n as the complex variable of integration. When this is done we get an integral with the path of integration L_1 shown in Fig. 5.1. Thus, for example, expression (4.16) for E is transformed into

$$E = \exp[-ix \sin\theta + iy \cos\theta] \left(-\frac{e^{iy} \sec\frac{\theta}{2}}{2i}\right) \int_{L_1} \left(\frac{iw}{2}\right)^n \frac{\Gamma(n+1)}{\sin \pi n} U_n(z) W_n(z') U_n(z_0')\, dn / W_n(z_0'). \tag{5.1}$$

At first sight it seems that not much can be done with this integral because the integral obtained by deforming L_1 into L_2 does not converge (this is explained in the discussion of Table 5.1). However, some ex-

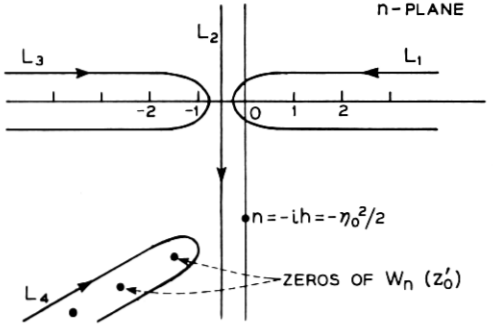

Fig. 5.1 — Paths of integration in the complex n-plane.

[15] Proc. Roy. Soc., London (A) **95**, p. 83, 1918.

perimentation shows that if we set $U_n(z_0') = -V_n(z_0') - W_n(z_0')$ in (4.16), the series splits into two series, one of which may be summed and the other may be converted into an integral along the path L_2 of Fig. 5.1:

$$\begin{aligned} E &= \exp[-ix\sin\theta + iy\cos\theta] + S_1 + S_2(h), \\ S_1 &= e^{iy}\sec(\theta/2)\sum_0^\infty n!(-iw/2)^n U_n(z)W_n(z'), \\ S_2(h) &= e^{iy}\sec(\theta/2)\sum_0^\infty n!(-iw/2)^n U_n(z)W_n(z')V_n(z_0')/W_n(z_0'). \end{aligned} \tag{5.2}$$

The series for S_1 may be summed by replacing $U_n(z)$ and $W_n(z')$ by their expressions (9.19) in terms of definite integrals, and interchanging the order of summation and integration. The resulting series may be summed and the integrations performed. The result is Sommerfeld's integral for a diffracted plane wave:

$$\begin{aligned} S_1 &= -(i/\pi)^{1/2} e^{-ix\sin\theta + iy\cos\theta}\int_{T_1}^\infty e^{-it^2}\,dt, \\ T_1 &= \eta\cos\frac{\theta}{2} - \xi\sin\frac{\theta}{2} = (2r)^{1/2}\sin\left(\frac{\varphi-\theta}{2}+\frac{\pi}{4}\right). \end{aligned} \tag{5.3}$$

The inversion of the order of summation and integration may be justified when $|w| = |\tan(\theta/2)| < 1$ (in which case the series in (5.2) converge) by using (1) the result that $|R_N| < |a^N/N!|$ when a is real in

$$\sum_0^{N-1}\frac{(ia)^n}{n!} = e^{ia} - R_N,$$

and (2) the inequality

$$\begin{aligned} \left[\int_0^\infty t^N \exp[-t^2 + 2^{1/2}bt]\,dt\right]^2 \\ < \int_0^\infty e^{-2(1-\alpha)t^2}t^{2N}\,dt\int_{-\infty}^\infty \exp[-2\alpha t^2 + 2^{3/2}bt]\,dt \\ < A2^{-N}b^{-1/2}N^{-1/4}N!\exp(2bN^{1/2}) \end{aligned}$$

This inequality holds when $N \gg b^2$ and at the same time $N \gg 1$. The value of A is independent of N and b is a number which exceeds $|\xi|$. In this work the parameter α has been arbitrarily introduced; and has then been chosen so as to make the product of the two integrals a minimum when N is large. This value of α is $bN^{-1/2}$.

When the series (5.2) for $S_2(h)$ is converted into a contour integral taken along the path L_1, by the procedure used to obtain (5.1), it is

seen that L_1 may be deformed into L_2 and we obtain

$$S_2(h) = \frac{e^{iy} \sec \frac{\theta}{2}}{2i} \int_{L_2} \left(\frac{iw}{2}\right)^n \frac{\Gamma(n+1)}{\sin \pi n} U_n(z) W_n(z') V_n(z_0')\, dn / W_n(z_0') \qquad (5.4).$$

Whether a particular integrand, such as the one shown in (5.4), converges at the ends $n = \pm i\infty$ of L_2 can often be decided from Table 5.1. This table gives a rough idea of the behavior of the various functions in terms of powers of i. For example, if the integrand should turn out to be proportional to $i^n = \exp(i\pi n/2)$ at $n = i\infty$, the integral will converge like $\exp(-\pi \mid n \mid /2)$.

TABLE 5.1

Function	Order of Magnitude — Rough Approximation	
	near $n = i\infty$	near $n = -i\infty$
i^n	0	∞
i^{-n}	∞	0
$\sin \pi n$	i^{-2n}	i^{2n}
$\Gamma(n+1)$	i^n	i^{-n}
$U_n(z)$	$i^{-3n/2}$	$i^{3n/2}$
$V_n(z)$	$i^{-3n/2}$	$i^{-n/2}$
$W_n(z)$	$i^{n/2}$	$i^{3n/2}$

The approximations for $\Gamma(n+1)$ follow from its asymptotic expression, and those for the parabolic cylinder functions come from Tables 12.2 and 12.4. The entries for the cylinder functions may also be surmised from expressions (9.4) which hold for $z = 0$.

Table 5.1 may be used to show that the integrand in (5.1) is of the order of i^n as $n \to -i\infty$. Hence there is no hope of deforming L_1 into L_2 in this case. On the other hand, the integrand in (5.4) is of the order of i^n as $n \to i\infty$ and of i^{-n} as $n \to -i\infty$, and therefore (5.4) converges exponentially. In fact, it converges for all real positive values of $w = \tan \theta/2$. This enables us to obtain an expression for the field which holds for $0 < \theta < \pi$ (i.e. it is not subject to the restriction $\mid w \mid < 1$ required by (4.16)). This expression, which is fundamental for our work, has the form

$$E = \exp[-ix \sin \theta + iy \cos \theta] + S_1 + S_2(h). \qquad (5.5)$$

Here S_1 and $S_2(h)$ are given by (5.3) and (5.4), respectively.

In working with (5.5) it is sometimes convenient to use the expression

$$\exp\,[-ix\sin\theta + iy\cos\theta] + S_1$$
$$= (i/\pi)^{1/2}\exp\,[-ix\sin\theta + iy\cos\theta]\int_{-\infty}^{T_1} e^{-it^2}\,dt \tag{5.6}$$

which follows from (5.3) and

$$\int_{-\infty}^{\infty}\exp\,(-it^2)\,dt = (\pi/i)^{1/2}. \tag{5.7}$$

The development leading to (5.5) shows that is satisfies the boundary condition $E = 0$ at $\eta = \eta_0$ for $0 < w < 1$. That (5.5) also satisfies the condition for the extended range $0 < w < \infty$ follows immediately from

$$\frac{e^{iy}\sec\frac{\theta}{2}}{2i}\int_{L_2}\left(\frac{iw}{2}\right)^n\frac{\Gamma(n+1)}{\sin\pi n}\,U_n(z)V_n(z')\,dn$$
$$= -(i/\pi)^{1/2}\exp\,[-ix\sin\theta + iy\cos\theta]\int_{-\infty}^{T_1}\exp\,(-it^2)\,dt \tag{5.8}$$
$$= -\exp\,[-ix\sin\theta + iy\cos\theta] - S_1$$

when we note that setting $z' = z_0'$ reduces $S_2(h)$ to the left hand side of (5.8) (with $z' = z_0'$).

Equation (5.8) is due to T. M. Cherry[16] who obtained it by expressing the cylinder functions as integrals and interchanging the order of integration (he works with the function $D_n(z)$ of our equations (9.2)). Substituting the integrals (9.19) for $U_n(z)$ and $V_n(z')$ in (5.8) and interchanging the order of integration leads to a similar derivation. Equation (5.8) may also be obtained by deforming L_2 into L_1 when $0 < w < 1$ and into L_3 when $1 < w < \infty$. This leads to the two series

$$e^{iy}\sec\frac{\theta}{2}\sum_{n=0}^{\infty}(-iw/2)^n n!\,U_n(z)V_n(z'), \tag{5.9}$$

$$-e^{iy}\sec\frac{\theta}{2}\sum_{n=-1}^{-\infty}(-iw/2)^n[\Gamma(n+1)U_n(z)]V_n(z') \tag{5.10}$$

which may be summed in much the same way as was (5.2) for S_1.

An expression for E which is useful in the study of the current density on the surface of the cylinder may be obtained from (5.5) by combining expression (5.8) for $\exp\,[-ix\sin\theta + iy\cos\theta] + S_1$ with expression (5.4)

[16] Expansions in Terms of Parabolic Cylinder Functions, Proc. Edinburgh Math. Soc., Ser. 2, **8**, pp. 50–65, 1948.

for $S_2(h)$:

$$E = \frac{e^{iy} \sec \frac{\theta}{2}}{2i} \int_{L_2} \left(\frac{iw}{2}\right)^n \frac{\Gamma(n+1)}{\sin \pi n} U_n(z) W_n(z') \left[\frac{V_n(z_0')}{W_n(z_0')} - \frac{V_n(z')}{W_n(z')}\right] dn. \tag{5.11}$$

When w exceeds unity (or when $w = 1$ and $\xi > \eta \geqq \eta_0 \geqq 0$) in (5.11), it may be verified with the help of Tables 12.2 and 12.4 that L_2 may be deformed into $L_3 + L_4$. When n is a negative integer the quantity within the brackets in (5.11) vanishes because of (4.8) and because $U_n(z) = 0$. The contribution of L_3 is zero since it encloses no poles. The contribution of L_4 is equal to the sum of the residues at the poles given by $W_n(z_0') = 0$. Hence, when $w > 1$,

$$E = -\pi e^{iy} \sec \frac{\theta}{2} \sum_{s=1}^{\infty} \left[\left(\frac{iw}{2}\right)^n \frac{\Gamma(n+1) U_n(z) W_n(z') V_n(z_0')}{\sin \pi n \partial W_n(z_0')/\partial n}\right]_{n=n_s} \tag{5.12}$$

where $n = n_s$ is the sth zero of $W_n(z_0')$. This series also converges when $w = 1$ and $\xi > \eta \geqq \eta_0 \geqq 0$ (which is roughly the shadow region). The preceding inequality does not necessarily specify the complete region of convergence.

Cherry[16] has also pointed out that the expression for a plane wave given by A. Erdélyi[17], namely (in our notation)

$$\exp[-ix \sin\theta + iy \cos\theta]$$

$$= -\frac{e^{iy} \sec \frac{\theta}{2}}{2i} \int_{L_2} \left(\frac{iw}{2}\right)^n \frac{\Gamma(n+1)}{\sin \pi n} [U_n(z) V_n(z') + U_n(-z) V_n(-z')]\, dn, \tag{5.13}$$

may be regarded as the sum of the negative of (5.8) and a similar expression with ξ and η replaced by $-\xi$ and $-\eta$. In informal discussions with the writer, Prof. Erdélyi has pointed out that the work leading to our expression (5.5) for the field may be considerably shortened by starting with some known integral for the impressed field, such as (5.13) or a related result. One way of doing this is to take

$$\exp[-ix \sin\theta + iy \cos\theta] + S_1,$$

[17] Proc. Roy. Soc Edinburgh, **61**, pp. 61–70, 1941.

as given by the left hand side of (5.8), to be the impressed field in the equation

$$E = \text{impressed field} + \text{reflected field}$$

From the form of (5.8) and the discussion of expression (4.6) (given between equations (4.14) and (4.15)) we are led to assume the reflected field to be an outgoing wave of the form

$$\frac{e^{iy}\sec\frac{\theta}{2}}{2i}\int_{L_2}\left(\frac{iw}{2}\right)^n\frac{\Gamma(n+1)}{\sin\pi n}\,U_n(z)W_n(z')a(n)\,dn$$

where $a(n)$ must be chosen so as to make E vanish on the surface of the cylinder. This gives $a(n) = V_n(z_0')/W_n(z_0')$ and leads directly to the expression (5.11) for E.

When the incident wave is vertically polarized, integrals for H may be obtained from the series of Section 4 in much the same manner as were the integrals for E. The analogues of the earlier results are

$$H = \exp(-ix\sin\theta + iy\cos\theta)$$

$$-\frac{e^{iy}\sec\frac{\theta}{2}}{2i}\int_{L_1}\left(\frac{iw}{2}\right)^n\frac{\Gamma(n+1)}{\sin\pi n}\,U_n(z)W_n(z')'U_n(z_0')\,dn/'W_n(z_0'), \tag{5.14}$$

$$H = \exp(-ix\sin\theta + iy\cos\theta) + S_1 + S_3(h), \tag{5.15}$$

$$S_3(h) = \frac{e^{iy}\sec\frac{\theta}{2}}{2i}\int_{L_2}\left(\frac{iw}{2}\right)^n\frac{\Gamma(n+1)}{\sin\pi n}\,U_n(z)W_n(z')\,'V_n(z_0')\,dn/'W_n(z_0'), \tag{5.16}$$

$$H = \frac{e^{iy}\sec\frac{\theta}{2}}{2i}\int_{L_2}\left(\frac{iw}{2}\right)^n\frac{\Gamma(n+1)}{\sin\pi n}\,U_n(z)W_n(z')\left[\frac{'V_n(z_0')}{'W_n(z_0')}-\frac{V_n(z')}{W_n(z')}\right]dn, \tag{5.17}$$

$$H = -\pi e^{iy}\sec(\theta/2)\sum_{s=1}^{\infty}\left[\frac{(iw/2)^n\Gamma(n+1)U_n(z)W_n(z')'V_n(z_0')}{\sin\pi n\partial'W_n(z_0')/\partial n}\right]_{n=n_s'} \tag{5.18}$$

In these formulas $'U_n(z)$, etc. are defined by (4.19); w, z, z' by (4.13), z_0' by (4.17). In (5.14) w is restricted to $0 < w < 1$. In (5.15) $S_3(h)$ is given by (5.16), and w may be anywhere in $0 < w < \infty$. In (5.17) w

may also lie anywhere in $0 < w < \infty$, but in (5.18) it is restricted to $1 < w < \infty$ except when $\xi > \eta$ (roughly the shadow region) in which case w may be unity. In (5.18) $n = n_s'$ is the sth zero of $'W_n(z_0')$. The zeros of $'W_n(z_0')$ interlace those of $W_n(z_0')$ shown in Fig. 5.1.

When $h = \eta_0^2/2 = 0$ the parabolic cylinder degenerates into a half-plane and our solutions reduce to Sommerfeld's expressions for waves diffracted by a half-plane. It may be shown that if

$$T_2 = \eta \cos\frac{\theta}{2} + \xi \sin\frac{\theta}{2} = (2r)^{1/2} \sin\left(\frac{\varphi + \theta}{2} + \frac{\pi}{4}\right), \tag{5.19}$$

we have

$$\begin{aligned} S_2(0) &= -(i/\pi)^{1/2} \exp\left[ix \sin\theta + iy \cos\theta\right] \int_{T_2}^{\infty} e^{-it^2}\, dt, \\ S_3(0) &= -S_2(0). \end{aligned} \tag{5.20}$$

When this expression for $S_2(0)$ is added to (5.6) we obtain Sommerfeld's result for the case of horizontal polarization.

One may verify that the series (5.12) leads to Sommerfeld's result as z_0' approaches zero. By neglecting $0(z^2)$ terms in (9.3) and setting $n_s = -2s + p_s$ for the sth zero of $W_n(z_0')$ we may obtain the following relations which are needed in the course of the verification

$$\begin{aligned} p_s &= -4iz_0'\Gamma(s + 1/2)/\pi\Gamma(s) + \cdots, \\ \partial W_n(z_0')/\partial n \text{ at } n_s &= \Gamma(s)/4 + \cdots, \\ V_n(z_0') \text{ at } n_s &= -2iz_0'\Gamma(s + 1/2)/\pi + \cdots, \\ \left[\frac{V_n(z_0')}{\sin \pi n \partial W_n(z_0')/\partial n}\right]_{n=n_s} &= 2/\pi + \cdots. \end{aligned} \tag{5.21}$$

6. SURFACE CURRENTS ON THE CYLINDER

As shown in Fig. 6.1, the surface current J on the perfectly conducting cylinder $\eta = \eta_0$ is parallel to the crest of the cylinder (and to the electric intensity E) when the incident wave is horizontally polarized. We have from Maxwell's equations in parabolic coordinates

$$\mathrm{J} = [-H_\xi]_{\eta=\eta_0} = (i\zeta_0)^{-1} (2r)^{-1/2} [\partial E/\partial\eta]_{\eta=\eta_0}. \tag{6.1}$$

Here H_ξ is the component of magnetic intensity in the ξ-direction. ζ_0 is the intrinsic impedance of free space given by $\zeta_0 = (\mu_0/\epsilon_0)^{1/2} = \omega\mu_0$ where the second part of the equation follows from $2\pi/\lambda = \omega(\mu_0\epsilon_0)^{1/2}$

and $\lambda = 2\pi$. The E_0 and the H_0 of the incident wave are related by $H_0 = E_0/\zeta_0 = 1/\zeta_0$ since $E_0 = 1$. In rational MKS units $\zeta_0 = 120\pi$ ohms.

The derivative in (6.1) may be obtained by differentiating expression (5.11) for E and then setting $\eta = \eta_0$. Use of the Wronskian (9.9) for $V_n(z_0')$, $W_n(z_0')$ then takes (6.1) into

$$\zeta_0 J = M_0 \int_{L_2} \frac{dn}{\sin \pi n} (iw)^n U_n(z)/W_n(z_0') \tag{6.2}$$

where $w = \tan(\theta/2)$, L_2 is shown in Fig. 5.1, z and z_0' are given by (4.13) and (4.17), and

$$M_0 = (i/8\pi r)^{1/2} e^{-ir} \sec\frac{\theta}{2}, \qquad r = (\xi^2 + \eta_0^2)/2. \tag{6.3}$$

In this Section r will be restricted to mean a radius vector drawn to the trace of the cylinder on the (x, y) plane of Fig. 6.1.

Closing L_2 on the right and on the left gives the two series

$$\zeta_0 J = 2iM_0 \sum_{n=0}^{\infty} (-iw)^n U_n(z)/W_n(z_0'), \qquad 0 < w < 1, \tag{6.4}$$

$$\zeta_0 J = -2i\pi M_0 \sum_{s=1}^{\infty} \left[\frac{(iw)^n U_n(z)}{\sin \pi n \, \partial W_n(z_0')/\partial n}\right]_{n=n_s}, \qquad 1 < w < \infty, \tag{6.5}$$

where n_s is the sth zero of $W_n(z_0')$ regarded as a function of n.

For the half-plane case $\eta_0 = 0$, and (9.4) gives

$$W_n(0) = -i^n/2\Gamma(1 + n/2).$$

In this case the series (6.4) may be expressed as an infinite integral

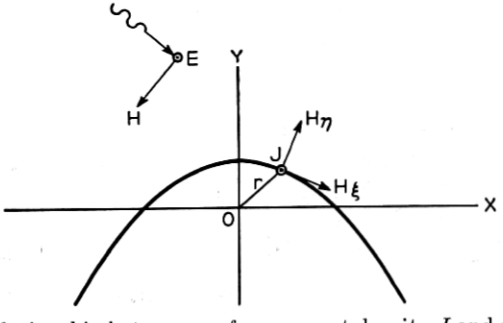

Fig. 6.1 — Relationship between surface current density J and electromagnetic field when incident wave is horizontally polarized. E and J are normal to the plane of the paper.

when the integral for $\Gamma(1 + n/2)$ is inserted and the sum (9.22) [i.e., the sum for the generating function of $U_n(z)$] used. Integrating part of the result gives

$$\zeta_0 J = (2/i\pi r)^{1/2} \cos\frac{\theta}{2}\left[e^{-ir} - 2i\xi \sin\frac{\theta}{2}\, e^{-ir\cos\theta}\int_{\xi \sin(\theta/2)}^{\infty} \exp(-it^2)\, dt\right]. \tag{6.6}$$

In (6.6) r is the distance along the half-plane as measured from the edge: $r = \xi^2/2 = |y|$. Positive values of ξ correspond to the shadowed side of the half-plane and negative values to the illuminated side. With this interpretation (6.6) agrees with the current density obtained from Sommerfeld's expression for the field.

Although (6.6) has been derived from (6.2) on the assumption that $0 < w < 1$ it also holds for $0 < w < \infty$ as may be shown by analytic continuation. Again, (6.6) may be obtained from (6.5).

Since the factor $r^{-1/2}$ comes from the multiplier M_0 in (6.4), it is possible that (6.6) may give one an idea of how the current density behaves near the crest of a thin cylinder which is almost, but not quite, a half-plane. Of course, r would have to be interpreted as shown in Fig. 6.1.

In order to study J when the radius of curvature of the cylinder is large compared to a wavelength we consider the case $\theta = \pi/2$, i.e. $w = 1$, in which the incident wave comes in horizontally. In this case most of the variation of the current density occurs near the crest of the cylinder where, as it turns out, ξ is of the order of $\eta_0^{1/3}$, η_0 being large.

At the beginning of the investigation rough calculations of the integrand in (6.2), based on the asymptotic expressions of Section 12, suggested that for small ξ and large η_0:

(a) Most of the contribution to the integral (6.2) comes from the neighborhood around point C shown on Fig. 6.2 where $m = n + 1 = z_0'^2/2 = -i\eta_0^2/2 = -ih$. Point C is a critical point associated with the asymptotic behavior of $W_n(z_0')$.

(b) The path of steepest descent for (6.2) roughly corresponds to the line ACD of Fig. 6.2, C being the high point of the path. Along this path $Im\,[f(t_0) - f(t_1)] = 0$ where $f(t) = -t^2 + 2zt - m\log t$, $m = n + 1$, is the function entering the definition (10.1) of the parabolic cylinder functions, and t_0, t_1 are the saddle points of $\exp[f(t)]$. This path in the n-plane separates the regions in which $W_n(z_0')$ has different asymptotic forms. It is the boundary of region III′ in Fig. 12.2 and has been studied in Sections 11 and 12.

Once (*b*) is verified the truth of (a) follows almost immediately since

the path of integration L_2 may be deformed into ACD without passing over any singularities of the integrand of (6.2).

In order to verify (b), we note that the entries in Table 12.3 for $W_n(z_0')$ show that along ACD

$$W_n(z_0') \sim A_0' \approx \exp [f(t_0)]. \tag{6.7}$$

Here the expressions for $W_n(z_0')$ along ACD are taken to be those corresponding to the regions I'b and II$'$ shown in Fig. 12.2. In making the last approximation in (6.7) we have neglected the slowly varying coefficient of the exponential function in the expression (12.9) for A_0'. Since $| \xi | \ll \eta_0$ we set $\xi = 0$ in $U_n(z)$. Then upon using the values (9.4) for $U_n(0)$, (6.7) for $W_n(z_0')$, and unity for w, we see that the integrand of (6.2) behaves like

$$\frac{i^n \exp [-f(t_0)]}{2 \sin (\pi n/2)\Gamma(1 + n/2)}. \tag{6.8}$$

On ACD we have, in dealing with $W_n(z_0')$, $-3\pi/2 < \arg m \leqq -\pi/2$. Hence, from $t_0 + t_1 = i^{-1/2}\eta_0$ and from $f(t_0) + f(t_1)$ as calculated from (12.9), we have

$$\begin{aligned} \exp [f(t_0)] &= \exp (\tfrac{1}{2}[f(t_0) + f(t_1)] + \tfrac{1}{2}[f(t_0) - f(t_1)]) \\ &\sim i^{n+1}(2\pi)^{-1/2}\Gamma(-n/2) \exp \left(-\frac{i\eta_0^2}{2} + \tfrac{1}{2}[f(t_0) - f(t_1)] \right) \end{aligned} \tag{6.9}$$

where we have used the second of expressions (12.10) to evaluate $\exp [m(1 - \log (m/2))/2]$. Substitution of (6.9) in (6.8) shows that the integrand behaves roughly like

$$\exp \left(\frac{i\eta_0^2}{2} - \tfrac{1}{2}[f(t_0) - f(t_1)] \right). \tag{6.10}$$

The truth of statement (b) then follows from the fact that the lines of steepest descent of (6.10) in the n-plane are given by $Im [f(t_0) - f(t_1)] = 0$. To see that C is the high point of ACD we use (12.9) to show that near C we have

$$f(t_0) - f(t_1) \approx (2/3z_0')(z_0'^2 - 2m)^{3/2}$$

where $m = n + 1$. Consequently, $f(t_0) - f(t_1)$ is real and positive on AC [where, near C, $\arg (z_0'^2 - 2m) = -\pi/6$] and on CD [where $\arg (z_0'^2 - 2m) = -3\pi/2$, m being in region II$'$ according to the convention used in (6.7)]. That C is the high point now follows from (6.10).

In accordance with statement (a), we must study the form assumed by the integrand of (6.2) when n is near point C.

When (1) n is near C, (2) η_0 is large, and (3) $|\xi| \ll \eta_0$ we have for the various terms in (6.2)

$$\begin{aligned} i^n/\sin \pi n &\sim 2i^{1-n} \\ \Gamma(1 + n/2)W_n(z_0') &\sim (\eta_0/4)^{1/3}(2\pi)^{1/2}i^{7/6} \exp[-i\eta_0^2/2]Ai(\alpha), \end{aligned} \tag{6.11}$$

$$2\Gamma(1 + n/2)U_n(z) \sim i^n \exp\left[\frac{i\xi^2}{2} + \xi\left(\frac{2m}{i}\right)^{1/2} - \frac{\xi^3}{6}\left(\frac{i}{2m}\right)^{1/2}\right] \tag{6.12}$$

where $Ai(\alpha)$ denotes the Airy integral defined by (13.12), $m = n + 1$, arg m is near $-\pi/2$, and

$$\begin{aligned} \alpha &= (2/i\eta_0^2)^{1/3}(m + i\eta_0^2/2), \\ d\alpha &= (2/i\eta_0^2)^{1/3}\, dn. \end{aligned} \tag{6.13}$$

Expression (6.11) comes from (13.21) and expression (6.12) comes from region Ia of Table 12.2 (strictly speaking, region Ib should be used but point C is so close to arg $m = -\pi/2$ that the simpler expression for Ia may be used). In obtaining (6.12) it is necessary to use the terms shown in the expansions (12.5) of t_0 and $\log t_1/t_0$. It may be shown that (6.12) also holds for negative values of ξ.

We now set $w = 1$ in (6.2) and change the variable of integration from n to α. Substituting for m in (6.12) its expression in terms of α, expanding in powers of α and neglecting higher order terms, converts the argument of the exponential function into

$$i\xi^2/2 - i\xi\eta_0 - i\gamma^3/3 + \alpha\gamma i^{1/3} \tag{6.14}$$

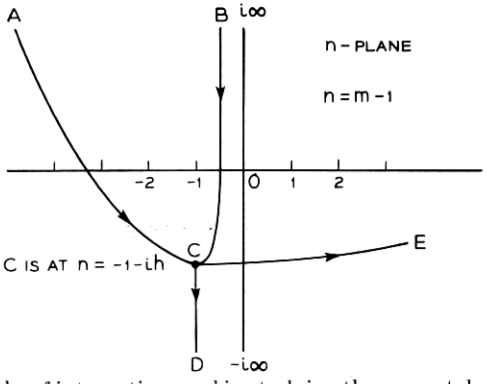

Fig. 6.2 — Paths of integration used in studying the current density and diffraction pattern when h is large. Path BCD is equivalent to path L_2 of Fig. 5.1. AC and CD are boundary lines which mark a change in the asymptotic behavior of $W_n(z_0')$. Far out towards A the line AC tends to become parallel to BC.

where

$$\gamma = \xi/(2\eta_0)^{1/3} = x/2h^{2/3} \tag{6.15}$$

When our approximations are set in (6.2) we obtain

$$\zeta_0 J \approx (i/2\eta_0)^{2/3}\pi^{-1} \exp\left[-i\xi\eta_0 - i\gamma^3/3\right] \int_{\infty \exp(-i2\pi/3)}^{\infty \exp(i2\pi/3)} \exp\left(i^{1/3}\gamma\alpha\right) d\alpha/Ai(\alpha). \tag{6.16}$$

Here we have taken the path of integration in the complex α-plane to be the transformed version of the path of steepest descent in the n-plane. That the path for (6.16) is still the one of steepest descent when $\gamma = 0$ and α is large follows from the asymptotic expansion (13.19) for $Ai(\alpha)$. It is interesting to note that near the crest of the cylinder $\xi\eta_0 + \gamma^3/3$ is approximately the distance along the cylinder as measured from the crest.

The expression (2.14) for $\zeta_0 J$ is obtained from (6.16) when $Ai(\alpha)$ is transformed by the relations (13.17).

When γ is positive the path of integration for α in (6.16) may be closed on the left to obtain a convergent series, the terms of which arise from the zeros of $Ai(\alpha)$. These zeros lie on the negative real α-axis starting with $\alpha = a_1 = -2.338 \cdots$, $a_2 = -4.087 \cdots$ The first fifty values of a_s and the corresponding values of the derivative $Ai'(a_s)$ have been tabulated*. Thus, when γ is positive,

$$\zeta_0 J \approx (2/i\eta_0^2)^{1/3} e^{-i\xi\eta_0 - i\gamma^3/3} \sum_{s=1}^{\infty} \frac{\exp\left(i^{1/3}\gamma a_s\right)}{Ai'(a_s)} \tag{6.17}$$

The leading term in this series leads to the approximation (2.19) when we use $Ai'(a_1) = .701 \cdots$ Expression (6.17) gives the form assumed by '6.5) when $w = 1$ and $h \to \infty$. For large values of s*

$$\begin{aligned} a_s &\sim -[3\pi(4s - 1)/8]^{2/3} \\ Ai'(a_s) &\sim -(-)^s \pi^{-1/2}(-a_s)^{1/4} \end{aligned} \tag{6.18}$$

When γ is large and negative an asymptotic expansion for $\zeta_0 J$ may be obtained by setting the asymptotic expansion (13.19) in (6.16) and using the method of steepest descent. It is found that the saddle point is at $\alpha = \alpha_0 = \gamma^2 i^{2/3}$ and the slope of the path of the steepest decent through it is given by $\arg(d\alpha) = -5\pi/12$. This leads to the expression for $\zeta_0 J$ which appears in (2.17).

When the incident wave is vertically polarized the magnetic intensity

* Reference 11, page 424.

H is parallel to the crest of the parabolic cylinder. Since the cylinder is a perfect conductor, the current density J_v on the surface $\eta = \eta_0$ is equal in magnitude to H and its direction is that of increasing ξ. Thus setting $z' = z_0'$ in expression (5.17) for H and using the Wronskian (9.9) gives

$$\begin{aligned} J_v &= N \int_{L_2} \frac{dn}{\sin \pi n} (iw)^n U_n(z) / {}'W_n(z_0'), \\ N &= e^{-ir} \left(\sec \frac{\theta}{2}\right) \Big/ 2\pi^{1/2}, \qquad r = (\eta_0^2 + \xi^2)/2, \end{aligned} \tag{6.19}$$

where ${}'W_n(z_0')$ is defined by (4.19).

Closing L_2 on the right and left leads to the analogues of (6.4) and (6.5):

$$J_v = 2iN \sum_{n=0}^{\infty} (-iw)^n U_n(z) / {}'W(z_0'). \qquad 0 < w < 1, \tag{6.20}$$

$$J_v = -2i\pi N \sum_{s=1}^{\infty} \left[\frac{(iw)^n U_n(z)}{\sin \pi n \partial' W_n(z_0')/\partial n} \right]_{n=n_s'}, \qquad 1 < w < \infty, \tag{6.21}$$

where n_s' is the sth zero of ${}'W_n(z_0')$. The zeros of both ${}'W_n(z_0')$ and $W_n(z_0')$ are enclosed by the path of integration L_4 shown in Fig. 5.1.

The current density on a half-plane is obtained by setting $z_0' = 0$ in (6.20), using ${}'W_n(0) = W_n'(0) = -i^{n-1}/\Gamma(n/2 + \frac{1}{2})$, from (9.4), and the generating function series (9.22) for $U_n(z)$:

$$J_v = 2(i/\pi)^{1/2} e^{-ir \cos \theta} \int_{\xi \sin (\theta/2)}^{\infty} e^{-it^2}\, dt \tag{6.22}$$

where r has the same significance as in (6.6). This agrees with the expression obtained from Sommerfeld's result for the half-plane.

When $w = 1$ and h is large, the path of steepest descent for (6.19) becomes the same as that for the case of horizontal polarization, namely ACD of Fig. 6.2. This follows from the fact that, as may be seen from (12.2), the controlling exponential functions for ${}'W_n(z_0')$ and $W_n(z_0')$ are the same. The analogue of (6.16) is obtained by using the approximation (13.24) for ${}'W_n(z_0')$:

$$J_v \approx (1/2\pi i) \exp [-i\xi\eta_0 - i\gamma^3/3] \int_{\infty \exp (i2\pi/3)}^{\infty \exp (-i2\pi/3)} \exp (i^{1/3}\gamma\alpha)\, d\alpha / Ai'(\alpha) \tag{6.23}$$

where $Ai'(\alpha)$ denotes $dAi(\alpha)/d\alpha$ and γ is given by (6.15).

For positive values of γ (6.23) and $d^2Ai(\alpha)/d^2\alpha = \alpha Ai(\alpha)$ lead to

$$J_v \approx -\exp\left[-i\xi\eta_0 - i\gamma^3/3\right] \sum_{s=1}^{\infty} \frac{\exp\left(i^{1/3}\gamma a_s'\right)}{a_s' Ai(a_s')} \tag{6.24}$$

where $a_1' = -1.019$, $a_2' = -3.248$, $\cdots$, etc. are the zeros of $Ai'(\alpha)$.* When we use $Ai(a_1') = 0.5357$ the leading term in (6.24) gives (2.19). For large values of s*

$$a_s' \sim -[3\pi(4s - 3)/8]^{2/3},$$

$$Ai(a_s') \sim -(-)^s(-a_s')^{-1/4}\pi^{-1/2}.$$

The expression (2.17) for J_v when γ is large and positive may be obtained by applying the method of steepest descent to (6.23). The asymptotic expression for $Ai'(\alpha)$ is obtained by differentiating (13.19).

When the cylinder is a good conductor, but not perfect, the expression for H analogous to (4.25) leads to an integral for J_v, obtained from (6.23) by substituting $Ai'(\alpha) + \ell Ai(\alpha)$ for $Ai'(\alpha)$, which is equivalent to one given by Fock.† Here $\ell = -(ih)^{1/3}\zeta/\zeta_0$ is assumed to be small compared to unity and ζ/ζ_0 is the ratio of the intrinsic impedance of the cylinder material to that of free space. Horizontal incidence, $\theta = \pi/2$, is assumed.

The analogue of (4.25) for H has the same form as (4.21) except that now $'U_n(z_0')$ is replaced by $'U_n(z_0') + \tau U_n(z_0')$, etc. The development leading from (4.21) through (5.15), (5.17), (6.19) to (6.23) may be carried out just as before. The work is also related to that given at the end of Section 7 where the effect of finite conductivity on the diffracted wave is briefly discussed.

A series corresponding to (6.24) may be derived from the integral. The exponential terms in this series are approximately $\exp\left[i^{1/3}\gamma(a_s' - \ell/a_s')\right]$, and are similar to those in (7.63). Since $\zeta_0 = (\mu_0/\epsilon_0)^{1/2}$ is real and $\zeta \approx (i\omega\mu/g)^{1/2}$ when $g \gg \omega\epsilon$ (the notation is explained in connection with (4.24); the g denoting conductivity should not be confused with the g defined by (7.20)) the quantity $-i^{1/3}\ell/a_s'$ has a positive part. Thus, the attenuation of J_v in the shadow is decreased slightly when the conductivity g of the cylinder is reduced from infinity to a large finite value.

7. FIELD AT A GREAT DISTANCE BEHIND THE PARABOLIC CYLINDER

The field at any point, for the case of horizontal polarization, is given by expression (5.5) with $S_2(h)$ given by (5.4). Since $S_2(h)$ is the

* Reference 11, page 424.
† Reference 5, page 418.

only troublesome term in (5.5) most of this section will be devoted to its study. Far behind the cylinder ξ and η are large and positive, and the corresponding terms in the integrand of (5.4) are

$$\Gamma(n+1)U_n(z)W_n(z') = (2i\xi/\eta)^n i^{3/2} e^{-i\eta^2}(1+f)/2\eta\pi^{1/2}, \tag{7.1}$$

where the asymptotic expressions (9.16) and (9.17) give

$$1 + f = 1 + \frac{in(n-1)}{4\xi^2} + \frac{i(n+1)(n+2)}{4\eta^2} + 0(n^4/r^2). \tag{7.2}$$

In writing the "order of" term it is assumed that ξ and η are both $0(r^{1/2})$ with $r \gg n^2$.

When (7.1) is put in (5.4) we obtain

$$S_2(h) = M_1 \int_{L_2} \frac{\beta^n i^{2n} V_n(z_0')(1+f)}{\sin \pi n W_n(z_0')}\, dn \tag{7.3}$$

where, from the expressions (4.1) for ξ and η,

$$M_1 = [(i/\pi)^{1/2} e^{-ir} \sec(\theta/2)]/4\eta, \tag{7.4}$$

$$\beta = \xi w/\eta = \xi[\tan(\theta/2)]/\eta = \cot(\varphi/2 + \pi/4)\tan(\theta/2).$$

Although it is not proved here, there is good reason to believe that (7.3) can be written as

$$S_2(h) = M_1 \int_{L_2} \frac{i^{2n}\beta^n V_n(z_0')}{\sin \pi n W_n(z_0')}\, dn + 0(h^3/r^{3/2}) \tag{7.5}$$

when r becomes large and we restrict ourselves to the region $|\varphi| < \pi/2$ in order to get $0(\xi^2) = 0(\eta^2) = 0(r)$. The first term contains r only through the factor M_1 and is of order $r^{-1/2}$. The "order of" term assumes h to be moderately large compared to unity but $h^2 \ll r$. When $h < 1$ the h^3 is to be replaced by unity.

The general idea leading to (7.5) is that (7.2) may be used over the portion of L_2 where the integrand is large and important. On the portion where (7.2) differs appreciably from unity the integrand is negligibly small. The important portion of L_2 runs from $n = \frac{1}{2}$ to $n = -\frac{1}{2} - ih$ (approximately). In particular the variation of $i^{2n}V_n(z_0')/\sin \pi n\, W_n(z_0')$ along L_2 may be summarized as follows: from $-\frac{1}{2}$ to $+i\infty$ it decreases exponentially as i^{2n}, from $-\frac{1}{2}$ to $-ih$ it is equal to $-2i$ plus an oscillating function of order unity, and from $-ih$ to $-i\infty$ it decreases slowly at first and then more rapidly until it goes down like i^{-2n} (steepest descent behavior). This may be shown with the help of Fig. 12.2, the entries for regions $I'a$ and II' in Table 12.3, and the following items [see (12.9) and Figs. 10.1 and 10.2 for $z = i^{-1/2}\eta_0$ with $-3\pi/2 \leqq \arg(i\eta_0^2$

$- 2m) < \pi/2)]$:

(a) $Re\ [f(t_1) - f(t_0)]$ is almost zero between $-\frac{1}{2}$ and $-ih$.

(b) $Im\ [f(t_1) - f(t_0)]$ is almost zero between $-ih$ and $-i\infty$.

(c) t_1/t_0 runs from zero to unity as n goes from -1 to $-1-ih$.

Items (a) and (b) are consistent with $f(t_0) - f(t_1) \approx (\frac{2}{3}z_0')(z_0'^2 - 2m)^{3/2}$ which holds when n is near $-ih$ and which was mentioned in connection with (6.10).

This concludes our discussion of the reasons for believing that (7.5) is true for general values of h. Now we shall check it for the special case $h = 0$.

When we set $h = 0$ (i.e. $z_0' = 0$) in (7.3), use (9.4) and close L_2 by an infinite semicircle, we obtain

$$S_2(0) \sim \frac{i^{3/2}e^{-ir}}{\pi^{1/2}2T_2}\left[1 - \frac{1}{2iT_2^2} + \cdots\right]. \tag{7.6}$$

This agrees with the first two terms in the asymptotic expansion of the Fresnel integral expression (5.20) for $S_2(0)$. In expanding (5.20) we need the first of the two asymptotic expansions (both of which hold for $T \gg 1$)

$$\int_T^\infty e^{-it^2}\,dt \sim -\frac{i\exp(-iT^2)}{2T}\left[1 - \frac{1}{2iT^2} + \cdots\right], \tag{7.7}$$

$$\int_{-\infty}^T e^{-it^2}\,dt \sim (\pi/i)^{1/2} + \frac{i\exp(-iT^2)}{2T}\left[1 - \frac{1}{2iT^2} + \cdots\right], \tag{7.8}$$

and also the first of the relations

$$\begin{aligned} x\sin\theta + y\cos\theta - T_2^2 &= -r, \\ T_2 &= \eta(1+\beta)\cos(\theta/2). \end{aligned} \tag{7.9}$$

In much of the following work we shall assume ξ and η to be so great that we can neglect the terms denoted by $0(h^3/r^{3/2})$ in (7.5). We shall use the asymptotic sign $\sim$ to acknowledge this omission.

From (7.4), β is equal to unity when $\varphi = \theta - \pi/2$. When r is very large this value of φ marks the shadow boundary. In the shadow $\beta > 1$ and in the illuminated region $\beta < 1$.

Closing L_2 on the right and on the left converts (7.5) into

$$S_2(h) \sim 2iM_1\sum_{n=0}^{\infty}\beta^n V_n(z_0')/W_n(z_0'). \tag{7.10}$$

$$S_2(h) \sim 2iM_1\left\{(\beta - 1)^{-1} - \pi \sum_{s=1}^{\infty}\left[\frac{i^{2n}\beta^n V_n(z_0')}{\sin \pi n\, \partial W_n(z_0')/\partial n}\right]_{n=n_s}\right\} \tag{7.11}$$

It can be shown that (7.10) converges if $\beta < 1$ (see (4.18)) and that (7.11) converges if $\beta > 1$ (see (12.13)). The term $1/(\beta - 1)$ in (7.11) comes from the poles of csc πn inside the path L_3 shown in Fig. 5.1

From (7.7) and

$$\begin{aligned} -x \sin\theta + y\cos\theta - T_1^2 &= r, \\ T_1 &= \eta(1+\beta)\cos(\theta/2) \end{aligned} \tag{7.12}$$

it may be shown that when $\beta > 1$, so that T_1 is negative, (5.6) has the asymptotic expression

$$\exp[-ix\sin\theta + iy\cos\theta] + S_1 \sim 2iM_1/(1-\beta). \tag{7.13}$$

When this is added to (7.11) the $1/(1-\beta)$ terms cancel leaving a series for E valid in the shadow where $\beta > 1$:

$$E \sim -2iM_1\pi \sum_{s=1}^{\infty}\left[\frac{i^{2n}\beta^n V_n(z_0')}{\sin \pi n\, \partial W_n(z_0')/\partial n}\right]_{n=n_s} \tag{7.14}$$

This series may also be obtained from the more general series (5.12) for E by using (7.1) and neglecting f.

We now take up the problem of finding the paths of steepest descent for the integral in (7.5) when β is near unity and h is large. When $\beta = 1$ and h is large, the integrand in (7.5) may be expressed in terms of $\exp[f(t_1) - f(t_0)]$ by using Table 12.3. In Section 6 it has been pointed out that the path of steepest descent for $\exp[f(t_1) - f(t_0)]$ is the path ACD of Fig. 6.2, with C being the high point. This suggests that the path ACD should be used to deal with the terms in (7.5) leading to $\exp[f(t_1) - f(t_0)]$. These terms are $U_n(z_0')/W_n(z_0')$ (introduced by the use of (4.8)) for the portion of L_2 between B and C, and $V_n(z_0')/W_n(z_0')$ for the portion between C and D. As a further argument supporting the use of the path AC we note that when n is on AC, i.e., on the edge of region $I'b$, Table 12.3 gives

$$U_n(z_0')/W_n(z_0') \sim -i(1 - i^{-4n})(t_1/t_0)^{1/2}\exp[f(t_1) - f(t_0)]. \tag{7.15}$$

Hence the variation of i^{2n} csc πn in the integrand of (7.5) is just cancelled by that of $(1 - i^{-4n})$ in (7.15). Consequently $i^{2n}U_n(z_0')/[\sin \pi n\, W_n(z_0')]$ varies as $\exp[f(t_1) - f(t_0)]$ along AC (the variation of t_1/t_0 is relatively small).

These considerations lead us to write (5.4) as

$$
\begin{aligned}
S_2(h) &= S_{21} + S_{22} + S_{23} \\
S_{21} &= -\int_B^C F\, dn, \\
S_{22} &= -\int_A^C F U_n(z_0')\, dn/W_n(z_0'), \\
S_{23} &= \int_C^D F V_n(z_0')\, dn/W_n(z_0'), \\
F &= e^{i\psi} \sec(\theta/2)(iw/2)^n \Gamma(n+1) U_n(z) W_n(z')/2i \sin \pi n.
\end{aligned} \tag{7.16}
$$

When instead of (5.4) the expression (7.5) for $S_2(h)$ is used we obtain

$$
\begin{aligned}
S_{21} &\sim -M_1 \int_B^C i^{2n}\beta^n\, dn/\sin \pi n, \\
S_{22} &\sim -M_1 \int_A^C i^{2n}\beta^n U_n(z_0')\, dn/[\sin \pi n W_n(z_0')], \\
S_{23} &\sim M_1 \int_C^D i^{2n}\beta^n V_n(z_0')\, dn/[\sin \pi n W_n(z_0')].
\end{aligned} \tag{7.17}
$$

In S_{22} it is permissible to swing AC from its original position BC because the zeros of $U_n(z_0')$ cancel those of $\sin \pi n$. When $\beta = 1$, AC and CD are the paths of steepest descent for S_{22} and S_{23} in (7.17) because $Im\,[f(t_1) - f(t_0)] = 0$ on ACD.

The asymptotic expression (7.17) for S_{21} may be evaluated by temporarily assuming β to be a complex number with $|\beta| < 1$ and $|\arg \beta| < \pi/2$. The integral along BC is the integral along BCE minus the integral along CE (see Fig. 6.2). Deforming BCE into L_1 of Fig. 5.1 shows that its contribution to S_{21} is $-2iM_1/(1-\beta)$. An infinite series for the integral along CE may be obtained by expanding $i^{2n}/\sin \pi n$ in powers of $\exp(-i2\pi n)$ and integrating termwise from $n = n_0 = -1-ih$ to $n = \infty - ih$, i.e., from C to E. In this way we obtain

$$
S_{21} \sim -2iM_1\left[\frac{1}{1-\beta} + \sum_{t=0}^{\infty} \frac{\exp(n_0 \log \beta - 2\pi t h)}{\log \beta - 2\pi i t}\right]. \tag{7.18}
$$

Despite the appearance of the right hand side, it is analytic around $\beta = 1$ and analytic continuation may be used to show that (7.18) holds for $0 < \beta < \infty$.

When h is large only the first term in the series is important and we have

$$
\begin{aligned}
S_{21} &\sim 2iM_1[(\beta-1)^{-1} - \beta^{-1-ih}/\log \beta] \\
&= 2iM_1(\beta-1)^{-1} + iM_2 g^{-1}
\end{aligned} \tag{7.19}
$$

where we have introduced two quantities which will be used later:

$$M_2 = 2M_1 h^{1/3}\beta^{-1-ih} = \left(\frac{i}{\pi}\right)^{1/2} \frac{h^{1/3}\exp[-ir + igh^{2/3}]}{2\xi \sin(\theta/2)}, \qquad (7.20)$$

$$g = -h^{1/3}\log\beta.$$

When $\beta = 1$

$$S_{21} \sim 2iM_1(ih' + \tfrac{1}{2}). \qquad (7.21)$$

When h is large most of the contributions to the integrals (7.17) for S_{22} and S_{23} come from around $n = n_0 = -1-ih$, and we may use the approximations

$$U_n(z_0')/W_n(z_0') \sim i^{-4/3}Ai(\alpha i^{-4/3})/Ai(\alpha), \qquad (7.22)$$

$$V_n(z_0')/W_n(z_0') \sim i^{4/3}Ai(\alpha i^{4/3})/Ai(\alpha), \qquad (7.23)$$

$$\alpha = (ih)^{-1/3}(n + 1 + ih), \qquad n - n_0 = \alpha(ih)^{1/3},$$

which come from (13.21). Setting these in the integrals (7.17) and using the fact that $i^{2n}/\sin \pi n$ is nearly $2i$ around n_0 leads to

$$S_{22} \sim -M_2 \int_{\infty \exp(i2\pi/3)}^{0} \exp(-i^{1/3}\alpha g)Ai(\alpha i^{-4/3})\, d\alpha/Ai(\alpha), \qquad (7.24)$$

$$S_{23} \sim -i^{2/3}M_2 \int_{0}^{\infty \exp(-i2\pi/3)} \exp(-i^{1/3}\alpha g)Ai(\alpha i^{4/3})\, d\alpha/Ai(\alpha), \qquad (7.25)$$

$$S_{22} + S_{23} \sim iM_2\Psi(g), \qquad (7.26)$$

where

$$\Psi(g) = i\int_{\infty i^{4/3}}^{0} \exp(-i^{1/3}\alpha g)Ai(\alpha i^{-4/3})\, d\alpha/Ai(\alpha) + i^{5/3}\int_{0}^{\infty i^{-4/3}} \exp(-i^{1/3}\alpha g)Ai(\alpha i^{4/3})\, d\alpha/Ai(\alpha). \qquad (7.27)$$

The expression (2.11) for $\Psi(g)$ is obtained from (7.27) by changing the variables of integration and using the transformations (13.17) for $Ai(\alpha)$.

Thus, when h is large and β near unity, (7.19) and (7.26) give

$$S_2(h) \sim 2iM_1(\beta - 1)^{-1} + iM_2[g^{-1} + \Psi(g)]. \qquad (7.28)$$

In the shadow, where $\beta > 1$ and g is negative, (7.13) and (7.28) give

$$E = \exp[-ix\sin\theta + iy\cos\theta] + S_1 + S_2(h) \sim iM_2[g^{-1} + \Psi(g)]. \qquad (7.29)$$

This and the series (7.14) for E suggest that $\Psi(g) + 1/g$ may be ex-

pressed as a series in which the parabolic cylinder functions in (7.14) are replaced by Airy integrals. One way of obtaining this series from (7.14) is to use the Airy integral approximations (13.21). The zeros $n_1, n_2, \cdots$ of $W_n(z_0')$ go into the zeros $a_1, a_2, \cdots$ of $Ai(\alpha)$ by virtue of the relation $n - n_0 = \alpha(ih)^{1/3}$ and we have

$$E \sim i^{-2/3} M_2 \sum_{s=1}^{\infty} \frac{\exp\left[-a_s g i^{1/3}\right]}{[Ai'(a_s)]^2}, \tag{7.30}$$

$$\Psi(g) + 1/g = -i^{1/3} \sum_{s=1}^{\infty} \frac{\exp\left[-a_s g i^{1/3}\right]}{[Ai'(a_s)]^2}, \tag{7.31}$$

where $g < 0$. Here, as in (6.17), $a_1 = -2.338 \cdots$ and $Ai'(a_1) = .701 \cdots$ In obtaining these relations we have used $i^{2n}/\sin \pi n \approx 2i$, and

$$Ai(a_s i^{4/3}) = -i^{5/3} Bi(a_s)/2 = i^{5/3}/2\pi Ai'(a_s), \tag{7.32}$$

where the first equation follows from (13.17) and the second from the Wronskian

$$Ai(\alpha)Bi'(\alpha) - Ai'(\alpha)Bi(\alpha) = 1/\pi. \tag{7.33}$$

The equal sign in (7.31) holds even though the steps leading to it indicate that $\sim$ should be used. This may be seen from an alternative derivation of (7.31) in which $Ai(\alpha i^{-4/3})$ in the first integral of (7.27) is replaced by the right hand side of*

$$Ai(\alpha i^{-4/3}) = -i^{4/3} Ai(\alpha) - i^{-4/3} Ai(\alpha i^{4/3}). \tag{7.34}$$

In the first portion the $Ai(\alpha)$'s cancel and the resulting integral contributes $-1/g$ to (7.27) (g must be negative for convergence). The second portion combines with the second integral in (7.27) to give a contour integral which leads to the series in (7.31) when the path of integration in the α-plane is closed on the left. The closure may be justified by the asymptotic expressions (13.19) and (13.20) for $Ai(\alpha)$ (again g must be negative).

Since the integrals in (7.27), and their equivalents in (2.11), converge uniformly for all finite values of g, $\Psi(g)$ is an integral function of g. When g is negative $\Psi(g)$ may be computed from the series (7.31). When g is positive I have not been able to find a practicable method of obtaining $\Psi(g)$ other than the numerical integration of (2.11). The results are shown in Table 2.1. Since $\Psi(g)$ is an integral function its Taylor's series about, say, $g = -.5$ converges for all values of g. The coefficients in this series may be computed from (7.31). However, I was unable to

* Reference 11, page 424.

obtain useful results by this method because the computation of the coefficients becomes more and more difficult.

When g is large and positive it may be shown that

$$\Psi(g) \sim -g^{-1} + (i\pi g)^{1/2} \exp(-ig^3/12). \tag{7.35}$$

The procedure used to establish (7.35) is much the same as that used to establish the more general result

$$S_{22} + S_{23} \sim -iM_2 g^{-1} - \left[\frac{h(1-\beta)}{r(1+\beta)}\right]^{1/2} \frac{\exp[-ir + 2ih(1-\beta)/(1+\beta)]}{\sin \frac{1}{2}(\varphi + \theta + \pi/2)}, \tag{7.36}$$

$$\frac{1-\beta}{1+\beta} = \frac{\sin \frac{1}{2}(\varphi - \theta + \pi/2)}{\sin \frac{1}{2}(\varphi + \theta + \pi/2)},$$

which holds when $h^{1/3}(1-\beta)$ is large and positive.

When φ is near $-\pi/2 + \theta$, (7.36) gives the same result as (7.26) plus (7.35). For φ near $-\pi/2 + \theta$,

$$g \approx h^{1/3}(1-\beta) \approx [2h^{1/3}/\sin\theta] \sin\frac{1}{2}\left(\varphi - \theta + \frac{\pi}{2}\right), \tag{7.37}$$

which shows that g is proportional to the cube root of the radius of curvature $2h/\sin^3\theta$ at the point where the incident ray is tangent to the cylinder.

When $\beta < 1$, (7.36) may be obtained from

$$S_{22} + S_{23} \sim -M_1 \int_C^E \frac{i^{2n}\beta^n}{\sin \pi n}\, dn - M_1 \int_{ACE} \frac{i^{2n}\beta^n U_n(z_0')}{\sin \pi n W_n(z_0')}\, dn. \tag{7.38}$$

The second integral in (7.38) represents, asymptotically, the wave reflected by the cylinder. This interpretation is suggested by the fact that, when the expression (7.1) for $\Gamma(n+1)U_n(z)W_n(z')$ is substituted in expression (5.1) for E, the resulting integral may be written as the second integral in (7.38).

The first term in (7.36) is obtained when $i^{2n}/\sin \pi n$ in the first integral of (7.38) is approximated by $2i$ and the result integrated. When the integrand of the second integral is examined with the help of Table 12.3, it is found to have a saddle point* at $m = m_1$ on the imaginary axis between $m = 0$ and $m = -ih$. Near m_1 the integrand is approximately

$$2\beta^{-1}(t_1/t_0)^{1/2} \exp[F(m)] \tag{7.39}$$

* It is interesting to note that a saddle point also appears in the study of reflection from a sphere. See page 86 of reference.[7]

where $F(m) = f(t_1) - f(t_0) + m \log \beta$ and $F'(m) = \log (t_0\beta/t_1)$. Here t_0 and t_1 are functions of m defined by (12.9). At m_1 we have $t_0\beta = t_1$ and this leads to

$$m_1 = -4ih\beta/(1+\beta)^2, \qquad F(m_1) = 2ih(1-\beta)/(1+\beta),$$
$$F''(m_1) = -(1+\beta)/m_1(1-\beta). \quad (7.40)$$

When we attempt to deform the path of integration ACE of the second integral in (7.38) into a path of steepest descent, we encounter no trouble near m_1 in regions $I'a$ and $I'b$. The path passes through m_1 with arg $(dm) = -\pi/4$. Soon after passing through m_1 the path of steepest descent strikes the boundary between $I'a$ and II' at a point we shall call G. At G the imaginary part of m is $2h(1-\beta)/(1+\beta) \log \beta$. The asymptotic approximation to the integrand changes its form at this point. The choice of the path from G out to ∞ is not important since it contributes little to the value of the integral. However, if we insist on following paths of steepest descent, it turns out that we must split the path of integration at G.

When $h^{1/3}(1-\beta) \gg 1$, it may be shown that the value of second integral in (7.38) is nearly equal to

$$-2M_1[-2\pi/\beta F''(m_1)]^{1/2} \exp [F(m_1)]$$

and this gives the second term in (7.36).

So far, in this section, we have been dealing with the case of horizontal polarization. Since the work for the case of vertical polarization (in which H plays the role of the wave function) follows much the same lines, we shall merely list the formulas corresponding to those already obtained for horizontal polarization. M_1, β and M_2, g are still given by (7.4) and (7.20), respectively.

$$S_3(h) = M_1 \int_{L_2} \frac{i^{2n}\beta^n\, 'V_n(z_0')}{\sin \pi n' W_n(z_0')}\, dn + 0(h^3/r^{3/2}), \quad (7.41)$$

$$S_3(0) = -S_2(0), \quad (7.42)$$

$$S_3(h) \sim 2iM_1 \sum_{n=0}^{\infty} \beta^n\, 'V_n(z_0')/'W_n(z_0'), \qquad \beta < 1 \quad (7.43)$$

$$S_3(h) \sim 2iM_1 \left\{ (\beta - 1)^{-1} - \pi \sum_{s=1}^{\infty} \left[\frac{i^{2n}\beta^n\, 'V_n(z_0')}{\sin \pi n\, \partial' W_n(z_0')/\partial n} \right]_{n=n_s'} \right\}, \quad (7.44)$$

$$\beta > 1 \text{ (shadow region)},$$

$$n_s' = s\text{th zero of } 'W_n(z_0'),$$

$$H \sim -2iM_1\pi \sum_{s=1}^{\infty} \left[\frac{i^{2n}\beta^n \, {}'V_n(z_0')}{\sin \pi n \, \partial' W_n(z_0')/\partial n} \right]_{n=n_s'}, \qquad \beta > 1 \tag{7.45}$$

$$\begin{aligned} S_3(h) &= S_{31} + S_{32} + S_{33}, \\ S_{31} &= S_{21} \text{ defined by (7.16)}, \\ S_{32} &= S_{22} \text{ with } {}'U_n(z_0')/{}'W_n(z_0') \text{ in place of } U_n(z_0')/W_n(z_0'), \\ S_{33} &= S_{23} \text{ with } {}'V_n(z_0')/{}'W_n(z_0') \text{ in place of } V_n(z_0')/W_n(z_0'), \end{aligned} \tag{7.46}$$

$$S_{32} \sim i^{2/3}M_2 \int_{\infty \exp(i2\pi/3)}^{0} \exp(-i^{1/3}\alpha g) Ai'(\alpha i^{-4/3}) \, d\alpha / Ai'(\alpha), \tag{7.47}$$

$$S_{33} \sim M_2 \int_{0}^{\infty \exp(-i2\pi/3)} \exp(-i^{1/3}\alpha g) Ai'(\alpha i^{4/3}) \, d\alpha / Ai'(\alpha), \tag{7.48}$$

$$S_{32} + S_{33} \sim iM_2\Psi_v(g), \tag{7.49}$$

$$\begin{aligned} \Psi_v(g) = i^{-1/3} &\int_{\infty \exp(i2\pi/3)}^{0} \exp(-i^{1/3}\alpha g) Ai'(\alpha i^{-4/3}) \, d\alpha / Ai'(\alpha) \\ &- i \int_{0}^{\infty \exp(-i2\pi/3)} \exp(-i^{1/3}\alpha g) Ai'(\alpha i^{4/3}) \, d\alpha / Ai'(\alpha), \end{aligned} \tag{7.50}$$

$$H \sim iM_2[g^{-1} + \Psi_v(g)], \qquad g < 0 \tag{7.51}$$

$$H \sim i^{-2/3}M_2 \sum_{s=1}^{\infty} \frac{\exp(-a_s' g i^{1/3})}{(-a_s')[Ai(a_s')]^2}, \qquad g < 0 \tag{7.52}$$

$$\Psi_v(g) + g^{-1} = -i^{1/3} \sum_{s=1}^{\infty} \frac{\exp(-a_s' g i^{1/3})}{(-a_s')[Ai(a_s')]^2}, \qquad g < 0 \tag{7.53}$$

$$\begin{aligned} &a_s' = \text{sth zero of } Ai'(\alpha), \qquad a_1' = -1.019, \qquad Ai(a_1') = 0.5357, \\ &Ai'(a_s' i^{4/3}) = -i^{1/3}Bi'(a_s')/2 = -i^{1/3}/[2\pi Ai(a_s')], \\ &Ai''(\alpha) = \alpha Ai(\alpha). \end{aligned} \tag{7.54}$$

When g is large and positive,

$$\Psi_v(g) \sim -g^{-1} - (i\pi g)^{1/2} \exp(-ig^3/12), \tag{7.55}$$

$$\begin{aligned} S_{32} + S_{33} \sim &-iM_2 g^{-1} \\ &+ \left[\frac{h(1-\beta)}{r(1+\beta)} \right]^{1/2} \frac{\exp[-ir + 2ih(1-\beta)/(1+\beta)]}{\sin \frac{1}{2}(\varphi + \theta + \pi/2)}. \end{aligned} \tag{7.56}$$

The change in sign of the second term on the right in going from (7.36) to (7.56) comes from (12.2) and the analogous expression for ${}'W_n(z_0')$

(only t_1 contributes to $U_n(z_0')$ and only t_0 to $W_n(z_0')$ at the saddle point m_1 of the second integral in (7.38)).

So far in this section the parabolic cylinder has been assumed to possess infinite conductivity. When the cylinder has a finite (but very large) conductivity, it may be shown that the field far out in the shadow is approximately

$$E \sim M_1 \int_{L_4} \frac{i^{2n}\beta^n}{\sin \pi n} \frac{V_n(z_0') + \sigma^{-1} {}'V_n(z_0')}{W_n(z_0') + \sigma^{-1} {}'W_n(z_0')}\, dn. \tag{7.57}$$

Equation (7.57) is suggested by (7.14) and (4.25). The analogue of (7.57) for vertical polarization may be obtained by replacing E, σ in (7.57) by H, τ so that ${}'V_n(z_0') + \tau V_n(z_0')$ appears in place of $V_n(z_0') + \sigma^{-1} {}'V(z_0')$, and so on.

When the parabolic cylinder functions are replaced by Airy integrals according to (13.21) and (13.24), equation (7.57) may be written as

$$E \sim i^{8/3} M_2 \int_{L_4'} \frac{[\exp(-\alpha g i^{1/3})] Ai[(\alpha + k) i^{4/3}]}{Ai(\alpha + k)}\, d\alpha \tag{7.58}$$

where g and M_2 are given by (7.20), α by (7.23) and

$$k = -(ih)^{-1/3}\zeta/\zeta_0. \tag{7.59}$$

$|k|$ is small compared to unity. L_4' is a path of integration in the α plane which encloses the zeros of $Ai(\alpha + k)$ in a clockwise direction. Changing the variable of integration in (7.58) to $u = \alpha + k$ enables us to conclude that

$$\left[\begin{matrix}E \text{ for finite} \\ \text{conductivity}\end{matrix}\right] \approx \left[\exp\left(-\frac{\zeta\psi}{\zeta_0}\right)\right] \left[\begin{matrix}E \text{ for infinite} \\ \text{conductivity}\end{matrix}\right]. \tag{7.60}$$

Since we have assumed $\theta = \pi/2$, the relation (7.60) holds in the region where the angle ψ defined by Fig. 2.3 is negative.

The analogue of (7.58) for vertical polarization is obtained by replacing E by H, omitting the $i^{8/3}$, and replacing the ratio of the Airy integrals by

$$Ai'[(\alpha + \ell/\alpha) i^{4/3}]/Ai'(\alpha + \ell/\alpha) \tag{7.61}$$

where

$$\ell = -(ih)^{1/3}\zeta/\zeta_0. \tag{7.62}$$

Even though h is large, ζ/ζ_0 is assumed to be so small that ℓ is small compared to unity. The path of integration L_4' must now enclose the zeros of $Ai'(\alpha + \ell/\alpha)$ which are close to those of $Ai'(\alpha)$ at $\alpha = a_s', s = 1,$

2, $\cdots$. It must not pass close to $\alpha = 0$ since the work leading to (7.61) assumes ℓ/α to be a small number. Changing the variable of integration to $v = \alpha + \ell/\alpha$, approximating ℓ/α, ℓ/α^2 by ℓ/v, ℓ/v^2, and evaluating the integral by considering the residues of the poles at $v = a_s'$ gives

$$H \approx i^{-2/3} M_2 \sum_{s=1}^{\infty} \left(1 - \frac{\ell}{a_s'^2}\right)^{-1} \frac{\exp\left[-i^{1/3} g(a_s' - \ell/a_s')\right]}{(-a_s')[Ai(a_s')]^2}. \tag{7.63}$$

This shows, to a first approximation, how the expression (7.52) is modified when the cylinder is a very good, but not perfect, conductor. Of course g must be negative in (7.63). Since ℓ in (7.62) varies as $h^{1/3}$ while k in (7.59) varies as $h^{-1/3}$ it appears that the field for vertical polarization is much more sensitive to changes in the conductivity than it is for horizontal polarization.

It may be verified that the change in the exponential terms in the series (7.30) and (7.52) produced by finite conductivity, namely

$$\begin{aligned} &a_s \text{ changes to } a_s - k \\ &a_s' \text{ changes to } a_s' - \ell/a_s', \end{aligned} \tag{7.64}$$

agrees, to a first approximation, with the change produced in the corresponding series (given, for example, by the series (27) and (28) on page 45 of Reference 7) for the propagation of radio waves over the earth's surface.

8. FIELD AT A GREAT DISTANCE BEHIND THE PARABOLIC CYLINDER WHEN $\theta = \pi/2$ AND h IS LARGE

In the work of Section 7 the angle of incidence θ may lie anywhere between 0 and π. Here we take $\theta = \pi/2$, which corresponds to the case shown in Fig. 2.3 and described in Section 2. Some simplification is obtained thereby. For example, the incident wave is now simply $\exp(-ix)$. We shall write the expressions for the horizontal and vertical polarization cases as

$$E = (e^{-ix} + S_1)_r + S_{21} + (S_{22} + S_{23}), \tag{8.1}$$

$$H = (e^{-ix} + S_1)_r + S_{21} + (S_{32} + S_{33}), \tag{8.2}$$

respectively. Here S_{21}, $\cdots$ are defined by (7.16) and (7.46) in which

$$\begin{aligned} &\theta = \pi/2, \qquad w = 1, \\ &\beta = \xi/\eta = \cot(\varphi/2 + \pi/4) = 1 - \varphi + \varphi^2/2 - \varphi^3/3 + \cdots \end{aligned} \tag{8.3}$$

Throughout this section β will be defined by (8.3), i.e., by (7.4) with

$\theta = \pi/2$. Also, from (5.3) and (5.6)

$$(e^{-ix} + S_1)_r = (i/\pi)^{1/2} e^{-ix} \int_{-\infty}^{T_1} e^{-it^2}\, dt, \qquad T_1 = 2^{-1/2}(\eta - \xi) = (2r)^{1/2} \sin(\varphi/2). \tag{8.4}$$

The subscript r is used to denote correspondence to a half-plane with its edge at $r = 0$.

When h is large, physical reasons lead us to expect a similarity between our field and the one behind a half-plane with its edge at the crest of the cylinder where $\rho = 0$ (see Fig. 2.3). The main part of this field is the analogue of (8.4):

$$(e^{-ix} + S_1)_\rho = (i/\pi)^{1/2} e^{-ix} \int_{-\infty}^{T_3} e^{-it^2}\, dt, \qquad T_3 = (2\rho)^{1/2} \sin(\psi/2), \tag{8.5}$$

where the subscript ρ indicates that $[\exp(-ix) + S_1]_\rho$ corresponds to diffraction behind the half-plane just mentioned.

In order to make use of the similarity between the field behind the cylinder and the half-plane with its edge at the crest of the cylinder, we change the polar coordinates from (r, φ) to (ρ, ψ). From

$$\rho e^{i\psi} = r e^{i\varphi} - ih \tag{8.6}$$

it may be shown that, when h^2/r is small,

$$(e^{-ix} + S_1)_r - (e^{-ix} + S_1)_\rho = (i/\pi)^{1/2} e^{-ix} \int_{T_3}^{T_1} e^{-it^2}\, dt = \frac{2iM_1}{\beta - 1} [e^{ih \sin \varphi} - 1] + 0(h^3/r^{3/2}) \tag{8.7}$$

where M_1 is obtained by putting $\theta = \pi/2$ in (7.4).

When we combine (8.7) and the expression (7.19) for S_{21} the $2iM_1/(\beta - 1)$ terms cancel leaving

$$(e^{-ix} + S_1)_r + S_{21} = (e^{-ix} + S_1)_\rho + \frac{2iM_1}{\beta - 1} e^{ih \sin \varphi} + i\frac{M_2}{g} + 0(h^3/r^{3/2}) + 0[M_1 \exp(-2\pi h)]. \tag{8.8}$$

The sum of the terms involving M_1 and M_2 may be expressed in a form which contains the expression $c(r)$ defined by (2.5) and the quantity b defined by

$$\begin{aligned} b &= -\log \beta = \log \tan\left(\frac{\varphi}{2} + \frac{\pi}{4}\right) = \varphi + \varphi^3/6 + \cdots \\ &= h^{-1/3} g, \\ \tanh b &= \sin \varphi. \end{aligned} \tag{8.9}$$

Replacing $c(r) \exp(ih \sin \varphi)$ by $c(\rho)$ plus a correction term then converts (8.8) into

$$\begin{aligned} (e^{-ix} + S_1)_r + S_{21} &= (e^{-ix} + S_1)_\rho \\ &+ \frac{c(\rho)[1 + \exp(2b_\rho)]^{1/2}}{2^{1/2}} \left[\frac{1}{1 - e^b} + \frac{\exp(ihb - ih \tanh b)}{b}\right]_\rho \\ &+ 0(h^3/r^{3/2}) + 0(r^{-1/2} e^{-2\pi h}), \end{aligned} \tag{8.10}$$

where the subscript ρ on the square brackets indicates that b is to be replaced by b_ρ defined by

$$b_\rho = \log \tan(\psi/2 + \pi/4) = \psi + \psi^3/6 + \cdots \tag{8.11}$$

The quantity within the square brackets in (8.10) is continuous at $b = 0$ where it behaves like (neglecting $0(b)$ terms but retaining $0(hb^2)$)

$$\tfrac{1}{2} + ihb^2/3 = \tfrac{1}{2} + ih^{1/3} g^2/3. \tag{8.12}$$

Expression (8.10) is to be used with $(S_{22} + S_{23})$ and $(S_{32} + S_{33})$ obtained from (7.17) and (7.46) (with $\theta = \pi/2$ and $w = 1$), respectively.

When ψ is small, expression (8.10) becomes

$$\begin{aligned} (e^{-ix} + S_1)_r + S_{21} &= (e^{-ix} + S_1)_\rho \\ &+ c(\rho) \left[\frac{1}{2} - \frac{1}{\psi} + \frac{h^{1/3} \exp(ig^3/3)}{g}\right]_\rho + \cdots . \end{aligned} \tag{8.13}$$

The subscript ρ on the square bracket indicates that g is to be replaced by g_ρ defined by

$$g_\rho = h^{1/3} b_\rho = h^{1/3} (\psi + \psi^3/6 + \cdots). \tag{8.13}$$

When, in accordance with (8.1) and (8.2), we add to (8.13) the approximations (7.26) and (7.49), namely

$$\begin{aligned} S_{22} + S_{23} &\sim iM_2 \Psi(g), \\ S_{32} + S_{33} &\sim iM_2 \Psi_v(g), \end{aligned} \tag{8.14}$$

we obtain

$$E = (e^{-ix} + S_1)_\rho + c(\rho)\left[\frac{1}{2} - \frac{1}{\psi} + \left\{\frac{1}{g} + \Psi(g)\right\} h^{1/3} \exp(ig^3/3)\right]_\rho + \cdots, \tag{8.15}$$

$$H = (e^{-ix} + S_1)_\rho + c(\rho)\left[\frac{1}{2} - \frac{1}{\psi} + \left\{\frac{1}{g} + \Psi_v(g)\right\} h^{1/3} \exp(ig^3/3)\right]_\rho + \cdots. \tag{8.16}$$

The terms neglected in (8.15) and (8.16) are the "order of" terms in (8.10), plus those neglected by virtue of ψ being small, plus the errors in (8.14) The errors in (8.14) are of two kinds namely those of $0(h^3/r^{3/2})$ and those due to approximating the parabolic cylinder functions by Airy integrals.

It is interesting to observe the forms assumed by (8.15) and (8.16) when $h = 0$ even though they are not supposed to hold for small values of h. In this case ρ, ψ go into r, φ and the right hand sides of (8.15) and (8.16) become the same, namely

$$(e^{-ix} + S_1)_r + c(r)/2. \tag{8.17}$$

The half plane results given in Section 2 become, for small values of φ,

$$\left.\begin{matrix} E \\ H \end{matrix}\right\} = (e^{-ix} + S_1)_r \pm c(r)/2 \tag{8.18}$$

where the upper sign corresponds to E and the lower one to H. Comparison of (8.17) and (8.18) shows that (8.15) for E reduces to the proper value but (8.16) for H fails to do so because the signs of $c(r)/2$ do not agree.

The discrepancy is apparently related to the approximations we have made in obtaining the expression (7.19) for S_{21} from (7.18) and to the errors introduced by approximating the parabolic cylinder functions by the Airy integrals. As we let $h \to 0$ in the more complete expression (7.18) for S_{21}, the value obtained for $S_{21} \to \infty$. This is explained by the fact that the upper limit of integration $-1 - ih$ (at point C) approaches the pole of the integrand of (7.17) at $n = -1$. This large value of S_{21} tends to be cancelled by the large value of S_{23} (for horizontal polarization). On the other hand our approximation (7.19) yields via (7.21) the value iM_1 for S_{21} and S_{31} when $h = 0$ and $\beta = 1$. The factor $h^{1/3}$ in M_2 makes our approximations for S_{22}, S_{23}, S_{32}, S_{33} in terms of Airy integrals vanish when $h = 0$.

Incidentally, if, instead of taking the point C of Fig. 6.2 to be at $-1 - ih$, we take it to be at $-\frac{1}{2} - ih$ (a choice which receives some support from the Airy integral representation obtained from the viewpoint of the differential equations discussed in the first part of Section 13), the approximate integrals of (7.17) and (7.46) may be integrated directly when $h = 0$ and $\beta = 1$. It is found that

$$S_{21} \sim -\frac{M_1}{\pi} \log 2, \qquad S_{22} \sim \frac{M_1}{\pi} \log 2 + \frac{iM_1}{2}, \qquad S_{23} \sim +iM_1/2,$$

$$S_{31} \sim -\frac{M_1}{\pi} \log 2, \qquad S_{32} \sim \frac{M_1}{\pi} \log 2 - \frac{iM_1}{2}, \qquad S_{33} \sim -iM_1/2,$$

and these add to give the values $S_2(0) \sim iM_1$, $S_3(0) \sim -iM_1$ required by the half-plane case.

It is seen that a rather thorough investigation of the errors introduced by our approximations would be required to resolve the discrepancy between (8.17) and (8.18). Since we do not intend to go into this subject, and since the errors we have made may be as large as the $\frac{1}{2}$ which appears within the square brackets of (8.15) and (8.16), we shall "split the difference" between the two polarizations and omit the $\frac{1}{2}$ altogether. This is done in Section 2 where $\tau \approx g_\rho$.

9. THE FUNCTIONS $U_n(z)$, $V_n(z)$, $W_n(z)$

The functions $U_n(z)$, etc., are defined for all values of z and n by the integrals

$$\begin{aligned} U_n(z) &= \frac{1}{2\pi i} \int_U t^{-n-1} e^{-t^2+2zt}\, dt, \\ V_n(z) &= \frac{1}{2\pi i} \int_V t^{-n-1} e^{-t^2+2zt}\, dt, \\ W_n(z) &= \frac{1}{2\pi i} \int_W t^{-n-1} e^{-t^2+2zt}\, dt. \end{aligned} \tag{9.1}$$

where the paths of integration U, V, W in the complex t-plane are shown in Fig. 9.1. The cut in the t-plane runs from $-\infty$ to 0 and has been introduced in order to make the function t^{-n-1} one-valued. In some of the later work the paths of integration will cross this cut. Of course, this requires close attention to arg t.

The initial and final points of the various paths (denoted in Fig. 9.1 by the subscripts i and f) are located at infinity. Arg $t = -\pi$ at U_i and W_f and $+\pi$ at U_f and V_i.

We shall give a summary of the properties of the functions (9.1)

which will be needed in our work. These functions are related to the parabolic cylinder function $D_n(z)$[18,19] through the equations

$$\begin{aligned} U_n(z) &= 2^{n/2}\, e^{z^2/2}\, D_n(2^{1/2}z)/\Gamma(n+1), \\ V_n(z) &= -i^{-n}\, 2^{n/2}\, e^{z^2/2}\, D_{-n-1}(-iz2^{1/2})/(2\pi)^{1/2}, \\ W_n(z) &= -i^{n}\, 2^{n/2}\, e^{z^2/2}\, D_{-n-1}(iz2^{1/2})/(2\pi)^{1/2}. \end{aligned} \tag{9.2}$$

We use the functions $U_n(z)$, etc., here instead of $D_n(z)$ because they seem to be more convenient for the particular problem we have to deal with.

From the definitions (9.1) it follows that $U_n(z)$, $V_n(z)$, $W_n(z)$ are one-valued analytic functions of z and n. By expanding $\exp(2zt)$ in (9.1) and integrating termwise it may be shown that

$$\begin{aligned} U_n(z) &= 2A\cos(\pi n/2) + 4zB\sin(\pi n/2), \\ V_n(z) &= -Ai^{-n} - 2zi^{-n+1}B, \\ W_n(z) &= -Ai^{n} - 2zi^{n-1}B, \end{aligned} \tag{9.3}$$

$$A = {}_1F_1\left(-\frac{n}{2}; \frac{1}{2}; z^2\right) \Big/ 2\Gamma\left(1+\frac{n}{2}\right),$$

$$B = {}_1F_1\left(\frac{1-n}{2}; \frac{3}{2}; z^2\right) \Big/ 2\Gamma\left(\frac{1+n}{2}\right).$$

When $z = 0$ and $U_n'(z) = d\,U_n(z)/dz$, etc.,

$$\begin{aligned} U_n(0) &= \frac{\cos(\pi n/2)}{\Gamma(1+n/2)}, \qquad V_n(0) = \frac{-i^{-n}}{2\Gamma(1+n/2)}, \\ & \qquad\qquad W_n(0) = \frac{-i^{n}}{2\Gamma(1+n/2)}, \\ U_n'(0) &= \frac{2\sin(\pi n/2)}{\Gamma\left(\frac{n+1}{2}\right)}, \qquad V_n'(0) = \frac{-i^{-n+1}}{\Gamma\left(\frac{n+1}{2}\right)}, \\ & \qquad\qquad W_n'(0) = \frac{-i^{n-1}}{\Gamma\left(\frac{n+1}{2}\right)}. \end{aligned} \tag{9.4}$$

[18] See E. T. Whittaker and G. N. Watson, *Modern Analysis*, Fourth Edition (1927) Cambridge Univ. Press pp. 347–354.

[19] W. Magnus and F. Oberhettinger, Formeln und Sätze für Speziellen Funktionen, 2nd Ed., Springer, 1948 Chap. 6 Section 3, and p. 227. A comprehensive account of $D_n(z)$ is given in the forthcoming work, *Higher Transcendental Functions*, compiled by the staff of the Bateman Manuscript Project.

Let $T_n(z)$ denote any one of $U_n(z)$, $V_n(z)$, $W_n(z)$, let primes denote differentiation with respect to z, and let asterisks denote complex conjugates. Then we have the following relations

$$T_n''(z) - 2zT_n'(z) + 2nT_n(z) = 0, \tag{9.5}$$

$$\frac{d}{dz}\left[e^{-z^2}T_n'(z)\right] + 2ne^{-z^2}T_n(z) = 0, \tag{9.6}$$

$$\frac{d^2}{dz^2}\left[e^{-z^2/2}T_n(z)\right] + (2n + 1 - z^2)e^{-z^2/2}T_n(z) = 0, \tag{9.7}$$

$$\begin{aligned} T_n'(z) &= 2T_{n-1}(z), \\ nT_n(z) &= 2zT_{n-1}(z) - 2T_{n-2}(z), \end{aligned} \tag{9.8}$$

$$\begin{aligned} U_n'(z)\,V_n(z) - U_n(z)\,V_n'(z) &= i2^n e^{z^2}/\pi^{1/2}\,\Gamma(n+1), \\ V_n'(z)\,W_n(z) - V_n(z)\,W_n'(z) &= i2^n e^{z^2}/\pi^{1/2}\,\Gamma(n+1), \\ W_n'(z)\,U_n(z) - W_n(z)\,U_n'(z) &= i2^n e^{z^2}/\pi^{1/2}\,\Gamma(n+1), \end{aligned} \tag{9.9}$$

$$U_n(z) + V_n(z) + W_n(z) = 0, \tag{9.10}$$

$$\begin{aligned} [V_n(z)]^* &= W_{n^*}(z^*),\ [W_n(z)]^* = V_{n^*}(z^*), \\ [U_n(z)]^* &= U_{n^*}(z^*), \end{aligned} \tag{9.11}$$

$$\begin{aligned} V_n(-z) &= i^{-2n}\,W_n(z),\ W_n(-z) = i^{2n}\,V_n(z), \\ U_n(-z) &= -i^{2n}\,V_n(z) - i^{-2n}\,W_n(z), \end{aligned} \tag{9.12}$$

$$V_{-n-1}(iz) = -i^{n+1}KU_n(z), \qquad W_{-n-1}(iz) = -i^{-n-1}KU_n(-z),$$

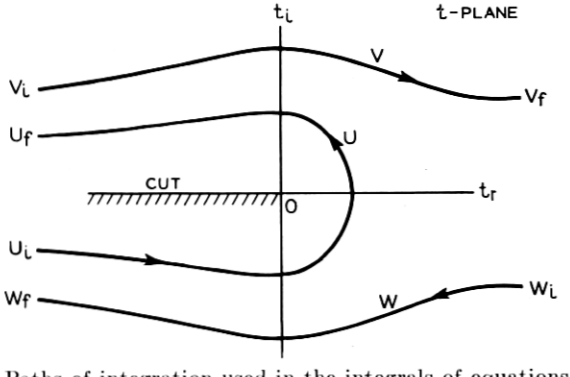

Fig. 9.1 — Paths of integration used in the integrals of equations (9.1) which define the functions $U_n(z)$, $V_n(z)$ and $W_n(z)$. The subscripts i and f stand for the "initial" and "final" points of the paths.

$$U_{-n-1}(iz) = i^{-n-1}(i^{2n} - i^{-2n})KW_n(z) = -(2i)^{-n}\pi^{1/2}e^{-z^2}W_n(z)/\Gamma(-n),$$
$$U_{-n-1}(-iz) = i^{n-1}(i^{2n} - i^{-2n})KV_n(z), \tag{9.13}$$
$$K = e^{-z^2}\Gamma(n+1)/\pi^{1/2}2^{n+1}$$

Equation (9.5) may be obtained from (9.1) by forming $T_n''(z) - 2zT'(z)$ and integrating by parts. Equation (9.10) follows from (9.1) upon joining the paths U, V, W to obtain a closed path of integration. From (9.11) it follows that when we have an expression for $V_n(z)$ which holds for all values of z and n, replacing i by $-i$ (or i^{-1}) gives the corresponding expression for $W_n(z)$. Equations (9.13) may be obtained by using the fact that $U_{-n-1}(iz)$ exp (z^2) etc. are solutions of the differential equations (9.5) and (9.7).

The relations (9.11) and (9.13) enable us to compute the values of $U_n(z)$, $V_n(z)$, $W_n(z)$ for $z = i^{1/2}\rho$ and $z = i^{-1/2}\rho$ and all n when the values of any two are given for $z = i^{1/2}\rho$ and $Re(n) \geqq -\frac{1}{2}$.

It may be verified that as z becomes large and n remains fixed the differential equation (9.5) has the asymptotic solutions

$$s_1(n,z) = \frac{2^n z^n}{\Gamma(n+1)}\,{}_2F_0\left(-\frac{n}{2}, \frac{1-n}{2}\,;\,;-1/z^2\right),$$
$$s_2(n,z) = \frac{z^{-n-1}e^{z^2}}{2\sqrt{\pi}}\,{}_2F_0\left(\frac{n+1}{2}, \frac{n+2}{2}\,;\,;1/z^2\right), \tag{9.14}$$

where

$$|\arg z| < \pi \text{ and } s_2(-n-1,iz) = i^n K s_1(n,z),$$

K being given by (9.13). In terms of these functions we have

$$V_n(z) \sim -is_2(n,z), \qquad 0 < \arg z < \pi$$
$$\sim -s_1(n,z) - is_2(n,z), \qquad -\pi/2 < \arg z < 0 \tag{9.15}$$
$$\sim -s_1(n,z) - i^{-4n+1}s_2(n,z), \qquad -\pi < \arg z < -\pi/2$$

$$W_n(z) \sim is_2(n,z), \qquad -\pi < \arg z < 0 \tag{9.16}$$

$$U_n(z) \sim s_1(n,z), \qquad -\pi/2 < \arg z < \pi/2. \tag{9.17}$$

The first expression for $V_n(z)$ in (9.15) follows when we note that the leading term may be obtained from (9.1) by choosing the path of integration V to be $t = z + \tau$ where τ runs from $-\infty$ to $+\infty$, and $|z|$ is supposed to be large. (9.17) follows from the first of (9.15) and the relation (9.13) between $V_{-n-1}(iz)$ and $U_n(z)$. Asymptotic expressions for $W_n(z)$ may be obtained by taking the conjugate complex of those

for $V_n(z)$. The second and third expressions for $V_n(z)$ follow from the other asymptotic expressions and (9.11), (9.12).

When $R(n) < 0$, the theory of gamma functions and (9.1) lead to

$$\begin{aligned}\Gamma(n+1)\Gamma(-n)U_n(z) &= -\pi \csc \pi n U_n(z) \\ &= \int_0^\infty \tau^{-n-1} \exp(-\tau^2 - 2\tau z)\, d\tau.\end{aligned} \tag{9.18}$$

By expressing $\sqrt{\pi} \exp[-(z-t)^2]$ as the integral of

$$\exp[-\tau^2 + 2i(z-t)\tau]$$

taken from $\tau = -\infty$ to $+\infty$ and substituting in (9.1) it may be shown that, when $R(n) > -1$,

$$\begin{aligned}U_n(z) &= Fi^n \int_{-\infty}^{\infty} e^{-t^2-2izt} t^n\, dt, \\ V_n(z) &= -Fi^{-n} \int_0^\infty e^{-\tau^2+2iz\tau} \tau^n\, d\tau, \\ W_n(z) &= -Fi^n \int_0^\infty e^{-\tau^2-2iz\tau} \tau^n\, d\tau, \\ F &= 2^n e^{z^2}/\Gamma(n+1)\pi^{1/2}.\end{aligned} \tag{9.19}$$

When n is not an integer the path of integration in the integral (9.19) for $U_n(z)$ is indented downward at the origin. Equations (9.19) may also be obtained from (9.1) by using (9.13) and (9.18).

When n is an integer

$$U_n(-z) = (-)^n U_n(z), \qquad V_n(-z) = (-)^n W_n(z), \tag{9.20}$$

and when n is a positive integer

$$\begin{aligned}U_n(z) = s_1(n, z) &= (-)^n \frac{e^{z^2}}{n!} \frac{d^n}{dz^n} e^{-z^2}, \\ U_{-n}(z) &= 0, \\ V_{-n}(z) = -W_{-n}(z) &= -is_2(-n, z) = -\frac{i}{\sqrt{\pi} 2^n} \frac{d^{n-1}}{dz^{n-1}} e^{z^2}.\end{aligned} \tag{9.21}$$

From Maclaurin's expansion and (9.21),

$$\sum_{n=0}^{\infty} t^n U_n(z) = \exp[-t^2 + 2zt]. \tag{9.22}$$

10. FORMULAS FOR THE SADDLE-POINT METHOD

Much of our work involves the behavior of the parabolic cylinder functions as functions of n when n is a large complex number. Although this subject has been studied by several writers,[20, 21, 22] their results are not in the form we require. As the work of Sections 6 and 7 shows, the paths of steepest descent for the integrals in our electromagnetic problem are intimately connected with the function $f(t_0) - f(t_1)$. In turn, this function is closely related to the saddle point method of evaluating $U_n(z)$, etc., for large values of n. For the sake of completeness, we shall outline this method. We shall pay special attention to the relative importance of the two saddle points as n moves about in its complex plane.

When we write the integrand of the integrals (9.1) as $\exp [f(t)]$ we obtain expressions of the form

$$U_n(z) = \frac{1}{2\pi i} \int_U \exp [f(t)]\, dt, \qquad f(t) = -t^2 + 2zt - m \log t, \qquad m = n + 1. \tag{10.1}$$

The saddle points of the integrand are at the points t_0 and t_1 in the complex t-plane where $f'(t)$ is zero:

$$2t_0^2 - 2zt_0 + m = 0, \qquad t_0^2 - zt_0 = -m/2,$$
$$t_0 = \frac{z + (z^2 - 2m)^{1/2}}{2}, \qquad t_0 + t_1 = z, \tag{10.2}$$
$$t_1 = \frac{z - (z^2 - 2m)^{1/2}}{2}, \qquad 2t_0t_1 = m.$$

Let the path of integration U of (10.1), for example, be deformed so as to pass through a saddle point, say t_0, along a path of steepest descent. Let

$$f(t) = f(t_0) - \sum_2^\infty b_k(t - t_0)^k/k!. \tag{10.3}$$

Then, if b_2 is not too small, the contribution of the region around t_0

[20] Nathan Schwid, The Asymptotic Forms of the Hermite and Weber Functions, Amer. Math. Soc. Trans. **37,** pp. 339–362, 1935. References to earlier work will be found in this paper. Schwid's work is based on R. Langer's study of the asymptotic solutions of second order differential equations.

[21] O. E. H. Rydbeck, The Propagation of Radio Waves, Trans. of Chalmers Univ. of Tech. **34,** 1944.

[22] G. N. Watson, Harmonic Functions Associated with Parabolic Cylinder Functions, Proc. London Math. Soc. (2) **17,** pp. 116–148, 1918.

to the value of the integral is exp $[f(t_0)]$ times

$$\frac{1}{2\pi}\int \exp\left[-\sum_2^\infty b_k(t-t_0)^k/k!\right]dt$$

$$\sim (2\pi b_2)^{-1/2}[1+\{-b_4B_2+10b_3^2B_3\} \tag{10.4}$$

$$+\{-b_6B_3+[35b_4^2+56b_3b_5]B_4-2100b_3^2b_4B_5+55(280)b_3^4B_6\}$$

$$+\cdots]$$

where $B_k = (2b_2)^{-k}/k!$. The sign of $(2\pi b_2)^{-1/2}$ is chosen so that the argument of the right hand side of (10.4) is equal to arg (dt) at $t = t_0$ on the path of steepest descent. The derivatives of $f(t)$ at t_0 give

$$b_2 = 2('_0 - t_1)/t_0, \qquad b_3 = 4t_1/t_0^2, \qquad b_4 = -12t_1/t_0^3,$$

$$-b_4B_2 + 10b_3^2B_3 = \frac{t_1(t_1+9'_0)}{24t_0(t_0-t_1)^3}. \tag{10.5}$$

The values of these quantities at the saddle point t_1 may be obtained by interchanging t_0 and t_1. If more terms of (10.4) are desired they may be obtained from the formal result

$$\frac{1}{2\pi}\int_{-\infty}^{\infty}\exp\left[-\sum_{k=2}^{\infty}\alpha_k t^k/k!\right]dt$$

$$\sim (2\pi\alpha_2)^{-1/2}\left[1+\sum_{k=2}^{\infty}Y_{2k}(0,0,-\alpha_3,-\alpha_4,\cdots,-\alpha_{2k})/k!(2\alpha_2)^k\right] \tag{10.6}$$

where $Y_n(a_1, a_2, \ldots, a_n)$ is the Bell exponential polynomial.[23] It is necessary to rearrange the terms given by (10.6) in order to get them in groups having the same order of magnitude. A more careful treatment of the terms in the asymptotic expansions for $D_n(z)$ has been given by Watson.[22] His method is similar to that used by Debye for Bessel functions.

In our work we shall deal with two different complex planes, and the reader is cautioned against confusing them. One is the complex t-plane, shown in Fig. 10.1, which contains the paths of integration for integrals such as (10.1). The other is the complex m-plane, shown in Fig. 10.2, which is introduced because we are often more interested in $U_n(z)$, etc., as functions of $m = n + 1$ than as functions of z. In the earlier sections

[23] E. T. Bell, Exponential Polynomials, Ann. of Math. **35,** pp. 258–279, 1934. The polynomials are tabulated up to $n = 8$ by John Riordan, Inversion Formulas in Normal Variable Mapping, Annals of Math. Stat. **20,** pp. 417–425, 1949.

we have spoken of the complex n-plane, but this is essentially the m-plane shifted by unity.

Since we are going to deal with a fixed value of z ($i^{1/2}\,\xi$ or $i^{-1/2}\,\eta$) but with a variable value of m, we make t_0 and t_1 one-valued functions of m by cutting the m-plane as shown in Fig. 10.2.

It may be shown that t_0 and t_1 lie in the opposite half-planes indicated in Fig. 10.1. This restricts arg t_0 to lie between arg $z - \pi/2$ and arg $z + \pi/2$. Arg t_1 is restricted to lie between arg $z - \pi$ and arg $z + \pi$ by the cut shown in Fig. 10.1. It may also be shown that

$$| t_0 | \geqq | t_1 |, \qquad | \arg t_0 - \arg t_1 | \leqq \pi. \tag{10.7}$$

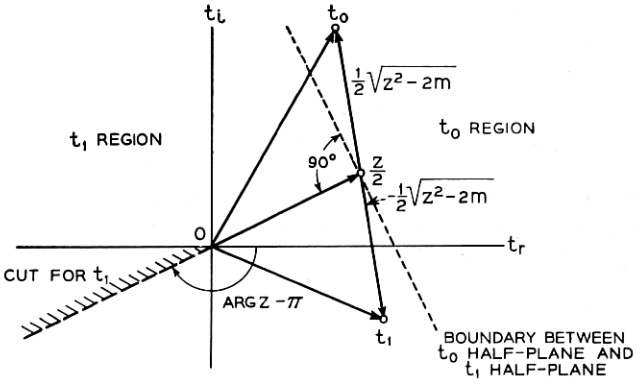

Fig. 10.1 — Diagram showing the half-plane regions to which the saddle points t_0 and t_1 are confined in the t-plane.

One might wonder why cuts in the m-plane are required since it has already been pointed out that $U_n(z)$, etc., are one-valued functions of $m = n + 1$. The trouble is that the asymptotic expressions for $U_n(z)$ are many-valued functions of m even though $U_n(z)$ itself is not.

Now that we have considered the saddle points t_0 and t_1, we turn to a consideration of the paths of steepest descent in the t-plane which pass through them.* The path of steepest descent which passes through t_0, for example, is that branch of the curve

$$Im\,[f(t) - f(t_0)] = 0 \tag{10.8}$$

for which t_0 is the highest point (i.e., $Re\,[f(t) - f(t_0)] \leqq 0$ on it). The

* Watson[22] has studied paths corresponding to $Re(n) > 0$ when z is any complex number, and has given curves which are related to some of those shown in Section 11.

paths of steepest descent may be shown to have the following properties:

1. Let $t = t_r + it_i = r \exp(i\theta)$. Then the paths of steepest descent either run out to $t_r = \pm \infty$ with $t_i \to Im\ z$ or spiral in to $t = 0$ as $r =$ (constant) exp $(-m_r\theta/m_i)$.

2. The steepest descent path through t_0 may be computed by a graphical method based on*

$$\arg(dt) = \arg t - \arg(t - t_0) - \arg(t - t_1). \tag{10.9}$$

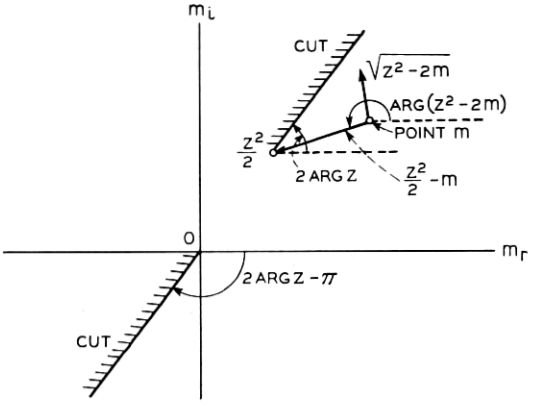

Fig. 10.2 — Diagram showing the cuts in the complex m-plane, $m = n + 1$.

If we draw the triangle $t_0\ 0\ t_1$ and bisect the interior angle at t_0 by the line b_0t_0 then

$$\arg(dt) \text{ at } t_0 = \text{angle } t_1t_0b_0. \tag{10.10}$$

If one goes clockwise in traveling from the side t_0t_1 to t_0b_0 then arg dt is negative. Likewise, arg (dt) at t_1 (on the path through t_1) is the angle between the side t_1t_0 and the bisector t_1b_1 of the interior angle at t_1.

3. When m has the critical value $z^2/2$ the saddle points coincide: $t_0 = t_1 = z/2$, and the paths of steepest descent start out from $t = z/2$ in the three directions arg $(t - z/2) =$ (arg z)$/3 + \delta$ where δ is 0, $2\pi/3$, or $-2\pi/3$.

4. Some of the paths of steepest descent change their character as m goes from one region of the m-plane to another. This is illustrated in Section 11 for the case $z = \rho \exp(i\pi/4)$ where it is shown that the

* A similar method was used in 1938 by A. Erdélyi in an unpublished study of the asymptotic behavior of confluent hypergeometric functions.

boundaries are given by

$$Im\,[f(t_0) - f(t_1)] = 0, \tag{10.11}$$

or a similar equation involving another pair of saddle points, e.g., t_1 and $t_1 \exp(i2\pi)$. In this equation z is regarded as fixed and t_0, t_1 are functions of m defined by (10.2). It should be noted that although (10.8) defines a path of steepest descent in the t-plane, (10.11) defines curves (boundaries of regions) in the m-plane.

5. If m is such that the path of integration for a particular function, say $U_n(z)$, passes through both t_0 and t_1, each one will contribute to the value of $U_n(z)$. Furthermore, if m is such that

$$Re\,[f(t_0) - f(t_1)] = 0, \tag{10.12}$$

t_0 and t_1 have the same height and the two contributions have a chance of cancelling each other and giving a value of zero for $U_n(z)$. Thus (10.12) or some similar equation defines the lines in the m-plane along which the zeros of $U_n(z)$, etc., (regarded as functions of m) are asymptotically distributed.

6. The lines in the m-plane defined by (10.11) and (10.12) may be obtained by substituting the values (10.2) for t_0 and t_1 in

$$f(t_0) - f(t_1) = t_0^2 - t_1^2 - 2t_0t_1 \log (t_0/t_1), \tag{10.13}$$

and setting the imaginary and real parts, respectively, to zero. However, instead of dealing with m directly it is easier to use $w = u + iv$ defined by

$$w = \log (t_0/t_1) = \log |t_0/t_1| + i(\arg t_0 - \arg t_1), \tag{10.14}$$

$$m = z^2/(\cosh w + 1), \tag{10.15}$$

where (10.15) follows from (10.14) and (10.2). Then (10.13) becomes

$$\begin{aligned} f(t_0) - f(t_1) &= m(\sinh w - w) \\ &= \frac{z^2(\sinh w - w)}{\cosh w + 1}. \end{aligned} \tag{10.16}$$

The inequalities (10.7) show that

$$u \geqq 0, \quad |v| \leqq \pi.$$

7. For the special case $z = \rho \exp(i\pi/4)$, (10.16) gives

$$\begin{aligned} (\cosh u + \cos v - v \sin v) \sinh u &= (\cosh u \cos v + 1)\, u, \\ (\cos v + \cosh u + u \sinh u) \sin v &= (\cosh u \cos v + 1)\, v, \end{aligned} \tag{10.17}$$

respectively, for $Im[f(t_0) - f(t_1)] = 0$ and $Re\,[f(t_0) - f(t_1)] = 0$. These equations are plotted in Fig. 10.3. It will be noted that a curve is shown for $v > \pi$ even though this puts w outside the allowed rectangle. This is done because one of the paths of integration, W, passes through both t_0 and $t_1 \exp(-i2\pi)$ when m is in a certain region, and the corresponding zeros of $W_n(z)$ lie on the curve defined by

$$Re\,[f(t_0) - f(t_1 \exp\{-i2\pi\})] = 0.$$

It may be shown that a curve corresponding to

$$f(t_0) - f(t_1 \exp\{-i2\pi\})$$

with $-\pi < v < \pi$ may be obtained from the curve corresponding to $f(t_0) - f(t_1)$ with $\pi < v < 3\pi$ by simply subtracting 2π from v. This is done on Fig. 10.3.

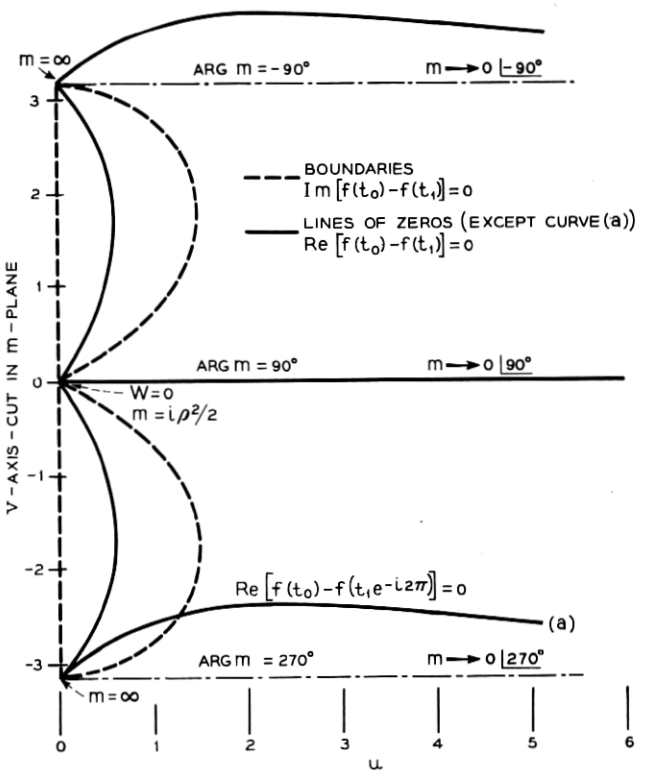

Fig. 10.3 — Boundaries of the regions shown in Fig. 11.2 and lines of zeros shown in Fig. 12.1 as they appear on the $w = u + iv$ plane when $z = i^{1/2}\rho$.

TABLE 11.1 — SADDLE POINT VALUES FOR REPRESENTATIVE VALUES OF m WHEN $z = i^{1/2}\rho$

Point Number	m/ρ^2		t_0/ρ		t_1/ρ		$\frac{f(t_0) + m \log \rho}{\rho^2}$	$\frac{f(t_1) + m \log \rho}{\rho^2}$
	Mod.	Arg.	Mod.	Arg.	Mod.	Arg.		
1	0.5	0°	1.07	57°	0.23	−57°	−0.013 + i0.550	1.21 + i0.450
2	1	0	1.20	64	0.42	−64	−0.080 + i0.021	1.77 + i0.979
3	0.550	0	1.09	58	0.25	−58	−0.017 + i0.500	1.28 + i0.500
4	0.005	0	1.00	45.1	0.0025	−45.1	−0.000 + i0.996	0.035 + i0.004
6	0.005	90	0.997	45	0.0025	45	0.004 + i1.000	0.004 + i0.035
8	0.005	180	1.00	44.9	0.0025	135.1	+0.000 + i1.004	−0.035 + i0.012
9	0.005	270	1.00	45	0.0025	225	−0.004 + i1.000	−0.020 − i0.035
10	0.005	−90	1.00	45	0.0025	−135	−0.004 + i1.000	0.012 − i0.035
11	0.550	180	1.09	32	0.25	148	0.017 + i1.36	−1.28 + i1.36
12	1	180	1.20	26	0.42	154	0.077 + i1.59	−1.77 + i2.55
13	1	90-ϵ arg $(z^2 - 2m) = 270$	0.71	90	0.71	0	1.07 + i1.35	0.5 + i1.35
—	1	90+ϵ arg $(z^2 - 2m) = -90$	0.71	0	0.71	90	0.5 + i1.35	1.07 + i1.35
14	0.5	90	0.5	45	0.5	45	0.39 + i1.10	0.39 + i1.10
—	1	270	1.37	45	0.37	225	−0.784 + i1.18	−3.93 − i1.87
—	1	−90	1.37	45	0.37	−135	−0.784 + i1.18	+2.35 − i1.87

The entries in this table must satisfy $t_0/\rho + t_1/\rho = i^{1/2}$. Equations (12.8) show that when all of the entries are replaced by their complex conjugates, a table for $z = i^{-1/2}\rho$ is obtained.

3. $m = (0.54953\ldots)\rho^2 \sim 0.55\rho^2$. Fig. 11.1 (b). This value of m marks the change in type of path. Since Im $f(t_1)$ = Im $f(t_0)$ is satisfied, the paths through t_0 and t_1 have the same equation [see (11.2)], and there is a chance for a situation like that at t_0 in Fig. 11.1 (b) to occur. The high point of the path U is at t_1, and it goes continually downhill on either side of t_1 although its direction changes sharply by 90° at t_0. The point $m = 0.55\rho^2$ is just one point on the boundary between regions in the m-plane corresponding to various types of paths. The boundary lines are obtained by solving condition (10.11) for m as outlined in Items 6 and 7 of Section 10. Mapping the boundary lines

$$\text{Im}\,[f(t_0) - f(t_1)] = 0$$

from the auxiliary w-plane (shown in Fig. 10.3) to the m-plane with the help of $m = i\rho^2/(\cosh w + 1)$ gives the boundaries between the regions

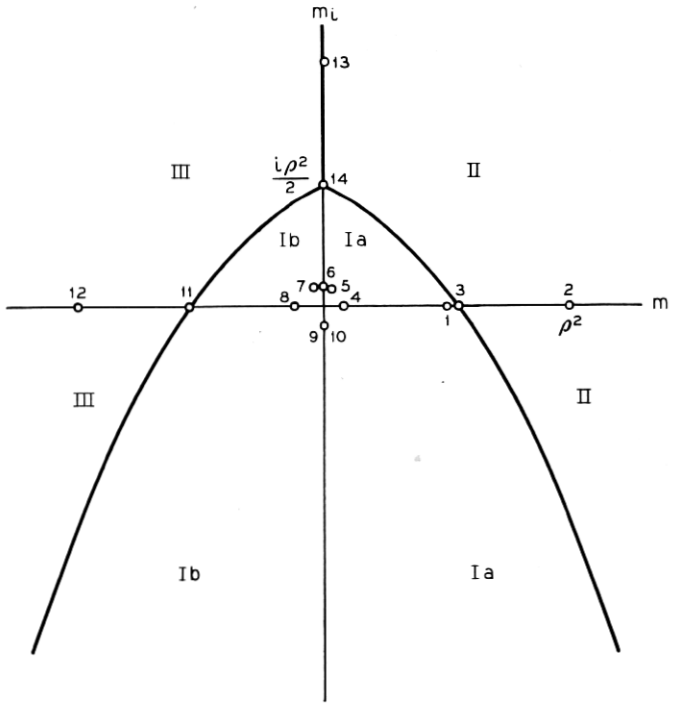

Fig. 11.2 — Regions of different types of paths of steepest descent, and hence different types of asymptotic expansions, when $z = i^{1/2}\rho$. Points numbered 1, 2, 3, are values of m corresponding to the paths of Figs 11.1 (a), (c), (b). Points designated by 5, 6, 7 correspond to Fig. 11.3(b). Points 4, 8, 9 correspond to Fig. 11.5 and points 11, 12, 13, 14 to Figs. 11.6 (a), (b), (c), (d).

I, II, III shown in Fig. 11.2. It may be verified that for large negative values of m_i the boundary lines in Fig. 11.2 are given approximately by

$$m_r = \pm 2^{3/2}\pi^{-1}\rho \mid m_i \mid^{1/2}. \tag{11.4}$$

There was a period, while these curves were being worked out, during which it appeared that the regions I, II, III told the entire story. However, when small values of m were studied it was found that region I splits up into the two sub-regions, Ia and Ib, such that the boundary between them is given by

$$\text{Im}\,[f(t_1) - f(t_1 e^{-2\pi i})] = 0. \tag{11.5}$$

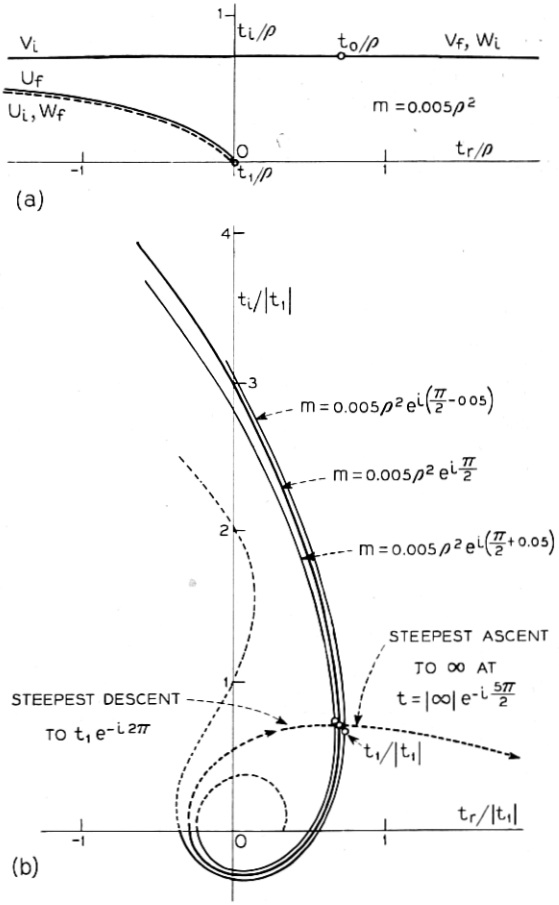

Fig. 11.3 — Paths of steepest descent for $\mid m \mid = 0.005\ \rho^2$, $z = i^{1/2}\rho$. Away from $t = t_1$ all paths look much like Fig. 11.3(a).

This is of the same form as (10.11). That $t_1 \exp(-2\pi i)$ is a saddle point follows from differentiation of the equation

$$f(te^{-2\pi i}) = f(t) + 2\pi i m_r - 2\pi m_i. \tag{11.6}$$

Combining (11.5) and (11.6) shows that the boundary between Ia and Ib is given by $m_r = 0$. This is indicated on Fig. 11.2.

We now examine the paths of steepest descent when m is small. Fig. 11.3 (a) gives a large view of all the paths, irrespective of arg m, when m^2/ρ is small.

4. $m = 0.005\rho^2$. Fig. 11.5 shows the vicinity around t_1.

5. $|m| = 0.005\rho^2$, arg $m = \pi/2 - 0.05$. Fig. 11.3 (b).

6. $|m| = 0.005\rho^2$, arg $m = \pi/2$. Fig. 11.3 (b). After passing through t_1 the path encircles the origin clockwise and runs down into the saddle point at $t = t_1 \exp(-2\pi i)$. Since m_i is positive, (11.6) shows that $t_1 \exp(-2\pi i)$ is lower than t_1. The path for arg $m = \pi/2 - 0.05$ suggests that from $t_1 \exp(-2\pi i)$ the path runs out to $\infty \exp(-\pi i)$ along the path of steepest descent which lies directly under (on the Riemann sheet for $-3\pi < \arg t < -\pi$) the path which runs from t_1 to $t = \infty \exp(i\pi)$. It follows from (11.6) that, as t traces out a path of steepest descent through t_1, $t \exp(-2\pi i)$ traces out a path of steepest descent through $t_1 \exp(-2\pi i)$ directly under the path through t_1.

7. $|m| = 0.055\rho^2$, arg $m = \pi/2 + 0.05$. Fig. 11.3 (b) shows that after passing through t_1 the path of steepest descent spirals in to $t = 0$. According to (11.3), the spiral is given by

$$r \approx (\text{constant}) \exp(-m_r\theta/m_i) \tag{11.7}$$

when r is small and θ large. Two things are to be noted. First, the type of path is different from that for arg $m = \pi/2 - 0.05$. Hence arg $m = \pi/2$ marks a change of type similar to that shown in Fig. 11.1 (b), except that here $t_1 \exp(-2\pi i)$ takes the place of t_0. Condition (11.5) takes the place of condition (10.11), and is satisfied by virtue of $m_r = 0$ when arg $m = \pi/2$.

The second thing to be noted is that up until now all of the paths of steepest descent have ended at $\pm\infty$ and U, V, W could be deformed into them without difficulty. How can we deform U, for example, into a path of steepest descent when the path through t_1 spirals in to $t = 0$? The way to deal with this problem is shown in Fig. 11.4 where U is continuously deformed into two portions, one coinciding with the path through t_1, as shown in Fig. 11.3 (b), and the other with the path of steepest descent through $t_1 \exp(-2\pi i)$. The second portion lies directly "underneath" the first portion.

In Fig. 11.4 the dashes mean, as before, that the path of steepest descent is on a sheet of the Riemann surface other than $|\arg t| < \pi$. The alternate dots and dashes are used to indicate that $|\arg t| > \pi$ and that in addition the path lies directly under the curve it parallels. Although in Fig. 11.4 the two kinds of dashed curves are joined at about arg $t = -3\pi - \pi/4$, they actually should spiral in to $t = 0$ before they connect.

8. $|m| = 0.005\rho^2$, arg $m = \pi$. Fig. 11.5. For arg $m = \pi$, (11.6) shows that t_1 and $t_1 \exp(-2\pi i)$ are of the same height.

9. $m = 0.005\rho^2$, arg $m = 3\pi/2$. For $\pi <$ arg $m < 3\pi/2$, $t_1 \exp(-2\pi i)$ is higher than t_1 and the paths spiral into $t = 0$ counterclockwise. At arg $m = 3\pi/2$ the rate of spiralling is zero and we have the path shown in Fig. 11.5 (which is the path for arg $m = \pi/2$ rotated by 180 degrees). Here arg $t_1 = 5\pi/4$.

10. $m = 0.005\rho^2$, arg $m = -\pi/2$. The paths for arg m equal to $-\pi/2$

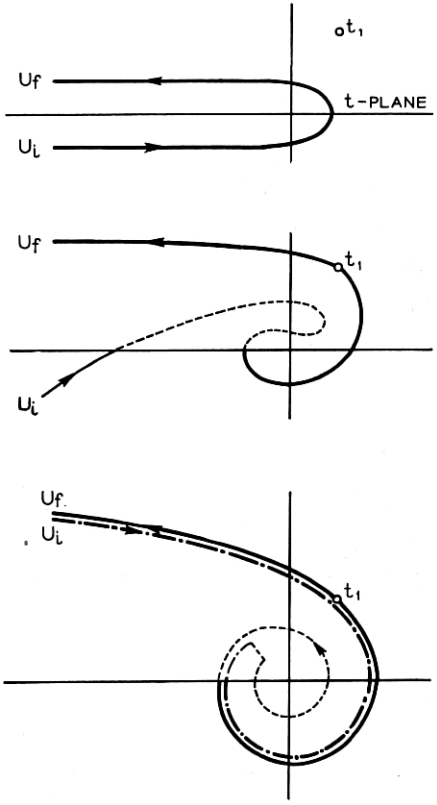

Fig. 11.4 — Deformation of path of integration U into path of steepest descent through t_1 when $m = 0.005\ \rho^2 \exp(i\pi/2 + i0.05)$.

and $3\pi/2$ have the same shape and both are highest at the saddle point whose argument is $-3\pi/4$. In both cases the contributions are the same and hence the value of $U_n(z)$, for example, is the same for arg $m = -\pi/2$ as for $3\pi/2$ (as it must be since our parabolic cylinder functions are one-valued functions of m).

Before leaving the region around $m = 0$ we point out that when $|m/\rho^2| \ll 1$ the path of steepest descent through t_0 is almost independent of arg m. Also, the curves of steepest descent for

$$1/\Gamma(m) = \frac{1}{2\pi i}\int_U e^t t^{-m}\, dt \tag{11.8}$$

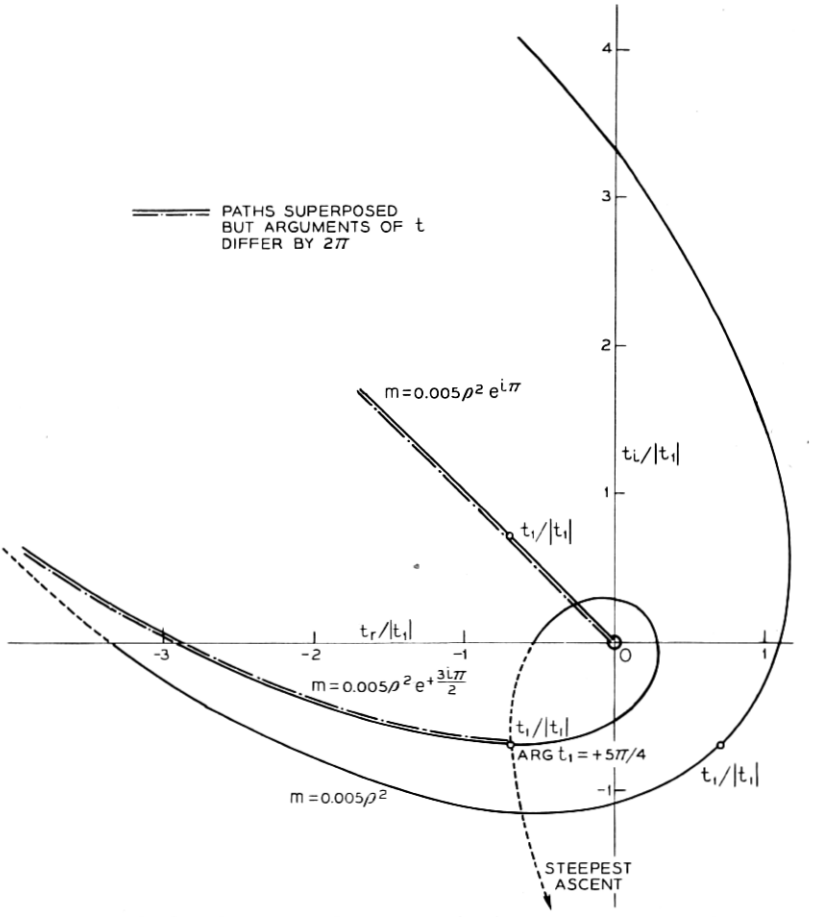

Fig. 11.5 — Paths of steepest descent for $|m| = 0.005\ \rho^2$, $z = i^{1/2}\rho$. These curves are much the same as those in Fig. 11.3(b) except for the values of arg m.

behave in much the same way as those just described. The line $m_r = 0$ divides the m-plane into two regions corresponding to different types of paths, and the negative real axis is a line of zeros corresponding to $Re\ [f(t_1) - f(t_1 \exp(-2\pi i))] = 0$ where $t_1 = m$ is the saddle point.

11. $|m| = 0.55\rho^2$, arg $m = \pi$. Fig. 11.6 (a). This value of m marks a change in the type of path.

12. $|m| = \rho^2$, arg $m = \pi$. Fig. 11.6 (b).

13. $|m| = \rho^2$, arg $m = \pi/2$, arg $(i\rho^2 - 2m) = 3\pi/2$. Fig. 11.6 (c). The complication of the paths in Fig. 11.6 (c) is due to the superposition of two boundaries in the m-plane. Im $f(t_0)$ = Im $f(t_1)$ accounts for

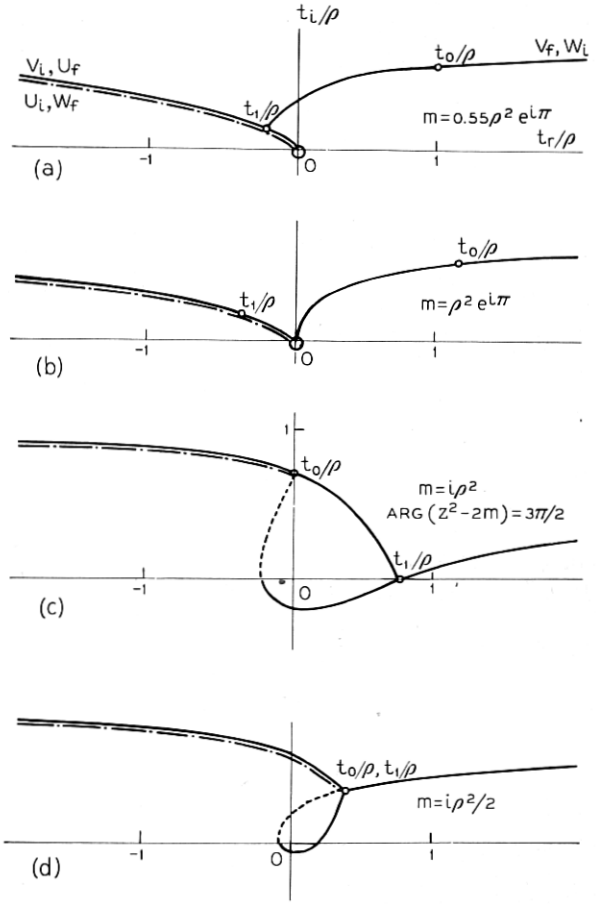

Fig. 11.6 — Paths of steepest descent for miscellaneous values of m with $z = i^{1/2}\rho$.

the path running from t_0 to t_1, and Im $f(t_1)$ = Im $f[t_0 \exp(-2\pi i)]$ for the one running from t_1 to $t_0 \exp(-2\pi i)$. The saddle points in order of their height are t_0, t_1, $t_0 \exp(-2\pi i)$, t_0 being the highest.

14. $m = i\rho^2/2$. Fig. 11.6 (d). Here $t_0 = t_1$ and the dashed lines go into the saddle point at $t_1 \exp(-2\pi i)$. The paths of steepest descent change their directions upon passing through the saddle points.

12. ASYMPTOTIC EXPRESSIONS FOR $U_n(z)$, $V_n(z)$, $W_n(z)$

The asymptotic expressions given here are for $z = i^{1/2}\rho$ and $z = i^{-1/2}\rho$ [with $i^{1/2} = \exp(i\pi/4)$] when n is not too close to $z^2/2$. As mentioned earlier, there is a close relation between our results and those given by Schwid.* The main difference is that we regard n as variable and z as fixed while Schwid regards z as variable with n fixed. Another point of difference is that in place of the $m = n + 1$ which appears in our expressions for t_0 and t_1 the quantity $n + \frac{1}{2}$ appears in Schwid's work. The quantity $2n + 1$ appears to enter naturally when the asymptotic values are obtained from the differential equations. This is seen when the *WKB* method is applied to equation (9.7).

By examining the paths of steepest descent shown in the figures of Section 11 we can determine the saddle points corresponding to $U_n(z)$, etc., (for $z = i^{1/2}\rho$) for various values of n. The contributions to the integral (10.1) from the saddle points t_0 to t_1 were discussed in Section 10. The contribution from the saddle point $t_1 \exp(-2\pi i)$ (which enters when $z = i^{1/2}\rho$) is, from (11.6), $\exp(i2\pi m)$ times the contribution from t_1.

Although we shall be concerned mainly with asymptotic expressions for the parabolic cylinder functions themselves, expressions for their derivatives may be readily obtained. Thus $U_n'(z) = dU_n(z)/dz$ has the asymptotic expression

$$\begin{aligned} U_n'(z) \sim\ & 2t_0\ [\text{contribution of } t_0 \text{ to } U_n(z)] \\ & + 2t_1\ [\text{contribution of } t_1 \text{ to } U_n(z)] \\ & + 2t_1\ [\text{contribution of } t_1 \exp(-2\pi i) \text{ to } U_n(z)] \end{aligned} \tag{12.1}$$

and similar expressions hold for $V_n'(z)$, $W_n'(z)$. These follow when we note that differentiation of the integrals (9.1), which define the functions, introduces a factor $2t$ into the integrand. Of course, if the path of integration does not pass throught a particular saddle point, its contribution to (12.1) is zero. Upon replacing t_0 and t_1 by their expressions

* Reference 20, page 478.

(10.2) and subtracting the corresponding expression for $zU_n(z)$ we obtain

$$\begin{aligned} {}'U_n(z) &= U_n'(z) - z\,U_n(z) \\ &\sim (z^2 - 2m)^{1/2}\,[(t_0 \text{ contribution}) - (t_1 \text{ contribution}) \\ &\qquad - (t_1 e^{-2\pi i} \text{ contribution})] \end{aligned} \tag{12.2}$$

where ${}'U_n(z)$ is the function defined by (4.19). The same is true for ${}'V_n(z)$ and ${}'W_n(z)$.

Consideration of the various paths of integration shown in Section 11 leads to the results shown in Table 12.1. The leading terms of the asymptotic expansions are listed for the various regions of the m-plane

TABLE 12.1 — LEADING TERMS IN THE ASYMPTOTIC EXPANSIONS FOR $U_n(z)$, $V_n(z)$, $W_n(z)$ WHEN $z = i^{1/2}\rho$, $\rho > 0$

Region in m-plane $m = n + 1$	$U_n(i^{1/2}\rho)$	$V_n(i^{1/2}\rho)$	$W_n(i^{1/2}\rho)$
Ia	A_1	A_0	$-A_0 - A_1$
II	$A_1 - A_0$	A_0	$-A_1$
Ib	$(1 - i^{4n})A_1$	A_0	$-A_0 - A_1 + i^{4n}A_1$
III	$(1 - i^{4n})A_1$	$A_0 - A_1$	$-A_0 + i^{4n}A_1$

shown in Fig. 11.2. If the next order terms are required, they may be obtained from (10.4) and (10.5).

The notation used in Table 12.1 is as follows:

$$z = i^{1/2}\rho, \qquad m = n + 1, \qquad i = \exp(i\pi/2),$$

$$-\pi/2 < \arg m \leqq 3\pi/2, \qquad -\pi/4 < \arg t_0 \leqq 3\pi/4,$$

$$-\pi/2 < \arg (i\rho^2 - 2m) \leqq 3\pi/2, \qquad -3\pi/4 < \arg t_1 \leqq 5\pi/4,$$

$$t_0 = [i^{1/2}\rho + (i\rho^2 - 2m)^{1/2}]/2, \qquad t_1 = [i^{1/2}\rho - (i\rho^2 - 2m)^{1/2}]/2,$$

$$\begin{aligned} A_0 &= [t_0^{1/2}(i\rho^2 - 2m)^{-1/4}/2i\pi^{1/2}] \exp f(t_0), \\ A_1 &= [t_1^{1/2}(i\rho^2 - 2m)^{-1/4}/2\pi^{1/2}] \exp f(t_1), \end{aligned} \tag{12.3}$$

$$f(t_0) = zt_0 + \frac{m}{2} - m \log t_0 = \frac{m}{2}\left(1 - \log \frac{m}{2} - \log \frac{t_0}{t_1}\right) + i^{1/2}\rho t_0,$$

$$f(t_1) = zt_1 + \frac{m}{2} - m \log t_1 = \frac{m}{2}\left(1 - \log \frac{m}{2} - \log \frac{t_1}{t_0}\right) + i^{1/2}\rho t_1.$$

Sometimes it is helpful to use

$$(2\pi)^{-1/2} \exp\left[\frac{m}{2}\left(1 - \log\frac{m}{2}\right)\right]$$

$$\sim \begin{cases} 1/\Gamma\left(\dfrac{m+1}{2}\right) = 1/\Gamma(1 + n/2) & \text{for} \\ & -\pi/2 < \arg m < \pi/2, \\ i^{-m}\Gamma\left(\dfrac{1-m}{2}\right)/2\pi = i^{-n-1}\Gamma(-n/2)/2\pi, & \\ & \pi/2 < \arg m < 3\pi/2, \end{cases} \tag{12.4}$$

where the last line is obtained by setting $m \exp(-\pi i)$ for m in the second line.

The asymptotic expansions for regions *Ib* and *III* may be obtained from those for *Ia* and *II* by using equations (9.11) and (9.13). However, the work is more difficult than one might suspect at first glance.

Incidentally, the leading terms in the asymptotic expansions (9.15) and (9.17), which hold when $\rho \to \infty$ and n remains fixed, may be obtained by considering the entries for *Ia* and *Ib* in Table 12.1.

It is sometimes convenient to use the limiting forms of the asymptotic expressions when $|m| \gg \rho^2$. In this case, for $z = i^{1/2}\rho$,

$$\begin{aligned} 2t_0 &\to z \pm i(2m)^{1/2}\left[1 - \frac{z^2}{2m}\right] + 0(m^{-3/2}), \\ 2t_1 &\to z \mp i(2m)^{1/2}\left[1 - \frac{z^2}{2m}\right] + 0(m^{-3/2}), \\ \log t_1/t_0 &\to \mp i\pi \pm iz(2m)^{-1/2}\left[2 + \frac{z^2}{6m}\right] + 0(m^{-5/2}), \end{aligned} \tag{12.5}$$

where the upper signs hold when $-\pi/2 < \arg m < \pi/2$ and the lower ones when $\pi/2 < \arg m < 3\pi/2$. Substituting (12.5) in (12.3), neglecting the higher order terms, and setting

$$\begin{aligned} B &= 2^{-3/2}\pi^{-1/2} \exp\left[\frac{m}{2}\left(1 - \log\frac{m}{2}\right) + i\rho^2/2\right], \\ \alpha_0 &= \exp\left[-\rho(2m/i)^{1/2}\right], \\ \alpha_1 &= \exp\left[\rho(2m/i)^{1/2}\right] = 1/\alpha_0, \end{aligned} \tag{12.6}$$

converts Table 12.1 into Table 12.2.

In this table B, α_0, α_1, are defined by (12.6); $m = n + 1$; $-\pi/2$

TABLE 12.2 — LEADING TERMS IN THE ASYMPTOTIC EXPANSIONS FOR $U_n(z)$, $V_n(z)$, $W_n(z)$ WHEN $z = i^{1/2}\rho$ AND $|2n| \gg \rho^2$

Region in m-plane ($m = n + 1$)	$U_n(i^{1/2}\rho)$	$V_n(i^{1/2}\rho)$	$W_n(i^{1/2}\rho)$
Ia	$i^n B\alpha_1$	$-i^{-n}B\alpha_0$	$B(i^{-n}\alpha_0 - i^n\alpha_1)$
II	$B(i^{-n}\alpha_0 + i^n\alpha_1)$	$-i^{-n}B\alpha_0$	$-i^n B\alpha_1$
Ib	$(1 - i^{4n})i^{-n}B\alpha_0$	$i^n B\alpha_1$	$B(i^{3n}\alpha_0 - i^{-n}\alpha_0 - i^n\alpha_1)$
III	$(1 - i^{4n})i^{-n}B\alpha_0$	$B(i^n\alpha_1 - i^{-n}\alpha_0)$	$B(i^{3n}\alpha_0 - i^n\alpha_1)$

$< \arg m \leqq 3\pi/2$; and in regions *Ia* and *Ib* $\arg m$ is approximately $-\pi/2$ and $3\pi/2$, respectively. Gamma functions may be introduced into the expression for B with the help of (12.4). It may be verified that the functions do not change, except for negligible terms, in crossing over the boundary from *Ia* to *Ib* (α_0 and α_1 are interchanged and B is changed by the factor $\exp(-m\pi i)$).

Since the zeros of our functions, regarded as functions of n, occur (asymptotically) when the contributions from two saddle points cancel each other, we may look at Table 12.1 and pick out regions which may possibly contain zeros. Thus, A_0 may equal A_1 along the line $|A_0| = |A_1|$, i.e. very nearly $Re[f(t_0) - f(t_1)] = 0$, in the m-plane. These lines were discussed in Item 7 of Section 10 and are plotted on the auxiliary w-plane in Fig. 10.3 When plotted on the m-plane the lines appear as shown in Fig. 12.1 The condition $Re[f(t_0) - f(t_1 \exp(-2\pi i))] = 0$ gives the line $|A_0| \approx |i^{4n}A_1|$ for some of the zeros of $W_n(i^{1/2}\rho)$.

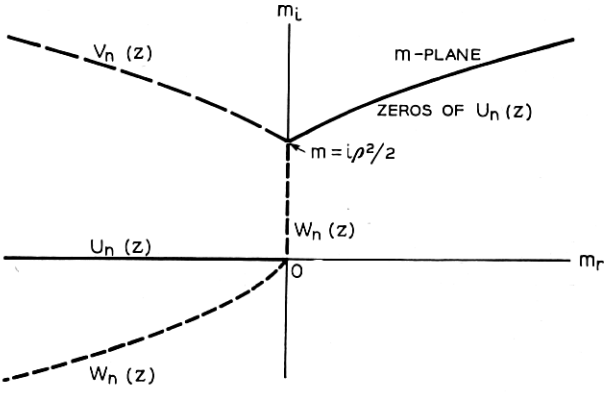

Fig. 12.1 — When $U_n(z)$, $V_n(z)$, and $W_n(z)$ are regarded as functions of n their zeros lie on the lines indicated when $z = i^{1/2}\rho$. The three branches coming out from $m = i\rho^2/2$ are lines along which $|A_0| \approx |A_1|$ and the three branch for $W_n(z)$ coming down from $m = 0$ is a line along which $|A_0| \approx |i^{4n}A_1|$ where A_0 and A_1 appear in Table 12.1.

The location of the zeros far out on the lines of Fig. 12.1 may be obtained by writing the appropriate expressions of Table 12.2 as proportional to B times a cosine or sine. Examination of the trigonometrical terms shows that

$$\begin{aligned} &U_n(i^{1/2}\rho) \text{ has zeros at } n \approx 2k + 1 + i^{1/2}4\rho k^{1/2}/\pi, \\ &V_n(i^{1/2}\rho) \text{ has zeros at } n \approx -2k + i^{3/2}4\rho k^{1/2}/\pi, \\ &W_n(i^{1/2}\rho) \text{ has zeros at } n \approx -2k + i^{-1/2}4\rho k^{1/2}/\pi, \end{aligned} \tag{12.7}$$

where k is a large positive integer. Of course, $U_n(z)$ also is zero when n is a negative integer.

So far we have been dealing with $z = i^{1/2}\rho$. Now we consider the case $z = i^{-1/2}\rho$.

Asymptotic expressions which hold when $z = i^{-1/2}\rho$ may be obtained from Table 12.1 by using the relations (9.11) between functions of z and of its complex conjugate z^*. Thus, for example, $V_{a+ib}(i^{-1/2}\rho)$ is equal to the complex conjugate of $W_{a-ib}(i^{1/2}\rho)$. These relations, and relations such as

$$\begin{aligned} &[t_0 \text{ for } z = i^{1/2}\rho,\ n = a - ib]^* = t_0 \text{ for } z = i^{-1/2}\rho,\ n = a + ib \\ &[f(t_0) \text{ for } z = i^{1/2}\rho,\ n = a - ib]^* = f(t_0) \text{ for } z = i^{-1/2}\rho,\ n = a + ib \end{aligned} \tag{12.8}$$

have been used in constructing Tables 12.3 and 12.4 from Tables 12.1 and 12.2 The interchange of $V_n(z)$ and $W_n(z)$ should be noted. The

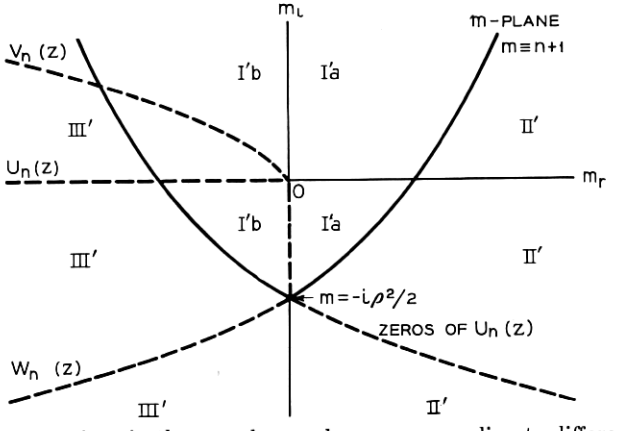

Fig. 12.2 — Regions in the complex m-plane corresponding to different asymptotic expressions when $z = i^{-1/2}\rho$. The lines on which the zeros of the various functions lie are shown by the dashed lines. The corresponding information for $z = i^{1/2}\rho$ is shown on Figs. 11.2 and 12.1.

TABLE 12.3 — LEADING TERMS IN THE ASYMPTOTIC EXPANSIONS FOR $U_n(z)$, $V_n(z)$, $W_n(z)$ WHEN $z = i^{-1/2}\rho$, $\rho > 0$

Region in m-plane $m = n + 1$	$U_n(i^{-1/2}\rho)$	$V_n(i^{-1/2}\rho)$	$W_n(i^{-1/2}\rho)$
Ia′	A_1'	$-A_0'-A_1'$	A_0'
II′	$A_1' - A_0'$	$-A_1'$	A_0'
Ib′	$(1 - i^{-4n})A_1'$	$-A_0' - (1 - i^{-4n})A_1'$	A_0'
III′	$(1 - i^{-4n})A_1'$	$-A_0' + i^{-4n}A_1'$	$A_0' - A_1'$

regions in the $m = n + 1$ plane corresponding to the different asymptotic expressions are shown in Fig. 12.2. The boundaries are simply those of Fig. 11.2 reflected in the real m-axis. The lines of zeros are also shown in Fig. 12.2, and are reflections of those of Fig. 12.1 except for the interchange of $V_n(z)$ and $W_n(z)$.

Table 12.3 may also be constructed by returning to the paths of integration shown in Section 11. It may be shown that corresponding to every path of steepest descent for $z = i^{1/2}\rho$, $n = n_1$ there is another path, obtained from the first by reflection in the real t-axis, which gives the path of steepest descent for $z = i^{-1/2}\rho$, $n = n_1^*$.

The notation used in Table 12.3 is as follows:

$$z = i^{-1/2}\rho,\ m = n + 1, \qquad i = \exp(i\pi/2),$$

$$-3\pi/2 \leqq \arg m < \pi/2, \qquad -3\pi/4 \leqq \arg t_0 < \pi/4,$$

$$-3\pi/2 \leqq \arg(-i\rho^2 - 2m) < \pi/2, \qquad -5\pi/4 \leqq \arg t_1 < 3\pi/4,$$

$$t_0 = [i^{-1/2}\rho + (-i\rho^2 - 2m)^{1/2}]/2, \qquad t_1 = [i^{-1/2}\rho - (-i\rho^2 - 2m)^{1/2}]/2,$$

$$A_0' = [t_0^{1/2}(-i\rho^2 - 2m)^{-1/4}/(-2i\pi^{1/2})]\exp f(t_0), \qquad (12.9)$$

$$A_1' = [t_1^{1/2}(-i\rho^2 - 2m)^{-1/4}/2\pi^{1/2}]\exp f(t_1),$$

$$f(t_0) = zt_0 + \frac{m}{2} - m\log t_0 = \frac{m}{2}\left(1 - \log\frac{m}{2} - \log\frac{t_0}{t_1}\right) + i^{-1/2}\rho t_0,$$

$$f(t_1) = zt_1 + \frac{m}{2} - m\log t_1 = \frac{m}{2}\left(1 - \log\frac{m}{2} - \log\frac{t_1}{t_0}\right) + i^{-1/2}\rho t_1.$$

Sometimes it is helpful to use

$$(2\pi)^{-1/2}\exp\left[\frac{m}{2}\left(1 - \log\frac{m}{2}\right)\right]$$

$$\sim \begin{cases} 1/\Gamma\left(\dfrac{m+1}{2}\right) = 1/\Gamma(1 + n/2) \text{ for } -\pi/2 < \arg m < \pi/2, & (12.10) \\ i^m\Gamma\left(\dfrac{1-m}{2}\right)\Big/ 2\pi = i^{n+1}\Gamma(-n/2)/2\pi, \quad -3\pi/2 < \arg m < -\pi/2. \end{cases}$$

TABLE 12.4 — LEADING TERMS IN THE ASYMPTOTIC EXPANSIONS FOR $U_n(z)$, $V_n(z)$, $W_n(z)$ WHEN $z = i^{-1/2}\rho$ AND $|2n| \gg \rho^2$

Region in m-plane $m = n + 1$	$U_n(i^{-1/2}\rho)$	$V_n(i^{-1/2}\rho)$	$W_n(i^{-1/2}\rho)$
Ia′	$i^{-n}B'\alpha_1'$	$B'(i^n\alpha_0' - i^{-n}\alpha_1')$	$-i^nB'\alpha_0'$
II′	$B'(i^n\alpha_0 + i^{-n}\alpha_1')$	$-i^{-n}B'\alpha_1'$	$-i^nB'\alpha_0'$
Ib′	$(1 - i^{-4n})i^nB'\alpha_0'$	$B'(i^{-3n}\alpha_0' - i^n\alpha_0'$ $- i^{-n}\alpha_1')$	$i^{-n}B'\alpha_1'$
III′	$(1 - i^{-4n})i^nB'\alpha_0'$	$B'(i^{-3n}\alpha_0' - i^{-n}\alpha_1')$	$B'(i^{-n}\alpha_1' - i^n\alpha_0')$

The notation used in Table 12.4 is as follows:

$$m = n + 1,\ i = \exp(i\pi/2), \qquad -3\pi/2 \leqq \arg m < \pi/2,$$

$$B' = 2^{-3/2}\pi^{-1/2}\exp\left[\frac{m}{2}\left(1 - \log\frac{m}{2}\right) - \frac{i\rho^2}{2}\right],$$

$$\alpha_0' = \exp[-\rho(2im)^{1/2}], \tag{12.11}$$

$$\alpha_1' = \exp[\rho(2im)^{1/2}] = 1/\alpha_0',$$

B' may be expressed in terms of gamma functions with the help of (12.10.).

Approximate expressions for the zeros are given by the complex conjugates of (12.7). For example, if k be a large positive integer such that $2k \gg \rho^2$, the zeros of $W_n(i^{-1/2}\rho)$ are at $n = n(k)$ where $i^{-n}\alpha_1' = \exp(i\pi k)$ and

$$n(k) \approx -2k + i^{-3/2}4\rho k^{1/2}/\pi - 4i\rho^2/\pi^2. \tag{12.12}$$

Here the approximation has been carried out one step further than in (12.7) We also have for the quantities in (7.11)

$$[\partial W_n(i^{-1/2}\rho)/\partial n]_{n=n(k)} \approx (-)^{k+1}B'i[\pi - \rho(i/k)^{1/2}], \tag{12.13}$$

$$[i^{2n}V_n(i^{-1/2}\rho)/\sin\pi n]_{n=n(k)} \approx (-)^{k+1}2B'i.$$

13. ASYMPTOTIC EXPRESSIONS FOR $U_n(z)$, ETC., WHEN n IS NEAR $z^2/2$

The asymptotic expressions given in Section 12 fail when n is near $z^2/2$. Expressions for the parabolic cylinder functions which hold for this region have been given by Schwid.* More recent studies of this sort, based on differential equations, have been made by T. M. Cherry[24] and F. Tricomi.[25] Their results suggest the possibility that our expressions

* Reference 20, page 478.

[24] Uniform Asymptotic Expansions, J. Lond. Math. Soc., **24**, pp. 121–130, 1949. Uniform Asymptotic Formulae for Functions with Transition Points, Am. Math. Soc. Trans., **68**, pp. 224–257, 1950.

[25] Equazioni Differenziali, Einaudi, Torino, pp. 301–308, 1948.

for the electromagnetic field which contain Airy integrals may be replaced by more accurate, but also more complicated, expressions. In dealing with our functions we shall work with the integrals and our procedure is somewhat similar to that used by Rydbeck.* First however, we point out that when we write (as suggested by the work of Cherry and Tricomi)

$$y = e^{-z^2/2}T_n(z), \qquad ax = z - (2n+1)^{1/2}, \qquad 2(2n+1)^{1/2}a^3 = 1, \tag{13.1}$$

the differential equation (9.7) for the parabolic cylinder functions goes into

$$\frac{d^2y}{dx^2} - xy = 2^{-4/3}(2n+1)^{-2/3}x^2y. \tag{13.2}$$

The Airy integrals $Ai(x)$ and $Bi(x)$ (and also $Ai[x \exp(\pm i2\pi/3)]$) discussed later in this section are solutions of

$$\frac{d^2y}{dx^2} - xy = 0, \tag{13.3}$$

and therefore we expect that approximate solutions of (13.2) are given by, for example,

$$y = c_1 Ai(xi^{\nu})[1 + 0(n^{-2/3})] \tag{13.4}$$

where the $0(n^{-2/3})$ term corresponds to the particular integral of (13.2) when the y on the right hand side is replaced by its approximate value $Ai(xi^{\nu})$. Here c_1 is independent of x (or z) but may depend on n, and ν may be 0 or $\pm 4/3$.

Since the labor of computing c_1 is considerable, we shall work out the approximations directly from the integrals.

We shall consider the case $z = i^{1/2}\rho$, $\rho > 0$, first. When $n + 1 = m = m_0 \equiv i\rho^2/2$ the saddle points t_0 and t_1 coincide at $t_2 \equiv i^{1/2}\rho/2$. Consequently only those portions of the paths of steepest descent which lie near t_2 are of importance. This is true even if m is not exactly equal to m_0. We therefore regard

$$f(t) = -t^2 + 2zt - m \log t \tag{13.5}$$

in (10.1) as a function of the two variables t and m (linear in m) with z fixed at $i^{1/2}\rho$. Expanding (13.5) about $t = t_2$, $m = m_0$ gives

$$f(t) = \frac{z^2}{2} + \left[\frac{m_0}{2} - \frac{m_0}{2}\log\frac{m_0}{2} - \frac{(m-m_0)}{2}\log\frac{m_0}{2}\right] - 4(t-t_2)^3/3z - 2(m-m_0)(t-t_2)/z + \cdots \tag{13.6}$$

* Page 87 of Reference 21 cited on page 478.

where we have used

$$t_2 = z/2 = i^{1/2}\rho/2 = (m_0/2)^{1/2} \tag{13.7}$$

and have arranged the terms within the brackets so that they represent the first two terms in the expansion of

$$\frac{m}{2} - \frac{m}{2}\log\frac{m}{2} \sim \log\left[(2\pi)^{1/2} \Big/ \Gamma\left(\frac{m+1}{2}\right)\right] \tag{13.8}$$

about m_0.

The paths of steepest descent in the t-plane when $m = m_0$ are shown in Fig. 11.6(d). The three branches start out from $t = t_2$ in the directions arg $(t - t_2) = 15°$, $135°$, and $-105°$. In this section we take the paths of integration to be those of Fig. 11.6(d) even when m is not exactly equal to m_0. Since we are dealing with asymptotic expressions we may confine our attention to the region around $t = t_2$ where the paths of integration are essentially straight lines [the contributions from $t_2 \exp(-2\pi i)$ are negligible].

When (13.6) is set in the integral

$$(1/2\pi i)\int \exp\,[f(t)]\,dt \tag{13.9}$$

we see that the initial directions of the branches are such as to make $(t - t_2)^3/z$ positive (arg $z = 45°$). Some study of (13.6) and of the Airy integrals we intend to use suggests that we change the variable of integration from t to s and introduce the parameter b where

$$t - t_2 = s(z/4)^{1/3}, \qquad b = (m - m_0)(2/z^2)^{1/3} = (m - m_0)/m_0^{1/3}. \tag{13.10}$$

This and (13.6) converts the integral (9.1) for $V_n(i^{1/2}\rho)$ into

$$V_n(i^{1/2}\rho) = \frac{(z/4)^{1/3}e^{z^2/2}}{i(2\pi)^{1/2}\Gamma\left(\dfrac{m+1}{2}\right)} \int_{\infty \exp(i2\pi/3)} \exp\,[-bs - s^3/3 + \cdots]\,ds. \tag{13.11}$$

When we use the Airy integral defined by

$$\begin{aligned} Ai(x) &= \pi^{-1}\int_0^\infty \cos\,(xt + t^3/3)\,dt \\ &= (i^{1/3}/2\pi)\int_{\infty \exp(i2\pi/3)} \exp\,[-i^{-2/3}xs - s^3/3]\,ds, \end{aligned} \tag{13.12}$$

we obtain

$$V_n(i^{1/2}\rho) \sim \frac{(z/4)^{1/3}e^{z^2/2}}{i(2\pi)^{1/2}\Gamma\left(\dfrac{m+1}{2}\right)} \frac{2\pi}{i^{1/3}}\,Ai(bi^{2/3}). \tag{13.13}$$

In order to obtain expressions corresponding to (13.13) for $U_n(z)$, $W_n(z)$ we examine Fig. 11.6(d). We have already seen that the limits of integration for s, in the integral (13.11) for $V_n(i^{1/2}\rho)$, are $[\infty \exp(i2\pi/3), \infty]$. In the same way it follows that the limits for $U_n(i^{1/2}\rho)$ and $W_n(i^{1/2}\rho)$ are $[\infty \exp(-i2\pi/3), \infty \exp(i2\pi/3)]$ and $[\infty, \infty \exp(-i2\pi/3)]$, respectively. When we take $s' = s \exp(\mp i2\pi/3)$ as new variables of integration (with the upper sign for $U_n(z)$ and the lower one for $W_n(z)$), the integrals corresponding to (13.11) go into Airy integrals.

We can write our results for $z = i^{1/2}\rho$, when n is close to $i\rho^2/2$, as follows:

$$\begin{aligned} U_n(i^{1/2}\rho) &\sim C i^{1/6} Ai(b i^{6/3}), \\ V_n(i^{1/2}\rho) &\sim C i^{-7/6} Ai(b i^{2/3}), \\ W_n(i^{1/2}\rho) &\sim C i^{9/6} Ai(b i^{-2/3}), \end{aligned} \tag{13.14}$$

where

$$\begin{aligned} C &= (\rho/4)^{1/3}(2\pi)^{1/2} e^{i\rho^2/2} / \Gamma\left(\frac{m+1}{2}\right), \\ b &= (2/\rho^2)^{1/3}(m - i\rho^2/2) i^{-1/3}, \\ i &= \exp(i\pi/2), \qquad m = n + 1. \end{aligned} \tag{13.15}$$

The asymptotic expansions whose leading terms are given by (13.14) may be obtained by the method used by F. W. J. Olver[26] to study Bessel functions.

$Ai(x)$ and its derivative have been tabulated for positive and negative values of x.* Here we shall use the definitions and results as set forth in Reference 11. These tables and (13.14) enable us to obtain values of $U_n(i^{1/2}\rho)$ along the rays in the m-plane defined by $\arg(m - i\rho^2/2) = \pi/6$ and $-5\pi/6$. Along the $\pi/6$ ray $bi^{6/3}$ is negative. Since the tables show that the zeros of $Ai(x)$ occur when x is negative, it follows that the zeros of $U_n(i^{1/2}\rho)$ occur on the $\pi/6$ ray. In the same way it is seen that the zeros of $V_n(i^{1/2}\rho)$ and $W_n(i^{1/2}\rho)$ occur on the $5\pi/6$ and the $-\pi/2$ rays, respectively. This agrees with Fig. 12.1.

The Airy integral defined by

---

* Reference 11, page 424.

[26] Some New Asymptotic Expansions for Bessel Functions of Large Orders, Proc. Cambridge Phil. Soc., **48**, pp. 414–427, 1952.

$$Bi(x) = \frac{i^{-2/3}}{2\pi}\left[\int_{\infty \exp(i2\pi/3)}^{\infty \exp(-i2\pi/3)} + \int_{\infty \exp(-i2\pi/3)}^{\infty}\right] \exp\left[-i^{-2/3}xs - s^3/3\right] ds \tag{13.16}$$

$$= \frac{1}{\pi}\int_0^\infty \left[\exp\left(-\frac{t^3}{3} + xt\right) + \sin\left(\frac{t^3}{3} + xt\right)\right] dt$$

is also tabulated in Reference 11 where it is shown that

$$\begin{aligned} Ai(xi^{4/3}) &= i^{2/3}[Ai(x) - iBi(x)]/2, \\ Ai(xi^{-4/3}) &= i^{-2/3}[Ai(x) + iBi(x)]/2. \end{aligned} \tag{13.17}$$

With the help of these relations we may evaluate the expressions (13.14) for $U_n(i^{1/2}\rho)$, etc., on any one of the six rays

$$\arg(m - i\rho^2/2) = \pm 5\pi/6, \pm/\pi/2, \pm\pi/6.$$

When b is a general complex number the expressions (13.14) may be evaluated with the help of the modified Hankel functions $h_1(\alpha)$, $h_2(\alpha)$ tabulated in Reference 27 for complex values of α. The relation needed is

$$\begin{aligned} Ai(\alpha) &= \frac{1}{2k}h_1(-\alpha) + \frac{1}{2k^*}h_2(-\alpha), \\ k &= (12)^{1/6}i^{-1/3}. \end{aligned} \tag{13.18}$$

When $|\arg\alpha| < \pi$ we have the asymptotic expansion

$$Ai(\alpha) \sim 2^{-1}\pi^{-1/2}\alpha^{-1/4}(\exp[-(2/3)\alpha^{3/2}])(1 - 5/48\alpha^{3/2} + \cdots) \tag{13.19}$$

and when $|\arg(-\alpha)| < 2\pi/3$ we have

$$Ai(\alpha) \sim \pi^{-1/2}(-\alpha)^{-1/4}\sin[(2/3)(-\alpha)^{3/2} + \pi/4]. \tag{13.20}$$

Both of these expansions follow from the discussion of the asymptotic behavior of $h_1(\alpha)$ and $h_2(\alpha)$ given by W. H. Furry and H. A. Arnold.[27]

Asymptotic expressions for $U_n(i^{-1/2}\rho)$, $\cdots$ valid when n is near $-i\rho^2/2$ may be obtained by applying the relations $U_n(z^*) = [U_{n*}(z)]^* \cdots$ given by (9.11) to the expressions (13.14) for $U_n(i^{1/2}\rho)$, $\cdots$:

$$\begin{aligned} U_n(i^{-1/2}\rho) &\sim C'i^{-1/6}Ai(b'i^{-6/3}), \\ V_n(i^{-1/2}\rho) &\sim C'i^{-9/6}Ai(b'i^{2/3}), \\ W_n(i^{-1/2}\rho) &\sim C'i^{7/6}Ai(b'i^{-2/3}), \end{aligned} \tag{13.21}$$

[27] Tables of the Modified Hankel Functions of Order One-Third and of Their Derivatives, Harvard Univ. Press, 1945.

where

$$\begin{aligned} C' &= (\rho/4)^{1/3}(2\pi)^{1/2}e^{-i\rho^2/2}/\Gamma\left(\frac{m+1}{2}\right), \\ b' &= (2/\rho^2)^{1/3}(m + i\rho^2/2)i^{1/3}, \\ i &= \exp(i\pi/2), \qquad m = n + 1. \end{aligned} \tag{13.22}$$

In (13.14) $bi^{6/3} = -b$ and in (13.21) $b'i^{-6/3} = -b'$ since $Ai(\alpha)$ is a single-valued function of α. It is interesting to note that the factor $i^{1/6}$ in the expression for $U_n(i^{1/2}\rho)$ gives the direction of that one of the three paths of steepest descent (in the t-plane) which is *not* traversed in getting $U_n(i^{1/2}\rho)$. The same sort of thing is true for the remaining expressions in (13.14) and (13.21).

The functions

$$'U_n(z) = \exp(z^2/2)\partial[U_n(z)\exp(-z^2/2)]/\partial z,$$

defined by (4.19), may be computed from (13.21) when $z = i^{-1/2}\rho$. We need the relations $\partial/\partial z = i^{1/2}\partial/\partial\rho$ and

$$\begin{aligned} m &= -i\rho^2/2 + b'(\rho^2/2i)^{1/3}, \\ \partial b'/\partial\rho &= (2/3)(2i\rho)^{1/3}(i - m/\rho^2) = i(2i\rho)^{1/3} - 2b'/3\rho, \end{aligned} \tag{13.23}$$

which follow from the definition of b'. When the differentiations are carried out we obtain

$$\begin{aligned} 'U_n(i^{-1/2}\rho) &\sim (2\rho)^{1/3}C'i^{-1/3}Ai'(b'i^{-6/3}), \\ 'V_n(i^{-1/2}\rho) &\sim (2\rho)^{1/3}C'i^{3/3}Ai'(b'i^{2/3}), \\ 'W_n(i^{-1/2}\rho) &\sim (2\rho)^{1/3}C'i^{7/3}Ai'(b'i^{-2/3}), \end{aligned} \tag{13.24}$$

In these expressions the prime on the Airy integral denotes its derivative:

$$Ai'(\alpha) = dAi(\alpha)/d\alpha. \tag{13.25}$$